Aggregation and Sedimentation of Fine Solids

by

Mehdi Omidghane

A thesis submitted in partial fulfillment of the requirements for the degree of

Doctor of Philosophy

in

Chemical Engineering

Department of Chemical and Materials Engineering
University of Alberta

Abstract

In many applications, it is desired to separate unwanted fine particulates from a liquid by gravity settling. An efficient separation, however, will be feasible only if a combination of aggregation and sedimentation occurs. To understand the kinetics of such a process, a mathematical model that accounted for aggregation and sedimentation was developed. The simulation was based on Smoluchowski's equation of population balance, with the collision frequency determined by Brownian motion and differential settling, while treating the aggregates as fractal objects as the particles collide and aggregate. One of the most important issues here is that aggregating systems, especially those encountered in particle technology and separation processes, often involve *non-uniform* particle distributions. Situations with evenly distributed aggregates are very rare in practice, but this continues to be the "default assumption" in many theoretical treatments. This study addressed this issue by developing a series of experiments and numerical model to properly account for non-uniform particle sizes and their spatial variations.

Our results showed that the rate of settling could be improved significantly if the particles aggregated (the settling time may be reduced from hours to minutes). Experimentally, we showed that, depending on the strength of interaction between the particles, different settling regimes were observed. It was also observed that under certain experimental conditions, an initial 'induction time' appeared before the apparent onset of sedimentation. It appears that the particles required some 'waiting time' before commencement of aggregation. Our simulations showed that the observed 'induction period' may in fact be a kinetic phenomenon that was independent of the nature of the inter-particle forces (i.e. on the microscopic scale, the particles began to aggregate immediately without any delay). Our simulation showed that inter-particle

attraction could significantly affect the rate of aggregation and sedimentation. Larger attractive forces also resulted in a perceptible clear liquid-suspension interface; as such forces diminished, the clear liquid-suspension interface became more diffuse and eventually appeared as a gradual concentration gradient. A novel approach was used to predict formation of this 'mud line.'

We have also demonstrated that sedimentation kinetics are largely insensitive to the initial particle size distribution; an explanation for this observation is discussed.

To my love, Marzieh

Acknowledgements

My deepest gratitude goes to my supervisors, Dr. Tony Yeung and Dr. Qi Liu. The superb mentorship I received from Dr Yeung, his kind attention and encouragement, and his trust in me were essential for the completion of this work.

I would like to thank my wife Marzieh for all of her support and encouragement. I could not have finished it without her by my side.

My gratitude extends to my colleagues Dr Feng Lin, Dr Leyli Mirmontazari, Amin Karkooti and Anita Bianchini for their valuable discussions and ideas.

I desire to acknowledge my dear friends in Edmonton for their invaluable friendship and help. Specially, I would like to appreciate Mohammad Saeid Amiri, Ehsan Jenab, Moslem Noori, Sadegh Amiri, Hadi Moosavi, Omid Taheri and Hamid Moghadas.

And last but not least my deepest gratitude goes to my mother and brother. I appreciate their love and support during all my studies. Without their support, trust and encouragement, none of my accomplishments were achievable.

The financial support of the project from Institute for Oil Sands Innovation at the University of Alberta is acknowledged and appreciated.

Table of Contents

List of Figures

List of Tables

Nomenclature

a	radius of particle
C	Smoluchowski rate constant
d_0	size of primary particles
d_{avg}	average size of aggregates
d_f	fractal dimension
d_i	size of aggregate i
d_{max}	size of largest aggregate
D	diffusivity
D_k	diffusivity of k-aggregate
g	gravitational acceleration
G	velocity gradient or shear rate
k	Boltzmann constant
$k_{m,avg}$	mass-weighted average size of particles
$k_{n,avg}$	number-weighted average size of particles
L	characteristic length
m_{tot}	total mass
n_k	number density of k-aggregates
n_{tot}	total number of aggregates
N	number of primary particles in the largest aggregate
N_{tot}	total number of primary particles
r	position
R	inner radius of tube
t	time
T	temperature
U	characteristic velocity
v	velocity
v_k	velocity of k-aggregate
V	volume of domain
z	vertical position
α	collision efficiency
β	collision frequency
ε	aggregate packing porosity
η	scaled size of aggregates
μ	viscosity of fluid
δ_k	travel distance of a k-aggregate
ρ_{agg}	density of aggregate

ρ_p	density of particle
φ	total number of primary particles
ψ	scaled particle size distribution

1 Introduction

1.1 Aggregation and Sedimentation of fine solids

Separation of fine particles from a fluid is one of the important processes in many industrial applications (e.g. in water treatment, mineral processing, and aerosol technology). There are several methods to separate particulates from a fluid [1]–[3]. However, when it comes to fine particles, most methods are not efficient and sufficiently reliable. The fine solids are typically in the colloidal or micron-sized range; they are not amenable to the usual methods of separation such as centrifugation or screening [2]. The removal of these solids from the fluid, however, can be accomplished through sedimentation under certain conditions. Sedimentation is the simplest and cheapest form of separation processes; it is the settling of small particles in a fluid under gravity. Despite its simplicity, it may be used to separate fine particulates. The main challenge to the separation of fine particulates — due to the small size — can be identified in two categories: (a) colloidal (sub-micron) particles are susceptible to thermal agitation and can be suspended indefinitely (an equilibrium situation); (b) even when the particles are larger than ~1μm, the settling velocity can be so slow that, on the time scales of the separation process, the particles are effectively 'neutrally buoyant.' In both situations, the remedy is to cause the particles to *aggregate*, as larger entities are not prone to Brownian motions and also will settle much faster.

Aggregation is a process where two or more suspended particles in a fluid combine together to form a larger particle. Efficient separation by sedimentation can be achieved following significant aggregation of particulates. The entire process (i.e. aggregation and sedimentation together) is carried out in a settling vessel.

The design of settling vessels must account for many parameters, but the key element is the settling velocity of the particulates, which is determined by the size of the particles and properties of the fluid. Designers size the vessels such that they ensure that the particulates have enough time to be removed from the fluid. If the particles, for any reason, do not aggregate, then only the initial size distribution of the particles matters; under this condition, the process time should be impractically long to allow enough settling time for the particles to be removed. On the contrary, if particles are able to aggregate, the settling time requirement, and therefore the size of the vessel will be reduced significantly. Therefore, it is necessary to investigate how the aggregation for a certain system can be improved. An understanding of the underlying mechanisms of aggregation will provide valuable information in efforts to enhance the aggregation.

In addition to mechanisms, the kinetics of aggregation should be taken into account in the design of the vessel. Kinetic study includes investigations of how different experimental conditions can influence the aggregation and, in turn, the rate of separation. Knowledge of process kinetics will be necessary to be able to design the equipment proficiently.

1.2 Motivation of this project

Canada has, in the form of oil sands, one of the largest petroleum resources in the world. These oil sands deposits are found mostly in the province of Alberta; it consists of a mixture of bitumen (a heavy form of crude oil [4]), silica sands, clay minerals and trace amounts of connate water. Such deposits are suitable for large-scale surface mining, in which the ores are recovered using open-pit mining technology. After it is mined, the ore is 'slurried' in massive amounts of water, and the bitumen is eventually separated from the sand through a flotation process. Despite the economic benefits brought on by the oil sands industry, the environmental impacts are also

considerable due to the extremely high demand for fresh water. The huge amount of water consumed everyday ends up in tailings ponds. These ponds in Northern Alberta are considered one of the largest human-made structures in the world that can be seen from space. With planned increases in oil production in the coming years (by up to five times the current level), this environmental impact will certainly become more serious. In view of this, an alternative *solvent-based* (or 'non-aqueous') extraction technique is proposed to replace the current water-based method. The basic principles of such a non-aqueous technology are simple: Mined oil sands are first mixed with an organic solvent in which bitumen is soluble. This mixture is then put through separation vessels where coarse sand grains and other solid particles are removed (Figure 1.1). The product of this non-aqueous process, as shown in the Figure 1.1, is solvent-diluted bitumen. This product stream should ideally be free of any suspended solids. Unfortunately, in reality, it is unavoidable to see fine solids entrained in the diluted bitumen (i.e. product) stream. These fine solids are highly undesirable as they can lead to fouling problems downstream.

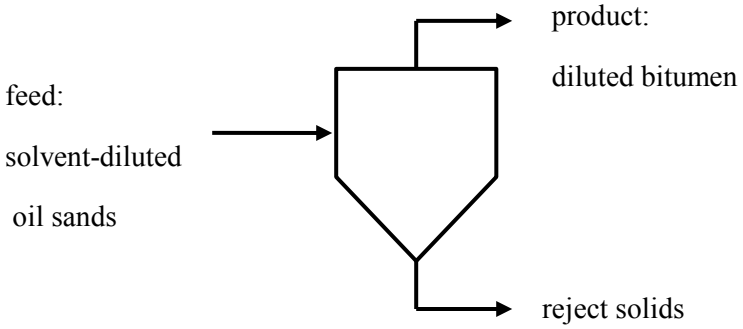

Figure 1.1. Schematic of the separation of coarse solids from solvent-diluted oil sands

Various non-aqueous processes had been proposed in the past decades for bitumen extraction, but no process design has progressed beyond large scale pilot tests. The two main obstacles to all the proposed non-aqueous processes are:

1. Entrained fine solids in the oil phase (i.e. diluted bitumen) can result in the fouling of pipelines and catalysts in downstream upgrading facilities.
2. The residual oil attached to the reject sand grains (underflow stream in Figure 1.1) will result in solvent loss and large scale environmental pollution.

To develop a successful non-aqueous (i.e. solvent-based) extraction process, the mechanisms which underlie the above two obstacles should be understood before development of any commercial operation.

One of the applications of this research will be on the basic science which underlies the first challenge: the removal of suspended fine solids from a hydrocarbon medium. The nature of the organic solvent plays a central role in the destabilization of suspended solids in diluted bitumen. A discussion of the background and motivation of this can be found in an earlier paper [5].

1.3 Thesis Objectives

A successful gravity separation process requires substantial aggregation followed by sedimentation. Here, sedimentation is the *collective* behaviour of a large number of aggregating and settling particles. Despite extensive studies in the literature regarding aggregation or sedimentation, very little work was done that consider both aspects at the same time. The overall dynamics that is crucial to evaluating the performance of a settling vessel is not yet understood.

There is a lack of knowledge in the literature to relate these two components (aggregation and sedimentation). The purpose of this research is to bridge the gap, and study the collective behaviour of sedimentation from first principles. The study will be then extended to examine the kinetics of the sedimentation in detail.

Empirical experiments on sedimentation produce valuable data, but they will not provide sufficient information required for a comprehensive kinetic study. A mathematical model which captures the intricate details of the phenomena seems inevitable. As a result, the study has been conducted by means of two approaches: (1) empirical experiments, and (2) numerical modeling.

The main objectives of this thesis can be listed as below:

- To conduct the experiments to measure the overall rates of settling under different conditions (including the nature of the suspension, fluid properties and the characteristics of particles such as size distribution).
- To create a model to simulate the aggregation of settling particles. All key factors should be considered in the model to minimize the simplifying assumptions.
- To use the model to facilitate experimental development.
- To use the modeling results to gain detailed insight into the sedimentation process.
- To predict the optimal condition (e.g. suspension medium properties) for the aggregation of fine particles.
- To use the results to identify the influence of different attributes (e.g. initial size distribution of the particles) on the design of separation vessels.

1.4 Thesis outline

This thesis is organized as follows: Given our objective of study discussed in Chapter 1, Chapter 2 reviews the relevant literature. A brief discussion of the background theory is presented in Chapter 2. Experimental procedures will be presented in Chapter 3. Chapter 4 is on the modeling procedure, and how a numerical method was employed to solve the equations. All the governing equations, along with the associated assumptions, will be presented in this chapter. Chapter 5 will be devoted to the preliminary results and brief discussion on model validation. The settling behaviour of a suspension, and the kinetics study and other relevant settling observables, will be addressed in Chapter 6. Chapter 7 will be dedicated to initial size distribution as it is the key consideration in the design of settling vessels. The conclusions will be presented in Chapter 8.

2 Literature review

2.1 Separation of Fine Particles from a fluid

Solid particles are found in many different types of suspensions. They come in various compositions, shapes and sizes. Solid particles suspended in gases (smoke) or liquids (dispersions) are the most common examples. Suspensions of very fine particles in a fluid (gas or liquid) are called colloidal dispersions. The size range of particles in the dispersed phase is roughly between 1 nm to 1μm — still much larger than the molecules of the dispersion medium. Such dispersions have been the subject of several studies in many fields of science [6].

In many applications, it is desired to have particles remain suspended in a fluid. In many others, the particulates are required to be separated from the fluid. The particles may contain important minerals, or they may be pollutants that must be removed. It is a very important phenomenon that underlies a wide variety of science application, such as atmospheric sciences and air pollution control, water and waste water treatment, the oil industry, etc. For example, in air pollution control, it is desired to remove any particulates from air (e.g. dust particles). Water or wastewaters are required to be free of any suspended particles. In a refinery, the product stream should ideally be free of any suspended solids as they may, for example, result in fouling problems downstream. Various methods and equipment have been developed in many industries to remove solids [7],[1]; settling tanks, thickeners, or centrifuges are some examples. The simplest and cheapest method is sedimentation.

Separation of solids from a fluid by gravitational sedimentation has long been used in many applications. Sedimentation is the settling of particles in a fluid under gravity. The process is based on the density difference between the two phases. It is an easy and cheap technique to separate particulates, and the equipment is often small and inexpensive; they can be used to process large amount of materials as they can be incorporated in several stages or in parallel. The simplest configuration is that the suspension enters from a side and leaves from another side. As the fluid flows through the vessel, the particles fall out and accumulate at the bottom.

If the particles are fine (≤ 10μm) and/or the density difference is small, the settling rate is quite low so that larger and more expensive equipment will be required to separate solids efficiently. In this case, the remedy is to make the particles aggregate.

2.2 Aggregation

Aggregation is a process in which two or more particles combine together to form a larger entity. The total number of particles reduces in aggregation (with each aggregate counting as one "particle"), while the total mass remains conserved. This is an important process in many fields relevant to the process of fine particle separation, and extensive studies can be found in the literature regarding this phenomenon [8], [9]. An understanding of the underlying mechanisms of aggregation will provide valuable information in efforts to remove the fine particles more efficiently. To illustrate this matter, let us look into an example: Experiments revealed that the choice of the suspending medium is one of the most important parameter affecting the rate of settling [5]; it is proposed that it has very strong effects on the aggregation of the fine solids. It is because we know that in the absence of aggregation, the type of suspending liquid has only a

very minor effect on the settling rate (e.g. Stokes velocity). Another example would be the water treatment; the chemistry of the medium affects the aggregation rate. The concentration of salt, pH, etc. would influence the aggregation and sedimentation.

The aggregation process is usually assumed to include two stages: First the particles are brought about together by collisions and second they should be held in contact by surface forces. In the following sections the mechanism of aggregation will be discussed. Here, we start with the inter-particle forces as it is the most important element in aggregation.

2.2.1 Inter particle forces

Several types of interactions between particles influence many of the important properties of solids suspensions [10]. These forces are short-ranged, in that their extents of influence are often much less than the size of the particles. Colloidal interactions have two major effects on the aggregation process: First, if strong repulsion exists between the particles, they repel each other and aggregation will occur only very slowly, if at all. In other words, the stability of suspended particles against aggregation is governed by the colloidal forces. Much less clear, but just as important, is the effect of colloid interactions on the strength of the aggregates; this property will determine whether the aggregates would break up under hydrodynamic shear forces. A brief description of the forces is given below:

Van der Waals Attraction

Van der Waals forces play a very important role in the interaction of colloidal particles; these forces often cause particles to aggregate in a suspension. The spontaneous electrical polarization is the source of these attractive forces. The magnitude of these forces depends on the properties

of the particles and of the intervening medium. Although at times repulsive, the van der Waals interaction between similar materials in a liquid is always attractive.

Electrical Double Layer Repulsion

When immersed in water, most particle surfaces are charged. If the aqueous solution contains dissolved ions (i.e. if it were an electrolyte), there would be an accumulation of counter ions around the particles to form an 'electrical double layer'. A part of these counter ions is compacted at the particle surface and forms a 'Stern layer,' while the remainder is distributed in the so-called diffuse layer, where the ions can move about via Brownian motions. As two particles come into close proximity, the electric double layers will be compressed. This results in a repulsive force which can stabilize particles in aqueous suspension.

Polymer Bridging

Adsorbed macromolecules, such as polymers, may play an important role in promoting aggregation through the so-called bridging mechanism. If polymers with an affinity for the particle surfaces were present in the solution, they can attach to two or more particles (i.e. forming a "bridge") and cause them to aggregate. However, the polymer needs to adsorb in such a way that a significant portion of the molecule will extend some distance into the continuous medium. In other words, the suspending liquid should be a "good solvent" for the polymer.

In this study, we have not planned to use polymers as an additive and hence the influence of polymer bridging on aggregation will not be studied.

Steric Repulsion

Although there is no significant double layer repulsion between surfaces in non-aqueous systems, stabilizing forces due to adsorption of macromolecules (e.g. polymers) may have to be included. As mentioned above, polymers at low surface concentrations could increase the aggregation rate through cross-bridging. In contrast, full (or close to full) surface adsorption can result in the opposite effect, i.e. enhanced stability by creating repulsive forces known as steric stabilization [11]. For example, in bitumen diluted systems, these forces arise from the adsorption of asphaltenes, which influence the process in a way similar to complete surface coverage by polymers. The larger molecules of asphaltenes can adsorb on surfaces in such a way that they extend some distance into the continuous medium, forming tails and loops which give enhanced stability against aggregation (Figure 2.1). The degree of stabilization depends on the thickness of the adsorbed layer relative to the particle size, and on the solvency of the medium for the stabilizing segments.

On the microscopic scale, very little is known about the surface forces of colloidal particles in oil sands systems. The two familiar types of colloidal interactions — the attractive van der Waals forces and the repulsive double layer interaction — form the basis of the well-known DLVO theory of colloid stability. In this theory, the repulsive force acts as a dispersion stabilizer, while the attractive force destabilizes the dispersed phase.

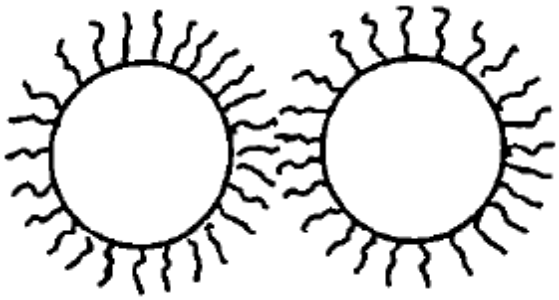

Figure 2.1. Prevention of particle contact by adsorbed macromolecules on solid surface [12]

2.2.2 Mechanism of aggregation

A key element to understanding the mechanics of aggregation is to determine how individual particles come into contact, and then remain together, to make a stable aggregate in various environments. Therefore, aggregation of particles can conceptually be divided into two steps: *transport*, which is the bringing of two particles into close contact, followed by *destabilization*, which is adhesion of the particles via short-range colloidal forces.

2.2.2.1 Collision frequency

The collision frequency, denoted β_{ij}, depends on the physical environment such as temperature, viscosity, shear stress and size of particles. It is a parameter reflecting how frequently particles of size i encounter and collide with particles of size j. It is generally accepted that there are three mechanisms which cause particle collision: Brownian motion (perikinetic aggregation), fluid shear (orthokinetic aggregation), and differential settling [8], [9], [12].

Brownian motion is the random movement of colloidal particles in a fluid, which can have the effect of bringing two entities together via diffusion. If the suspension is subjected to fluid shear, particle transport will be brought about by fluid motion, which can greatly increase the rate of

collision; this is called orthokinetic aggregation. Differential settling occurs when larger aggregates settle more rapidly than smaller ones; such relative motion can result again in particles collisions. For simple cases, with the particles considered spherical, the collision frequency is calculated as follows [12]:

Perikinetic: $$\beta_{ij} = \frac{2kT}{3\mu}\frac{(a_i + a_j)^2}{a_i a_j} \quad (1)$$

Orthokinetic: $$\beta_{ij} = \frac{4}{3}G(a_i + a_j)^3 \quad (2)$$

Differential settling: $$\beta_{ij} = \left(\frac{2\pi g}{9\mu}\right)(\rho_s - \rho)(a_i + a_j)^3(a_i - a_j) \quad (3)$$

In the above expressions, a_i is the radius of particle i and G is the velocity gradient or shear rate. In our settling study, no shear is applied to the suspension. As such, collision between particles will result only from Brownian motion and differential settling. Brownian motion is often the dominant mechanism of transport for colloidal (i.e. submicron) particles. As the aggregates grow in size, however, differential settling gradually becomes the more important transport mechanism.

2.2.2.2 Collision efficiency

Not all collisions result in successful aggregation. It depends whether the suspension is destabilized or not. The fraction of collisions which result in flocculation, called the collision efficiency, is usually denoted by the symbol α. In the limit of very large number of collisions, α is defined as

$$\alpha \equiv \frac{\text{number of collisions resulting in aggregation}}{\text{total number of collisions}}$$

Aggregation is not possible if there is strong repulsion between the particles — in which case the suspension is stable, and α is equal to zero. On the other hand, the collision efficiency approaches unity, and the suspension is destabilized when there is strong attraction between particles such that they are likely to stick to each other on contact. It is a function of the surface properties of the particles and colloidal interactions [13]. The collision efficiency thus should be incorporated into the rate expressions.

The collision efficiency and the stability of suspended particles against aggregation are usually assumed independent of the transport mechanism. It is dependent only on inter-particle forces. There are, nevertheless, observations that suggest the contrary [14].

2.2.3 Structure of aggregates

When two particles collide and aggregate, the simplest picture is that spherical particles come together to form a larger sphere of the same total volume. Although unrealistic except for the coalescence of liquid drops, this scenario has often been assumed in many treatments of aggregation kinetics. In reality, the aggregate, which is formed from many primary particles, is typically of a branched and random structure; the "compactness" of an aggregate can be characterized by its *fractal dimension* (see Figure 2.2) [15], [16].

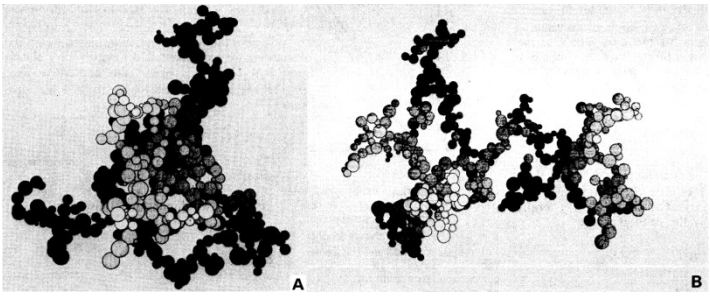

Figure 2.2. Fractal shape of aggregates: (a) packed, and (b) loose structure (modified from [17])

For a solid object, its mass m is proportional to the third power of its characteristic length L (i.e. $m \sim L^3$). For fractal objects, however, the exponent is less than 3. The mass of a fractal object scales as

$$m \sim L^{d_f}$$

where d_f is the fractal dimension. Figure 2.3 illustrates how the fractal dimension can be measured experimentally. Fractal dimension indicates how densely the primary particles are distributed in the aggregate. The fractal dimension can range of 1 (for rod-like objects) to 3 (for solid objects); a denser packed aggregate has higher fractal dimension. The fractal dimension is an important parameter as it determines the effective size and settling velocity of non-compact aggregates [18].

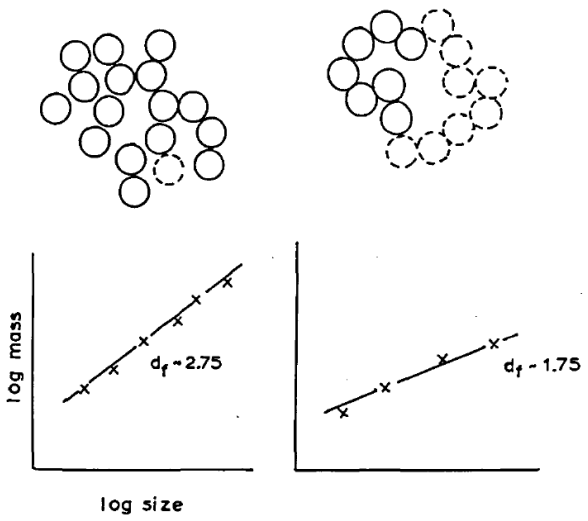

Figure 2.3. Schematic illustration on how fractal dimension is calculated under various conditions [12].

Several experimental studies of the fractal nature of aggregates have been reported. The fractal dimension has been measured by various techniques, such as image analysis [19]–[21], settling

velocity measurement [22], [23], Xray or light scattering [24], [25], and electron microscopy [17]. Experiments show that fractal dimension of aggregates formed from smaller particles depends on the transport mechanism which is involved in the aggregation process. Ref [22], [26] reported that fluid shear (i.e. orthokinetic aggregation) results in creation of aggregates with fractal dimension greater than 2.4, whereas aggregates created by differential sedimentation has lower fractal dimension — in the range of 1.6 to 2.3. It is also reported that the fractal dimension is between 1.6 and 1.9 for rapid aggregation (i.e. when $\alpha = 1$), and between 2 and 2.3 for slow aggregation (i.e. $\alpha \ll 1$) [12], [27]. Lin et al. [28] showed that in the regime of slow aggregation (or reaction-limited aggregation), the aggregates had a fractal dimension $d_f = 2.1$ [28].

2.3 Previous studies

Despite extensive studies in the literature regarding aggregation [29]–[33] or sedimentation [7], [34], the results were limited to either process; very little work was done that consider both aspects at the same time. Furthermore, the solution were for special cases or they were carried out with simplifying assumptions which apply only to highly idealized — even unrealistic — situations [35]–[38]. A few studies, for example, assumed that aggregation was driven by differential settling (which implied sedimentation), but the number densities of the aggregates were assumed independent of the fluid depth. In other words the spatial variation in particles density has been overlooked. Some other studies considered the sedimentation of particles, but differential settling was not taken into account as the mechanism of aggregation [39]. Also, the

attachment probability α was in most cases assumed to be 100% (the so-called rapid aggregation scenario), which cannot be a general occurrence.

It is true that all features relevant to sedimentation (e.g. fractal dimension, etc.) have been the subject of various investigations, but they are treated only in a fragmentary way; there is, to date, no study that considers all the important issues simultaneously. Many early models assumed all aggregates to have fractal dimension $d_f = 3$, which is correct only for the coalescence of liquid drops [40]–[44]. Other studies, while acknowledging the fractal nature of the aggregates, had neglected to account for other properties affected by non-compact structures (e.g. settling velocity and the rate of collision) [45]. Other researchers later made all necessary modifications to their models for fractal aggregates [26], [46], but the mechanism of transport was limited to orthokinetics, not differential settling.

With regard to experimental measurement, it is practical to track only a very limited number of observables; some examples are "mud line" level [47],[48], turbidity [49],[50], mass concentration of solids at a fixed location [5], settling balance [51], and aggregation time [52]. In some studies [53], imaging techniques were used to investigate aggregation and sedimentation. We, however, can gain only limited knowledge of process kinetics by these experimental works.

In many studies (see Ref [45], [54], [55]), the collision efficiency and fractal dimension were estimated by fitting the experimental results to modeling results. It is often assumed that the collision efficiency is independent of the transport mechanism, so that it can be generalized to aggregation resulting from other transport mechanisms.

In most studies, a simple case of mono-size dispersion is assumed as the initial state of the particles; there are few papers in which a ploy-disperse size distribution is considered [54]; none

of these studies, however, deal with effect of all the important issues mentioned earlier; e.g. differential settling as the dominant mechanism of particle transport. A large body of literature is dedicated to the modeling (see Ref [56]). Among the three transport mechanisms mentioned earlier, fluid shear has been central to many studies[26], [41], [54]–[59], while differential settling, which is the most dominant mechanism when particles settle, was overlooked in research projects. Differential settling was taken into account as the main mechanism in some works [52], but again the sedimentation was not considered in the study.

Here in this study, we followed two approaches to investigate the aggregation and sedimentation systems while spatial variation of particles density is taken into account: 1) Experimental; and 2) modeling work. Brownian motion would be the dominant transport mechanism in aggregation of fine particles while differential settling becomes dominant for larger aggregates as they grow. The aggregates were treated as fractal objects. In following chapters, we will first describe the experimental procedure and then continue with explanation of our modeling scheme.

3 Experiments procedure

In this study, two sets of experiments were conducted by using two different methods: *ashing technique* and *settling balance*. The first method (i.e. ashing technique) was mainly used to investigate the aggregation and sedimentation of bitumen coated particles in several organic solvents. The second method, the settling balance, was used in our group for a wide range of different suspensions. The main objective of both experiments was to determine the settling rate. The settling rate of particles can be used as an indicator of kinetics of aggregation. Particles that aggregate faster make larger particles, so the rate of settling can be used to indicate how fast the fine particles can form aggregates.

A major advantage of these two methods is that they can be used for dark and opaque liquids (when the mud line is impossible to locate). The traditional method in which the interface between the top clear liquid and the cloudy suspension is recorded over time is only practical if the interface can be detected. The traditional method, which is based on optical detection of the sludge zone interface, was not applicable to dark liquids.

3.1 Ashing technique

In a non-aqueous process, an organic solvent is mixed with oil sands to dissolve the bitumen. Based on experience, we know it is possible to exploit the solvent property to maximize the elimination of solids. For reasons not yet fully understood, some solvents are known to facilitate the sedimentation of suspended fines. To evaluate this capability, a series of settling tests were conducted in organic solvent mixtures which include an aliphatic component (either paraffinic *n*-heptane or naphthenic cyclohexane) and an aromatic component (toluene). By changing the

volume fraction of toluene in the mixture, the aromatic content of the solvent was adjusted. It is known [60] that aromatic solvents have much higher asphaltene solubility. Hence, the interaction of the solvent with adsorbed asphaltenes on particle surfaces could be studied in our experiments.

Materials

Silica beads of diameter 0.25 μm (Fiber Optic Center, New Bedford, MA) were first surface-treated as follows: The beads as received were heated in an oven at 400ºC for 30 minutes to eliminate any possible surface contamination. They were then dispersed in toluene-diluted bitumen and stirred for 2 hours to allow adsorption of bitumen materials onto the silica surfaces. (Toluene-diluted bitumen was a 1:1 mixture, by weight, of toluene and an extra heavy crude oil known as bitumen; the latter was supplied by Syncrude Canada Ltd.) Next, the silica beads were washed multiple times (i.e. repeated centrifugation and decantation) in toluene until the supernatant was clear; this ensures that the only bitumen components that remain in suspension are those that are irreversibly adsorbed onto the bead surfaces. The solids were then recovered and dried. The resulting silica beads were rendered hydrophobic and mimicked the indigenous solids in oil sand ores [5].

The treated solids were dispersed in three different types of solvent: toluene, *n*-heptane and cyclohexane. These solvents were chosen to represent the three low molecular weight components in crude oil, namely, the aromatics, alkanes and cycloalkanes. All solvents were HPLC grade.

Experimental Procedures for Sedimentation Test

The following test was designed for quantifying sedimentation rates in the event that the suspending liquid is completely opaque (e.g. crude oil) [5]. Model solids (0.25-μm, surface-modified silica) at 2.0 wt% were suspended in a hydrocarbon (toluene, *n*-heptane or cyclohexane); they were agitated vigorously by sonication. At time $t = 0$, the agitation ceased and the particles were allowed to settle. A series of small samples, each of volume 0.5 mL, were drawn from a fixed location (1 cm from the free surface) at specific times. The silica was isolated from each sample (by vaporizing all organic matter in an oven) and its mass m was determined using a microbalance (Mettler Toledo, model MX5). A plot of m vs. t served as an empirical representation of the sedimentation process (see Figure 3.1). A minimum of three runs were made for each system.

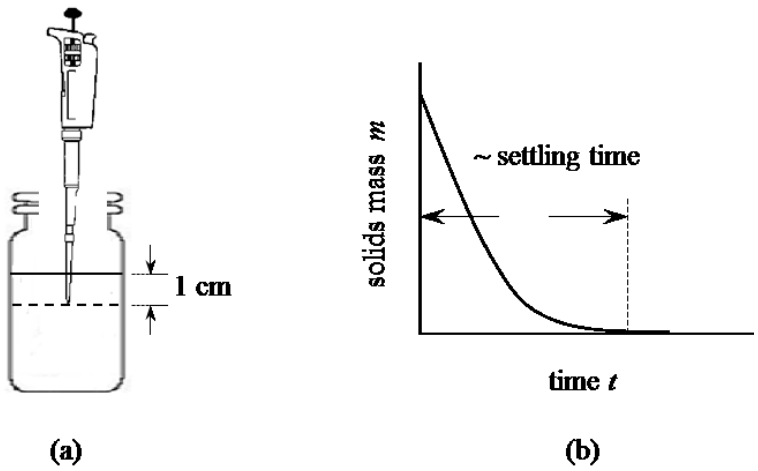

Figure 3.1. Schematic of the sedimentation test. A suspension of solids begins settling at time $t = 0$. (a) Small samples were drawn from a fixed location, and the mass of the solids, m, was determined; (b) typical — or expected — plot of m vs. t. The "settling time" as shown is not a precisely defined quantity.

3.2 Settling Balance

In this method, the settling rate of particles is measured by tracking the solids content at a fixed location over time using a sedimentation balance (KRÜSS K100). This device comprises of a tray that goes into the suspension at the time $t = 0$, and collects the falling solids overtime. The location of the tray remains constant at a distance below the liquid surface during the experiment. The tray is connected to a sensitive balance and a computer that records the weight of collected solids over time. The experimental setup is shown in Figure 3.2a.

A suspension of evenly dispersed particles in liquid (i.e. water, for example) was prepared by adding silica particles to the suspending liquid. The particles were 0.25, 0.5, and 1μm silica particles. This method was mainly used to investigate the effect of initial size distribution on the aggregation and settling in water, thus the particles were clean uncoated powders of just different sizes. Silica particles with a given size, or a mixture of different sizes, were used to make the suspension. The suspension was then agitated by sonication for about one minute. The sample is then put into the settling balance. The balance is equipped with a built-in magnetic stirrer that kept the suspension well-mixed and the particles dispersed before commencement of each test. In this study, the suspensions were stirred for two minutes. In case when the pH had to be lowered, a certain amount of hydrochloric acid was injected to the suspension just before the experiments began. The amount of hydrochloric acid was calculated according to the required pH. When the stirrer was switched off, the suspended particles begin to settle to the bottom. The particles were deposited on the tray, and the weight gain is recorded over time. The sedimentation rate can be determined by analysing the amount of mass that the tray receives. It can be used to gain knowledge about the kinetics of aggregation as the particles fall faster when they aggregate; in that case a larger amount of mass is collected in short time periods.

A typical plot of the solids mass vs. time is shown in Figure 3.2b. The time at which the stirrer is stopped and particles start falling was defined as the starting time (i.e. $t = 0$). The time that the mass on the probe reaches a constant value is taken as a measure of the solids settling time.

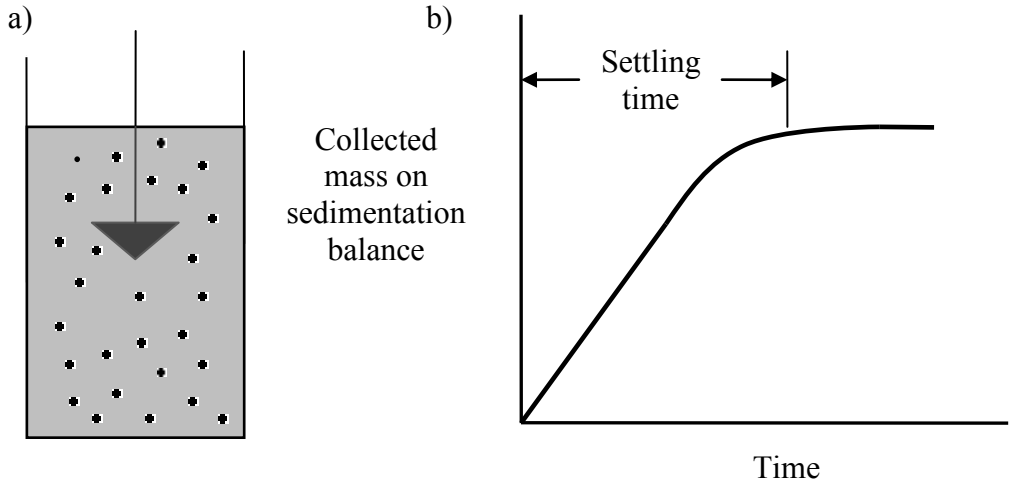

Figure 3.2. a) Sedimentation experimental set up; b) a typical plot of the solids mass m vs. time t in settling experiments.

4 Modeling

The aim of this section is to model the sedimentation of aggregating particles in a settling column. As such, the population of aggregates is a function of time and position. It is impossible to characterize *empirically* a sedimentation process to the level of details as one can do in a numerical simulation (i.e. population of all class size of aggregates as a function of time and position). Experimentally, it is practical to track only a very limited number of observables. However, to reconcile these few observables with the fundamental mechanisms of sedimentation, a "full blown" simulation of the sedimentation process appears inevitable. With regard to theoretical simulation: although by no means straightforward, it is in principle possible to predict the detailed evolution of a suspension. The results of such a calculation, which contain full information on a sedimentation process, can be summarized as follows:

$$n_k = n_k(z\,,t)\;;\;\; k = 1, 2, 3\,, \cdots \tag{4}$$

where n_k is the number density of aggregates containing k primary particles (also called the "k-aggregates"), z is the depth in the quiescent fluid (often measured from the free surface), and t is the time (with $t = 0$ marking the beginning of aggregation). After such a detailed calculation, one may then extract, from the massive amount of information embodied, the few observables that are accessible through experimentation. To date, there has been no theoretical or numerical study that provides the level of detail as expressed in Eq. (4).

In this study, we report a numerical procedure which we have developed for simulating the sedimentation of particles. The initial PSD of the particles can be arbitrary, and the simulation

allows for adjustable α, d_f, solid-liquid density difference and liquid viscosity. Particle transport in the liquid is by perikinetics and differential settling; orthokinetics (i.e. shear-driven collisions) is not included. We do not follow the trajectories of individual particles (as done in granular /particles dynamics); instead, the number concentrations of the k-aggregates, n_k, are treated as continuous functions of position and time. For simplicity, only gradients in the vertical direction are considered. The evolution of the aggregates is tracked using local population balance, while accounting for variations with position and time. The results of such calculations are summarized in the form of Eq. (4), from which empirical observables can be extracted. The simulation software is, however, only limited to suspensions of low solids concentrations. As such, the modelling of complex phenomena, such as hindered settling or sludge formation, is beyond our current capability.

4.1 Equations

4.1.1 Population balance: the Smoluchowski equation

Sedimentation is the *collective* behaviour of a large number of aggregating and settling particles. To predict sedimentation, the population balance of interacting particles and aggregates should be tracked over time. The population balance equation is well-established in the literature owing to Smoluchowski's work [40], which considered particle aggregation to be analogous to a series of chemical reactions. The Smoluchowski equation assumes that the aggregation is a second-order process in which the rate of collision/conversion between two species is proportional to the product of their number concentrations; the rate constant is denoted C_{ij}, where i and j are the sizes (i.e. numbers of constituent primary particles) of the two aggregates. For a suspension with aggregates of all sizes; the rate of change of n_k is given by the Smoluchowski equation

$$\frac{dn_k}{dt} = \frac{1}{2}\sum_{\substack{i+j=k \\ i=1}}^{i=k-1} C_{ij}\, n_i n_j - n_k \sum_{i=1}^{\infty} C_{ki} n_i \tag{5}$$

where the first term represents the combining of two smaller aggregates into a k-aggregate, and the second term accounts for the loss of k-aggregates as they join others to form larger structures; equation 5 assumes no breakage of aggregates. The rate constant C_{ij} is the product of the collision rate β_{ij} and the collision efficiency α, i.e.

$$C_{ij} = \alpha\, \beta_{ij} \tag{6}$$

In the context of our earlier discussion, β_{ij} is associated with the transport of the aggregates, while α is determined by close-range colloidal interactions. In this study, no shear is applied on the suspension; thus, collisions between particles result only from Brownian motion and differential settling.

Note that the Smoluchowski equation (Eq. 5) has no explicit dependence on spatial coordinates. As such, the equation may be applied in two ways: (a) globally, for a closed and well-mixed system in which the total mass is fixed, and the n_k's have no gradients; or (b) locally, as a "chemical reaction" equation, while allowing the n_k's to be functions of position and time. The latter situation, which is of course much more complex, is unfortunately also the case for sedimentation.

The size of aggregates

Consider an aggregate of k primary particles (i.e. a k-aggregate); the primary particles are assumed spherical with diameter d_0. The effective diameter of the k-aggregate, according to the characteristics of fractal structures, is given by

$$d_k = d_0 \cdot k^{1/d_f} \tag{7}$$

If the size of primary particles is assumed to be 1μm, for a fractal dimension of 1.5, 1000 primary particles are needed to build an aggregate with 100 μm diameter. It is worth noting that particles gradually adhere together to make such an aggregate, and smaller aggregates, each one composed of a number between 1 and 1000 particles, are formed in the intermediate stages. As a result, one would expect to see 1000 types of aggregates, which necessitate solving 1000 simultaneous differential equations. The number of equations needed is a function of the largest allowable aggregate size and the fractal dimension.

4.1.2 Settling velocity and collision kernels

In case of settling in a gravitational field, a particle rapidly reaches its terminal falling velocity as the gravitational force becomes equal to drag and buoyancy forces. Stokes Law expresses the settling velocity of a sphere of density ρ_p and diameter d as

$$v = \frac{(\rho_p - \rho) g d^2}{18\mu} \tag{8}$$

where g is the gravitational acceleration, and ρ and μ are the density and viscosity of the suspending medium. The porous nature of aggregates requires modifications of their hydrodynamic properties. The main parameter that should be modified is the Stokes settling velocity. For a k-aggregate with fractal dimension d_f, its settling velocity v_k is given by [52]

$$v_k = \frac{\Delta\rho g d_0^2}{18\mu} \left(\frac{d_k}{d_0}\right)^{d_f - 1} \tag{9}$$

(Note that in the special case of coalescing droplets, with $d_f = 3$, the above expression reduces to the familiar Stokes settling velocity for spheres.) The other property of importance is $\Delta\rho_k$, the effective density of a k-aggregate *in excess* of the fluid density; it is given by

$$\Delta\rho_k = \Delta\rho\,(1 - \varepsilon_k) \tag{10}$$

where $\Delta\rho$, as noted earlier, is the density difference between the solid and the fluid, and

$$\varepsilon_k = 1 - (D_k/D_0)^{d_f - 3} \tag{11}$$

is the porosity of a k-aggregate.

With the above modifications for fractal structures, the collision kernels for the two transport mechanisms (Eq. 1 and 3) become [61]

Perikinetics: $$\left(\beta_{ij}\right)_{\text{peri}} = \frac{2kT}{3\mu}\left(\frac{1}{i^{1/d_f}} + \frac{1}{j^{1/d_f}}\right)\left(i^{1/d_f} + j^{1/d_f}\right) \tag{1a}$$

Differential Settling: $$\left(\beta_{ij}\right)_{\text{ds}} = \frac{\pi}{72}\frac{\Delta\rho g}{\mu}\, d_0^{3-d_f}\left(d_i + d_j\right)^2\left(d_i^{d_f-1} - d_j^{d_f-1}\right) \tag{3a}$$

where d_i is the "diameter" of the k-aggregate, kT is the thermal energy, $\Delta\rho$ is the solid-fluid density difference, g is gravitational acceleration, and μ is the fluid viscosity. When both transport mechanisms are present, the total rate of collision (β_{ij} in Eq. 5) is just the sum of the two frequencies, i.e.

$$\beta_{ij} = \left(\beta_{ij}\right)_{\text{peri}} + \left(\beta_{ij}\right)_{\text{ds}} \tag{12}$$

4.1.3 Assumptions

1- In a concentrated suspension, the frictional force exerted at the particles may be increased because of flow pattern changes. Thus, the sedimentation rate of particles may be less

than the expected terminal velocity. In this study, the concentration of solid particles was assumed to be sufficiently low (i.e. dilute suspensions) to avoid hindered settling phenomena. (The volume fraction of solids was around 0.5%).

2- To avoid excessive computational complexity, we assumed all aggregates to have a common fractal dimension of 2. It is reported that aggregates created by differential sedimentation has fractal dimension in the range of 1.6 to 2.3 (see section 2.2.3). In this study, it was assumed that the fractal dimension d_f of all aggregates were equal.

3- The equations apply when the Reynolds number is very low ($Re < 0.5$). The Reynolds number for the primary particles in this study is quite less than one ($Re \ll 1$). It may be about 0.1 for the largest aggregates.

4- The aggregates were assumed to be fractal objects, but they were treated as spherical particles to estimate the drag forces.

5- It was also assumed, consistent with equation 5, that all aggregations were irreversible (i.e. no breakage of aggregates, as the hydrodynamic shear created by settling motion is minimal).

4.1.4 General smoluchowski equation with spatial variation

Through his 1916 and 1917 papers, Smoluchowski had laid a timeless foundation for the study of aggregation kinetics ([40],[62]). We present here a small extension to Smoluchowski's work as we attempt to account for spatial variations in particle densities. Aggregated structures do not, in general, distribute themselves evenly in space. Similar equations had been proposed in the past which included gradient terms ([9], [46], [55], [63]), but they were tailored for either macromolecular structures (50 nm or smaller) or applications involving vigorous (i.e. turbulent) mixing; there was also no treatment of non-uniform particle distributions in those studies. Here,

we apply the convection-diffusion equation of aggregation (based on population balance) to four simple situations; particular attention will be given to the inhomogeneous distributions of particles.

Aggregation kinetics with density and velocity gradients

Consider a suspension of aggregates in a fluid. The size of each aggregate is specified by the number of primary particles within it. Thus, a "k-aggregate" is one with k primary particles; its diffusivity is denoted D_k. We assume all primary particles to be of the same size. Let n_k be the number density of the k-aggregates (units of m^{-3}), and $\mathbf{v}_k$ be the macroscopic velocity of such entities. In general, both n_k and $\mathbf{v}_k$ are functions of position $\mathbf{r}$ and time t, i.e.

$$n_k = n_k(\mathbf{r}, t)\,; \quad \mathbf{v}_k = \mathbf{v}_k(\mathbf{r}, t)$$

It should be noted that $\mathbf{v}_k$, the macroscopic velocity of the k-aggregates, can in general be different from $\mathbf{v}_{\text{fluid}}$, the local fluid velocity [64].

Population balance: The convection-diffusion equation

As defined earlier, n_k is the number density of the k-aggregates, and $\mathbf{v}_k$ the macroscopic velocity of the same entities. Both n_k and $\mathbf{v}_k$ can be functions of position $\mathbf{r}$ and time t, i.e. $n_k = n_k(\mathbf{r}, t)$ and $\mathbf{v}_k = \mathbf{v}_k(\mathbf{r}, t)$. If the aggregates are sufficiently small, they will be susceptible to thermal agitations; the resulting diffusivity of the k-aggregates is denoted D_k. In general, the transport of aggregates can be by convection and/or diffusion; the associated fluxes of the k-aggregates are, respectively, $n_k\mathbf{v}_k$ and $-D_k\,\boldsymbol{\nabla} n_k$. We also define $\dot{n}_k$ to be the rate at

which k-aggregates are created per unit volume. Expressions for $\dot{n}_k$ are given by Smoluchowski (Eq. 5).

Consider now an arbitrary control volume (i.e. one with stationary boundaries) in space. The number of k-aggregates within the control volume changes with time according to

$$\frac{\partial}{\partial t}\int n_k \, \mathrm{d}V = -\oint (n_k \mathbf{v}_k - D_k \, \boldsymbol{\nabla} n_k) \cdot \hat{\mathbf{e}} \, \mathrm{d}S + \int \dot{n}_k \, \mathrm{d}V \tag{13}$$

where $\hat{\mathbf{e}}$ is the unit outward normal. Converting the surface integral to volume integral, and noting that the control volume is arbitrary, we arrive at Eq. (14), the convection-diffusion equation of aggregation (assuming constant D_k):

$$\frac{\partial n_k}{\partial t} + \boldsymbol{\nabla} \cdot (n_k \mathbf{v}_k) = D_k \, \nabla^2 n_k + \dot{n}_k \tag{14}$$

The ratio of convective to diffusive contributions (i.e. $|\boldsymbol{\nabla} \cdot (n_k \mathbf{v}_k)|/|D_k \nabla^2 n_k|$) is the Péclet number (Pe). In the high Pe limit, Eq. (14) simplifies to

$$\frac{\partial n_k}{\partial t} + \boldsymbol{\nabla} \cdot (n_k \mathbf{v}_k) = \dot{n}_k \quad (\mathrm{Pe} \gg 1) \tag{14a}$$

The term $\dot{n}_k$ in Eq. (14) or (14a) represents the rate of production of k-aggregates. Following Smoluchowski [40], [62], we write

$$\dot{n}_k = \frac{1}{2}\sum_{i=1}^{k-1} C_{i,k-i} \, n_i \, n_{k-i} - \sum_{i=1}^{N-k} C_{k,i} \, n_k \, n_i \; ; \quad k = 2, 3, \cdots, N-1 \tag{15}$$

where $C_{i,j}$ is the rate constant for the i- and j-aggregates, and N is the maximum aggregate size. For $k = 1$ and N (the smallest and largest aggregates), we have

$$\dot{n}_1 = -\sum_{i=1}^{N-1} C_{1,i}\, n_1\, n_i \quad \text{and} \quad \dot{n}_N = \frac{1}{2}\sum_{i=1}^{N-1} C_{i,N-i} n_i\, n_{N-i} \tag{16}$$

In addition, the total number of primary particles (i.e. mass of all aggregates/mass of one primary particle) is given by

$$N_{\text{tot}} = \int \sum_{k=1}^{N} k n_k \, \mathrm{d}V \tag{17}$$

Clearly, by mass conservation, N_{tot} must be invariant with time. This condition is in fact already built into the Smoluchowski equations and need not be imposed separately. A proof of this mass conservation property is given as follows.

Mass balance

N_{tot} is the total number of constituent particles in a control volume; it is given by Eq. (17). From Eqs. (13) and (17), it follows that

$$\frac{\partial N_{\text{tot}}}{\partial t} = -\oint \sum_{k=1}^{N} k[(n_k \mathbf{v}_k - D_k \boldsymbol{\nabla} n_k) \cdot \hat{\mathbf{e}}] \, \mathrm{d}S + \int \sum_{k=1}^{N} k \dot{n}_k \, \mathrm{d}V \tag{18}$$

The principle of mass balance can now be stated as follows: Any change in N_{tot} within the control volume must be due to mass fluxes through its boundaries, i.e.

$$\frac{\partial N_{\text{tot}}}{\partial t} = -\oint \sum_{k=1}^{N} k[(n_k \mathbf{v}_k - D_k \boldsymbol{\nabla} n_k) \cdot \hat{\mathbf{e}}] \, \mathrm{d}S \tag{19}$$

Comparing this equation with (18), the requirement of mass balance reduces to

$$\int \sum_{k=1}^{N} k\dot{n}_k \, \mathrm{d}V = 0 \tag{20}$$

As the control volume is arbitrary, the integrand must itself vanish. We have therefore the following final equation of mass balance:

$$\sum_{k=1}^{N} k\dot{n}_k = 0 \tag{21}$$

where $\dot{n}_k$ are the Smoluchowski expressions given by Eqs. (15) and (16).

Proof of the mass balance equation

For simplicity, and without loss of generality for the proof, we ignore all rate constants (i.e. by setting $C_{ij} = 1$). The Smoluchowski expressions (Eqs. 15 and 16) thus become

$$\dot{n}_k = \frac{1}{2} \sum_{i=1}^{k-1} n_i \, n_{k-i} - \sum_{i=1}^{N-k} n_k \, n_i \;\; ; \quad \text{for } k = 2, 3, \cdots, N-1 \tag{22}$$

and

$$\dot{n}_1 = -\sum_{i=1}^{N-1} n_1 \, n_i \;\; ; \quad \dot{n}_N = \frac{1}{2} \sum_{i=1}^{N-1} n_i \, n_{N-i} \tag{23}$$

Eq. (21) can be proved by induction as follows: We begin with a "base case," with $N = N_0$, in which Eq. (21) can be verified directly. The easiest case would be for $N_0 = 2$. Now suppose the value N_0 is increased by 1; Eq. (21) must still hold, i.e. we must have

$$\sum_{k=1}^{N_0} k \, \dot{n}_k = \sum_{k=1}^{N_0+1} k \, \dot{n}_k = 0$$

Next, let Δ to be the algebraic difference between the two sums, i.e.

$$\Delta \equiv \sum_{k=1}^{N_0+1} k\,\dot{n}_k \; - \sum_{k=1}^{N_0} k\,\dot{n}_k$$

Clearly, for Eq. (21) to be satisfied, Δ must vanish identically. From the Smoluchowski expressions, it is easy to show that

$$\Delta = \; -\sum_{k=1}^{N_0} k\,n_k\,n_{N_0+1-k} \; + \frac{1}{2}(N_0+1)\sum_{i=1}^{N_0} n_i\,n_{N_0+1-i}$$

Writing i as k in the second sum, we get

$$\Delta = \; \sum_{k=1}^{N_0}\left(\frac{N_0+1}{2} - k\right) n_k\,n_{N_0+1-k} \tag{24}$$

To demonstrate that $\Delta = 0$, we substitute the index $N_0 + 1 - k$ with the new variable l:

$l = N_0 + 1 - k$; or $k = N_0 + 1 - l$

In terms of l, Eq. (24) becomes

$$\Delta = \; -\sum_{l=1}^{N_0}\left(\frac{N_0+1}{2} - l\right) n_l\,n_{N_0+1-l} \tag{25}$$

Comparing Eqs. (24) and (25), it is clear that Δ must be zero. This in turn means that Eq. (21), the mass conservation equation, is identically satisfied with the Smoluchowski expressions.

Applications of the General Equation of Aggregation

The main difficulty with Eq. (14) is determination of the aggregate velocity field $\mathbf{v}_k(\mathbf{r},t)$; in many situations (particularly when particle inertial effects are significant), one may need to resort to numerical means. Here, we examine four simple cases in which such a difficulty can be avoided. Rather than obtaining full solutions to Eq. (14), we will focus only on aspects related to the spatial variations of n_k. In the first three cases, we assume small and neutrally buoyant particles in the low Stokes number regime. Also, it is assumed that there are initially only primary particles that are distributed uniformly in space, i.e.

$$\left.\begin{array}{l} \Delta\rho = 0 \quad \text{and} \quad \mathbf{v}_k = \mathbf{v}_{\text{fluid}} \equiv \mathbf{v} \\ \\ n_1(\mathbf{r},0) = n_0 = \text{constant}\,; \quad n_k(\mathbf{r},0) = 0 \ \text{ for } \ k \geq 2 \end{array}\right\} \text{ Cases 1, 2 and 3}$$

where $\Delta\rho$ is the density difference between the dispersed and continuous phases.

Case 1: Perikinetic aggregation in quiescent fluid

Here, $\mathbf{v} = 0$ and there are no gradients in n_k; the conduction-diffusion equation (Eq. 14) reduces to $\partial n_k/\partial t = \dot{n}_k$. Also, the "collision kernels" $C_{i,j}$ have no spatial dependence. Since the initial particle distribution is uniform, the n_k's will remain also uniform as they evolve over time. Solutions to this problem were first discussed by Smoluchowski (1917) and subsequently by many others ([9], [12], [62]).

The remaining cases (Cases 2, 3 and 4) are in the high Péclet number regime for which Eq. (14a) applies.

Case 2: Orthokinetic aggregation in simple shear flow

In Cartesian coordinates, simple shear is characterized by

$$v_x = Gy\,; \quad v_y = v_z = 0$$

where G is the shear rate (a constant). This flow field is created, for example, by relative lateral motion between parallel plates. For infinite plates, there are no gradients of any quantity in the lateral directions; in particular, we have $\partial n_k/\partial x = 0$. As such, the term $\nabla \cdot (n_k \mathbf{v}_k)$ in Eq. (14a) vanishes identically. Just as in Case 1, the collision kernels $C_{i,j}$ contain no spatial dependencies; this leads again to a situation in which the n_k's remain uniform in space as their values evolve over time.

At the initial stage of aggregation, we can make the usual (and rather crude) "nearly monodisperse" approximation: that all aggregates have roughly the same size as the primary particles. This leads to an exponentially decaying $\sum n_k$ — the total number of aggregates (of any value k) per unit volume [12]. Specifically, we have

$$\sum n_k/n_0 = \exp(-t/\tau_G) \tag{26}$$

The time constant τ_G in Eq. (26) is

$$\tau_G = \frac{\pi}{4\Phi} \cdot \frac{1}{G} \tag{27}$$

where Φ is the volume fraction of the dispersed phase. The aggregate number density $\sum n_k$ can be detected, for example, through turbidity measurement [65]. Thus, for Case 2, one expects the suspension turbidity to decrease exponentially, with a characteristic time τ_G, while remaining spatially uniform throughout.

Cases 1 and 2 were first discussed by Smoluchowski (1917), with the implicit (and of course correct) assumption that the aggregates are uniformly distributed in space. In what follows, we will examine situations in which the n_k's are non-uniform.

Case 3: Orthokinetic aggregation in Poiseuille flow

Here, we have laminar flow in a tube of inner radius R and infinite length. The velocity field is expressed in cylindrical coordinates as

$$v_r = v_\theta = 0\,; \quad v_z = v_0\,[1 - (r/R)^2]$$

For an infinitely long tube, we have $\partial n_k/\partial z = 0$. Thus, the term $\boldsymbol{\nabla} \cdot (n_k \mathbf{v}_k)$ in Eq. (14a) again vanishes. However, unlike in the previous cases, the collision rates $C_{i,j}$ have here spatial dependencies. In particular, the shear rate, given by $G = |\partial v_z/\partial r|$, is now a linear function of the radius r:

$$G = \frac{2v_0}{R^2}\, r \tag{28}$$

Substituting Eq. (28) into Eq. (27), we see that for orthokinetic aggregation in Poiseuille flow, the turbidity would exhibit radial variations as time progresses. In particular, the turbidity near the axis remains relatively constant, while that near the tube wall will show the fastest decrease with time. This effect will be especially apparent in its 2-D projection, i.e. if the aggregation process were observed in a direction perpendicular to the cylinder axis.

Case 4: Sedimentation in a quiescent fluid

In this case, the density difference $\Delta\rho$ must clearly not vanish. With regard to the velocity $\mathbf{v}_k$, its only non-zero component will be in the downward ($+z$) direction; it is denoted v_k. For

simplicity, we assume Stokes flow for even the largest coalesced droplets. Thus, for a fluid of viscosity μ and primary particles of diameter d_0, we have

$$v_k = \frac{\Delta\rho g}{18\mu}\left(d_0\, k^{1/3}\right)^2. \tag{29}$$

This velocity has evidently no dependence on spatial coordinates. Assuming $\mathrm{Pe} \gg 1$, the equation of aggregation (Eq. 14a) becomes

$$\frac{\partial n_k}{\partial t} = -v_k \frac{\partial n_k}{\partial z} + \dot{n}_k \tag{30}$$

It is shown in later that the Péclet number for sedimentation depends very strongly on the particle size, i.e. $\mathrm{Pe} \sim d^4$. As such, the crossover condition, at which $\mathrm{Pe} \approx 1$, can practically be the demarcation between the $\mathrm{Pe} \ll 1$ and $\mathrm{Pe} \gg 1$ regimes.

Estimating the Péclet Number

The Péclet number is the ratio of convective to diffusive rates of transport. It is commonly expressed as

$$\mathrm{Pe} = UL/D \tag{31}$$

where U and L are, respectively, the characteristic velocity and characteristic length, and D is the diffusivity of the dispersed particles. For spheres of radius a undergoing Brownian motion, D is given by the Einstein-Stokes relation:

$$D = \frac{kT}{6\pi\mu a} \tag{32}$$

We now examine the Péclet number in two scenarios.

Particles in shear flow at low Stokes number

There are two length scales in this situation, namely, a for the particles and L for the flow field. Smaller particle size means higher diffusivity; for $a \sim 10$ nm, we have $D \sim 10^{-10}$ m^2/s (using viscosity of liquid water). This leads to the relation

$$\mathrm{Pe} \sim 10^{10}\, UL \quad (\mathrm{SI\ units})$$

Thus, in most "normal" situations, we have $\mathrm{Pe} \gg 1$ and Eq. (14a) can be applied. However, this will no longer be the case when the physical dimensions are reduced. For example, when 10-nm colloidal particles are transported in microchannels, with $L \sim 10\ \mu\mathrm{m}$ and $U \sim 10\ \mu\mathrm{m/s}$, the Péclet number is not $\gg 1$, and the full convection-diffusion equation must be solved.

Sedimentation of particles in quiescent liquid

Here, the characteristic length is the particle size, i.e. $L \sim a$; the characteristic velocity is the Stokes settling velocity given by $U \sim \Delta\rho g a^2/\mu$. Putting these into (31) and (32), we have

$$\mathrm{Pe} \sim \frac{\Delta\rho g}{kT} \cdot a^4 \tag{33}$$

Let us now consider the "crossover" condition for which $\mathrm{Pe} \sim 1$: assuming $\Delta\rho \sim 10^3$ kg/m^3 (e.g. silica beads in water), the crossover particle size is about 1 μm. Because of the strong dependence of Pe on a, particles that are smaller or larger than the crossover size will quickly enter the $\mathrm{Pe} \ll 1$ or $\mathrm{Pe} \gg 1$ regime.

4.2 Numerical scheme for handling temporal and spatial variation

The equations described above can be used to model the sedimentation of settling particles in a column. The number densities of particles (as well as the aggregates that are created by aggregation) are functions of position and time. This means that at any instant, the number densities of particles varies over depth of a column, for example. To implement the modeling, we followed two separate procedures: 1) Conducting population balance at each time step for all positions by applying the Rosenbrock technique (discussed below), followed by relocation of aggregates due to settling; and 2) providing a numerical solution for general Smoluchowski equation. In both cases, the numerical scheme would require that time and position be discretized.

4.2.1 Rosenbrock method

With adhesion between particles, a suspension of primary solids will very quickly acquire aggregates of all sizes. The time rate of change of n_k (number density of k-aggregates) is given by Eqn. (5); the index k in the equation ranges from 1 to N, where N is the size of the largest aggregate. As such, Eqn. (5) represents a set of N differential equations which must be integrated simultaneously over time; this is already a non-trivial task. The complexity of the problem is *greatly* exacerbated when, in the general case, the n_k's are functions also of position. In such a situation, Eqn. 5 captures only the *local* kinetics of aggregation — which we will here call the Smoluchowski kinetics. In addition to Smoluchowski kinetics, spatial variations in n_k must also be tracked based on mass conservation.

We non-dimensionalize all variables with the following basis parameters: d_0, v_0 and n_0. The first two parameters are, respectively, the size and Stokes settling velocity of a single primary

particle; n_0 is the imaginary number concentration in the situation when all particles exist as singlets ($k = 1$) and are evenly distributed in space. The dimensionless form of the Smoluchowski equation is

$$\frac{dn_k^*}{dt^*} = \frac{1}{2}\sum_{i=1}^{i=k-1} C^*{}_{i,k-1}\, n_i^* n_{k-i}^* - n_k^* \sum_{i=1}^{N-k} C^*{}_{k,i} n_i^* \tag{34}$$

where

$$n_k^* \equiv \frac{n_k}{n_0}\ ; \quad v_k^* \equiv \frac{v_k}{v_0}\ ; \quad t^* \equiv \frac{t v_0}{d_0}\ ; \quad z^* \equiv \frac{z}{d_0}\ . \tag{35}$$

The collision kernel for differential settling is non-dimensionalized as follows:

$$C_{i,j}^* \equiv C_{i,j} \cdot \frac{n_0\, d_0}{v_0} \tag{36}$$

Discretization

The problem is treated numerically as follows:

Sedimentation clearly creates non-uniform particle distributions, but we are at least fortunate that there is only one spatial coordinate this is of relevance, namely, the fluid depth. As such, the functions n_k have two independent variables: the vertical position z and the time t (see Eq 4). There is no hope of solving such a problem analytically [66], [67]. In this study, we will simulate the sedimentation process by discretizing both space and time.

Since this is a one-dimensional problem, we need only focus on a vertical fluid column of unit cross section. We envision this fluid column to be divided into thin horizontal layers — or "bins" — each of the *same* thickness Δz. As such, the continuous variable z is coarse-grained

into an integer i_z which is the bin number (we let i_z increase in the downward direction). To customize to our numerical scheme, the number density function $n_k(z,t)$ is rewritten as

$$n_k(z,t) \rightarrow n(k,i_z)|_t \ ,$$

where $n(k,i_z)$ is a two-dimensional array with the index k denoting the aggregate size and i_z specifying the bin number (i.e. the depth). Entries of this 2-D array are the corresponding aggregate densities at time t. These aggregate densities are updated as time progresses. As sedimentation is not history-dependent, there is no need to archive past entries of $n(k,i_z)$.

As mentioned earlier, we divide time also into a series of short durations Δt. However, unlike discretization of space, the series of time steps can be non-uniform (this will be further discussed below). At every time step, the following two operations are performed:

- Over a short time interval Δt, each bin is treated as a closed system (i.e. borders between adjacent bins are "sealed"). Within each bin, the aggregates are assumed to be uniformly distributed, thus allowing Smoluchowski kinetics to apply. At the end of each time interval, the number densities are updated based on a simple Euler formula, i.e.

$$n(k,i_z)|_{t+\Delta t} = n(k,i_z)|_t + \frac{\mathrm{d}n_k}{\mathrm{d}t} \cdot \Delta t \qquad (37)$$

  where the "conversion rates" $\mathrm{d}n_k/\mathrm{d}t$ are calculated from Eq. (5) using local aggregate densities. This updating is carried out for all aggregate sizes and in every bin (i.e. for all values of k and i_z).

- Before proceeding to the next time step (and after *all* bins are updated according to Eq. 37), aggregates are relocated to lower bins if their settling velocities are sufficiently high; the new location of an aggregate depends on its travel distance over the time interval Δt.

Specifically, the travel distance of a k-aggregate is $\delta_k = v_k \Delta t$, where v_k is given by Eq. (9). This travel distance leads to a downward migration of the k-aggregate by j bins, where j is an integer (which can be 0, 1, 2 …) satisfying the relation

$$j \Delta z < \delta_k < (j+1) \Delta z .$$

This relocation scheme is clearly approximate; its accuracy improves as $\Delta z \to 0$. In our simulation, relocation of the k-aggregates is done by adjusting their number densities in the two bins (current bin and the j^{th} bin below). To be clear, let us suppose the current bin number is i_z and that $j \geq 1$ for the k-aggregates; in such a case, the following two steps are carried out (in the context of a computer code):

$$n(k, i_z + j) = n(k, i_z + j) + n(k, i_z) ;$$

$$n(k, i_z) = 0 .$$

If $j = 0$ (i.e. no downward migration), the above steps are bypassed. Two practical points should be noted here: (a) aggregate relocation must begin from the bottom and proceed upward; (b) the lowest bin should be treated as a "sink" for all aggregates.

We now comment on the time step Δt: The modelling of sedimentation is inherently a "stiff" problem in that some aggregate densities in the Smoluchowski equation (Eq. (5)) vary much more rapidly than others; for this reason, a sufficiently small Δt must be used in Eq. (37) to maintain a numerically stable and accurate solution. To use the same Δt for the entire sedimentation process would be unwise as the time interval could, for a given error tolerance, be considerably lengthened at certain stages of the simulation. In this study, a modified Runge-Kutta algorithm, called the Rosenbrock method, was used. With this approach, the time step is not fixed. An automatic step size adjustment is applied to regulate the time step Δt according to

the local truncation error at each iterative step. Details of the Rosenbrock method can be found in Ref [68]. A brief discussion of how this adaptive algorithm was applied to the present problem is given in Apendix A.

4.2.2 General Smoluchowski equation

There is no hope of any analytical solution to Eq. (30). Here, we will solve the equation numerically by evaluating spatial gradients ($\partial n_k/\partial z$ in Eq. 30) using backward difference approximation, and marching forward in time with a simple Euler approach. Details of this numerical scheme are outlined below.

We first non-dimensionalize all variables with the following basis parameters: d_0, v_0 and n_0. The first two parameters are, respectively, the diameter and Stokes settling velocity of a primary particle; the third is $n_0 = N_{\text{tot}}/V$, where N_{tot} is given by Eq. (17) and V is the volume of the domain. Note that n_0 and d_0 are not dimensionally independent; this will be addressed below. The dimensionless form of Eq. (30) is

$$\frac{\partial n_k^*}{\partial t^*} = -v_k^* \frac{\partial n_k^*}{\partial z^*} + \dot{n}_k^* \tag{38}$$

where

$$n_k^* \equiv \frac{n_k}{n_0}\ ;\quad \dot{n}_k^* \equiv \frac{d_0}{n_0 v_0}\dot{n}_k\ ;\quad v_k^* \equiv \frac{v_k}{v_0}\ ;\quad t^* \equiv \frac{t v_0}{d_0}\ ;\quad z^* \equiv \frac{z}{d_0}\,. \tag{39}$$

The collision kernel for differential settling is likewise non-dimensionalized as follows:

$$C_{i,j}^* \equiv C_{i,j} \cdot \frac{n_0\, d_0}{v_0}\,. \tag{40}$$

Substituting Eq. (3) into (40), and recognizing that $v_0 = \Delta\rho g d_0^2/18\mu$, we obtain

$$C_{i,j}^{*} = \frac{\pi}{4}\left(d_i^{*} + d_j^{*}\right)^2 \left|(d_i^{*})^2 - \left(d_j^{*}\right)^2\right| \cdot (n_0 {d_0}^3) \qquad (41)$$

where $d_i^{*} \equiv d_i/d_0$. With the above scaling, the only required input parameter is $n_0 d_0^3$. In our simulation, we have chosen plausible values of d_0 and n_0.

Eq. (38) is integrated numerically using finite difference (specifically, backward difference) approximation for spatial derivatives, and simple Euler formula to advance in time.

4.2.3 Computer code in FORTRAN

FORTRAN is one of the oldest programming languages which is still popular in the field of high performance computing. It is often referred to as a scientific language as it is suitable to model a wide range of applications in scientific and engineering problems. Despite the ease of coding in FORTRAN, the programs run almost as efficiently as those written in machine language.

Due to these facts, we have used FORTRAN to implement our numerical model. The source code is described in Appendix B. The FORTRAN code then was compiled and executed by submitting batch jobs on WestGrid[1] to take advantage of parallel programming and fulfill the large memory requirement. WestGrid is a facility which provides high performance computing mainly in Western Canada.

4.2.4 Parallel programming

As will be shown later, the program is quite time consuming. Even for a small system consisting of not many sizes of aggregates, it takes several days to run the model. It is because all types of aggregates interact with one another and one needs therefore to keep track of the number

[1] https://www.westgrid.ca

densities of all aggregate sizes — at every time step and at all positions. Single processors, even the fastest ones, provide only limited computational power; the problem can be solved much faster by using multiple processors. A major advantage of parallel programming is that we can extend the model to a larger number of aggregate sizes.

The numerical code should be developed in a parallelized way so that the work is distributed across multiple processors. Some code modifications or reformulation of algorithms would be necessary to enhance parallelization. This introduces additional programming complexity to computer codes, but it will bring along significant time-saving advantages. There are several techniques to develop parallel programs [69],[70].

Here, we used OpenMP to run the source codes in parallel. OpenMP is a shared-memory programming technique to run a computer code on a number of processors. It uses a set of 'compiler directives' to facilitate parallelism in the source code. The computer code should be developed such that computational work is decomposed across multiple processors. More details on parallel processing are available in the book by Chandra et al [71]. Here in this study, by using six processors working in parallel, the speed was improved 33%.

5 Simplified cases and model validation

5.1 A dimensionless settling curve

The equations as described earlier were solved numerically using both Rosenbrock method and general PDE form (see previous sections for the details). In this section, for the sake of obtaining preliminary results, we assume, entirely arbitrarily, that the maximum aggregate size is 100 (i.e. the largest drops are from the coalescence of 100 primary droplets). We also neglect all other "complexities" of aggregation; these include: collision efficiency (i.e. we assume rapid coagulation), fractal nature of aggregates (i.e. we consider only droplet coalescence), and aggregate breakup; these aspects will be taken into account in later sections.

The equations were scaled so the required input parameters are d_0 and n_0. The parameters d_0 and n_0 are the size and the number density of primary particles, respectively; the third parameter is defined as $n_0 = N_{\text{tot}}/V$, where N_{tot} is the total number of primary particles. Here, we have chosen the values of $d_0 = 5\,\mu m$ and $n_0 = 5 \times 10^{16}\,m^{-3}$ (number density equal to 2 wt% of silica particles suspended in an organic solvent). Regarding the initial and boundary conditions: we had specified an initial mixture of 90 wt% singlets (i.e. individual primary particles) and 10 wt% doublets — both uniformly distributed in space at time $t = 0$. We envision the domain to be a vertical settling column. The boundary conditions are zero mass flux at the top and bottom of the column. The fractal dimension is set to 3. The settling column is 5 cm in height; it is discretized into 500 segments, each with therefore a thickness of $\Delta z = 100\,\mu m$. For the PDE

solution, the dimensionless time step $\Delta t^* = 0.0002$ is chosen small enough that the solution remains stable. The Rosenbrock method uses a varying time step.

The settling curves obtained using both simulations (i.e. Rosenbrock and PDE solution) will be presented next. The experiment to be modelled was the settling balance (see Figure 3.2), in which the cumulative amount of mass collected on a tray was determined as a function of time. Here, the tray was located at a depth of 5 cm from the free surface.

5.1.1 Rosenbrock method

First, mass conservation was checked upon completion of the modeling. The total mass of particles is shown in Figure 5.1. Since the mass should be conserved in the settling column, the total mass plotted versus time is a straight line. Total mass has been determined by calculating total number of primary particles, N_{tot}, as below

$$N_{\text{tot}} = \int \sum_{k=1}^{N} k n_k \, dV \tag{17}$$

where k is the size of each aggregate which is the number of primary particles within it, and N is the maximum aggregate size. n_k is the number density of the k-aggregate. The total mass, m_{tot}, is

$$m_{\text{tot}} = N_{\text{tot}} \times \text{mass of one primary particle} \tag{42}$$

Here, in Figure 5.1 $m_{\text{tot}}/m_{\text{tot},0}$ was plotted, where $m_{\text{tot},0}$ is the total mass at time $t = 0$.

The settling curve obtained from the Rosenbrock simulation is shown in Figure 5.2. All quantities are expressed in their non-dimensional forms (see earlier sections for definitions). Total number density of primary particles, φ , is determined from

$$\varphi = \sum_{k=1}^{N} k n_k \tag{43}$$

Figure 5.2 shows the cumulative amount of mass collected at a tray 5 cm deep over time. Note that the amount of mass has been divided by total mass at $t = 0$ (i.e. $m_{\mathrm{tot},0}$), and then plotted versus time.

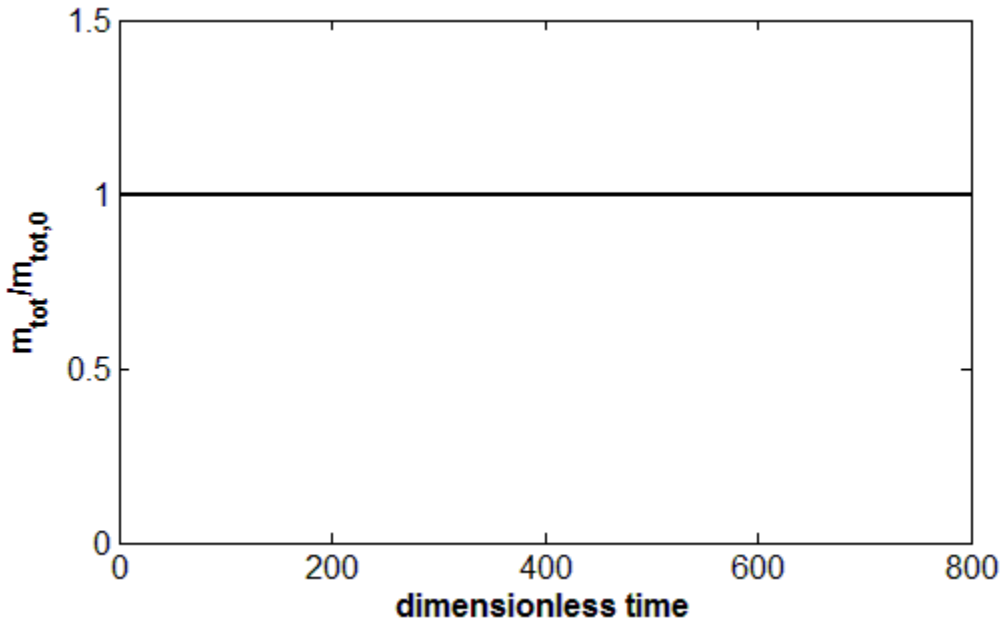

Figure 5.1. Conservation of mass; $m_{\mathrm{tot}}/m_{\mathrm{tot},0}$ was plotted where $m_{\mathrm{tot},0}$ is the total mass at time $t = 0$. The graph was obtained by using the results from Rosenbrock method.

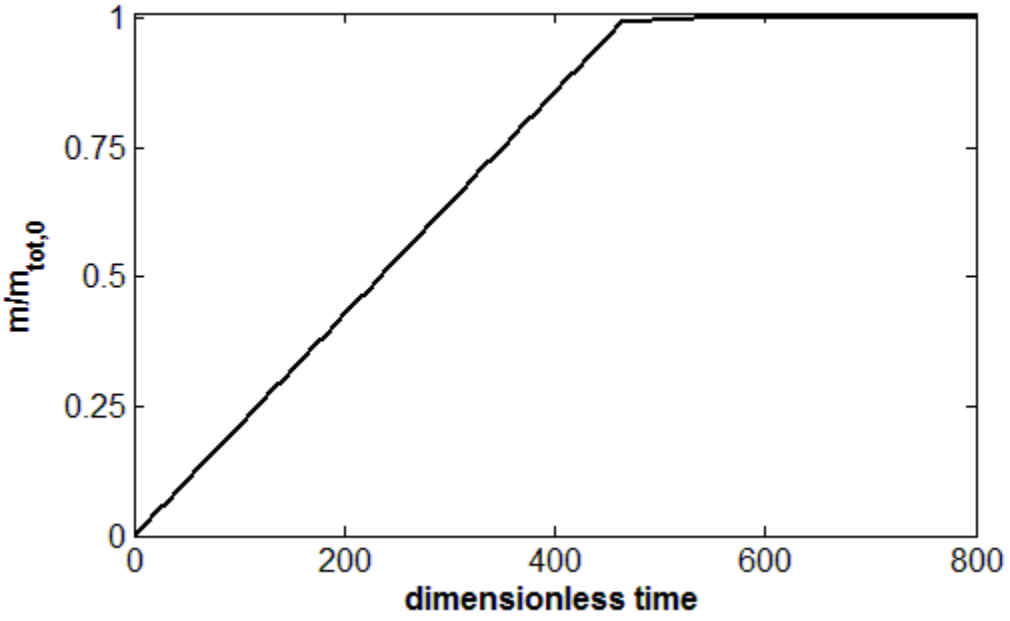

Figure 5.2. The cumulative mass collected at a plate 5 cm deep. The amount of mass was divided by total mass at $t = 0$, and then plotted versus time. The graph was obtained by using the results from Rosenbrock method.

Mesh size dependency

The number of spatial and time steps depends on how fine the grids were selected during discretization. As check, the simulations are repeated with both and reduced to half their values to ensure that the results are reproducible. Figure 5.3 shows the settling curves when $\Delta z = 50$ μm. The original plot was shown for comparison. There is good agreement between two curves, illustrating that the results are independent of the size of vertical segments (i.e. bin sizes used in spatial discretization) in the settling column.

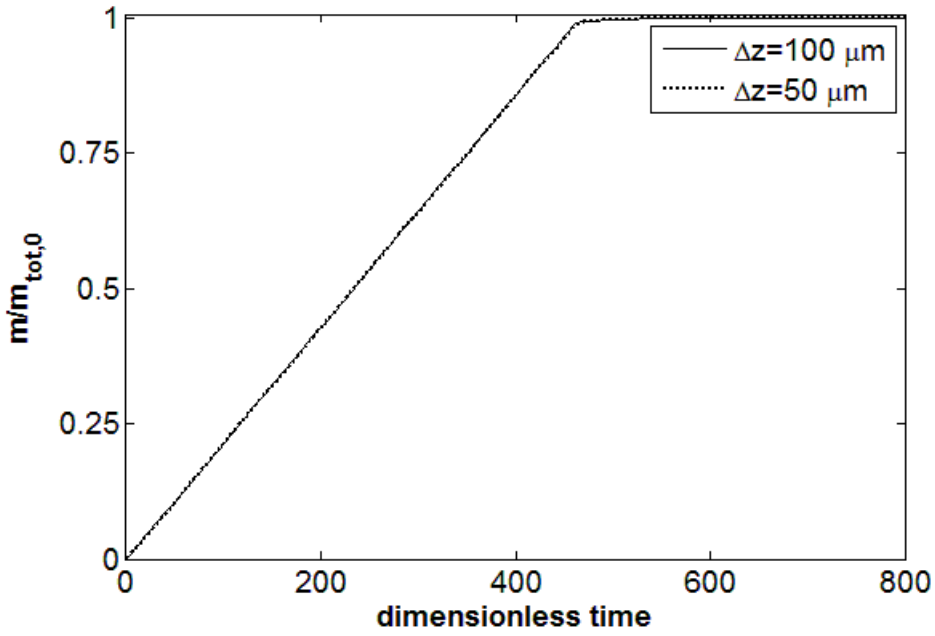

Figure 5.3. The cumulative mass collected at a plate 5 cm deep when step size is reduced to half ($\Delta z = 50\ \mu m$) compared to the result obtained by step size $\Delta z = 100\ \mu m$.

If the step size is twice as large, (i.e. $\Delta z = 200$ μm), we will still obtain the same results; see Figure 5.4. This shows that the mesh size was small enough that we can save on time by using the larger step size.

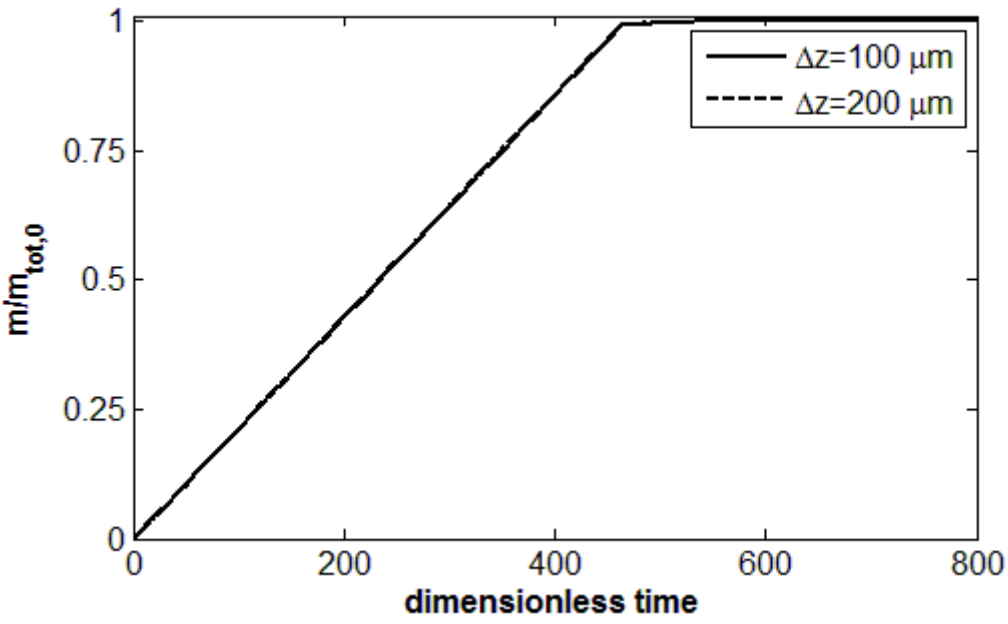

Figure 5.4. The cumulative mass collected at a plate 5 cm deep when step size is twice larger ($\Delta z = 200\ \mu m$) compared to the result obtained by step size $\Delta z = 100\ \mu m$.

5.1.2 General Smoluchowski equation

There is no hope of any analytical solution to Eq. (30). Therefore, it was integrated numerically using finite difference (specifically, backward difference) approximation for spatial derivatives, and simple Euler formula to advance in time. Details of this numerical scheme were outlined in Section 4.2.2. Figure 5.5 shows the total mass of particles in order to check for mass conservation. The total mass has been determined by the same approach used for the results obtained from Rosenbrock method (see Eq. 42).

The settling curve is also plotted in Figure 5.6. All the quantities are determined in the same way as that used for the Rosenbrock method (see the section above for details). The only difference is that the raw data were obtained by solution of Eq. (30).

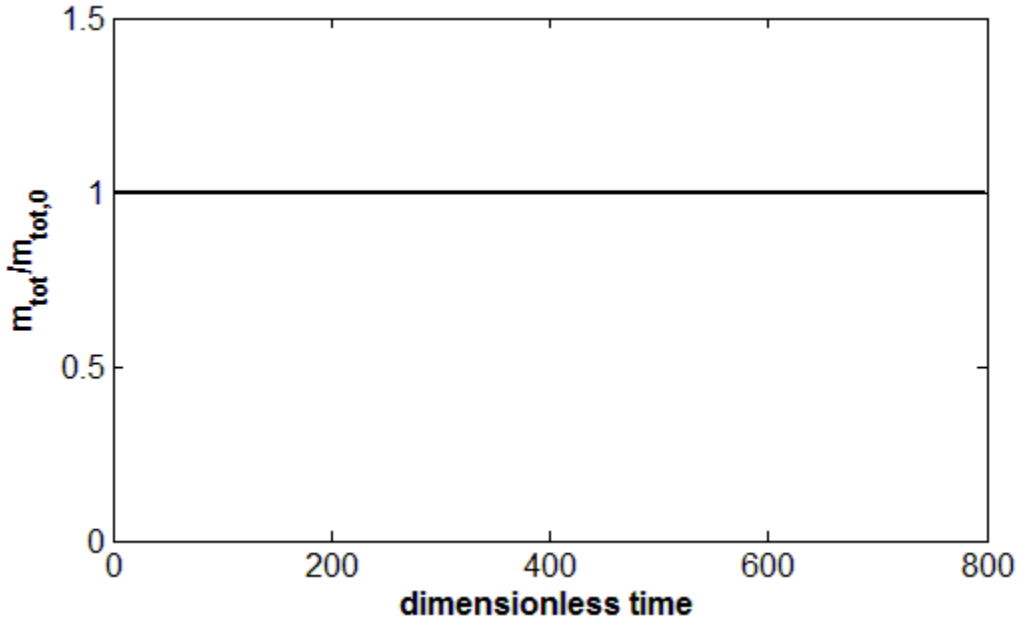

Figure 5.5. Conservation of mass; the graph was obtained by integrating Eq. (30).

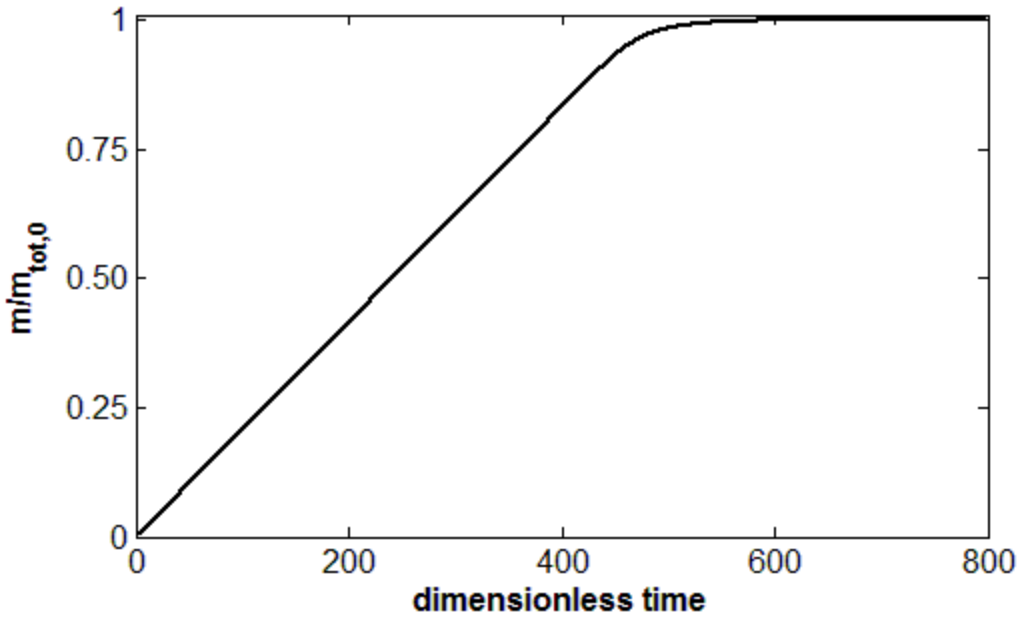

Figure 5.6. The cumulative mass collected at a plate 5 cm deep. The amount of mass was divided by total mass at $t = 0$, and then plotted versus time. The graph was obtained by using the results from integrating Eq. (30).

Mesh size dependency

In order to show that the results are independent of step sizes, the simulations are repeated with both and reduced to half their values to ensure that the results are reproducible. Figure 5.7 and 5.8 show the settling curves when Δz and Δt are reduced to half, respectively.

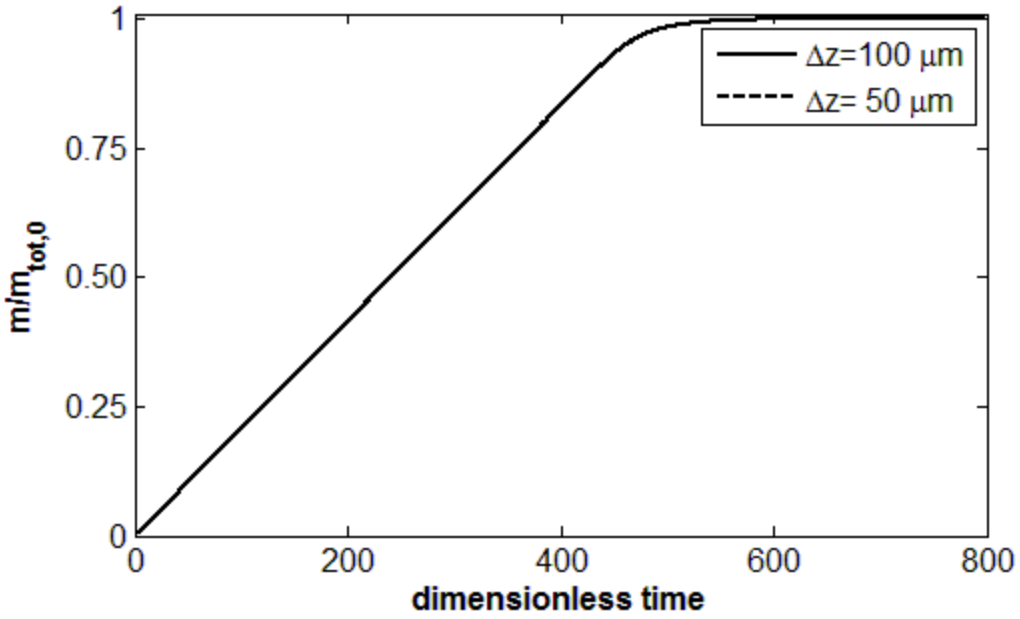

Figure 5.7. The cumulative mass collected at a plate 5 cm deep when Δz is reduced to half compared to the result obtained by step size $\Delta z = 100$ μm . The results were obtained by integrating Eq.(30).

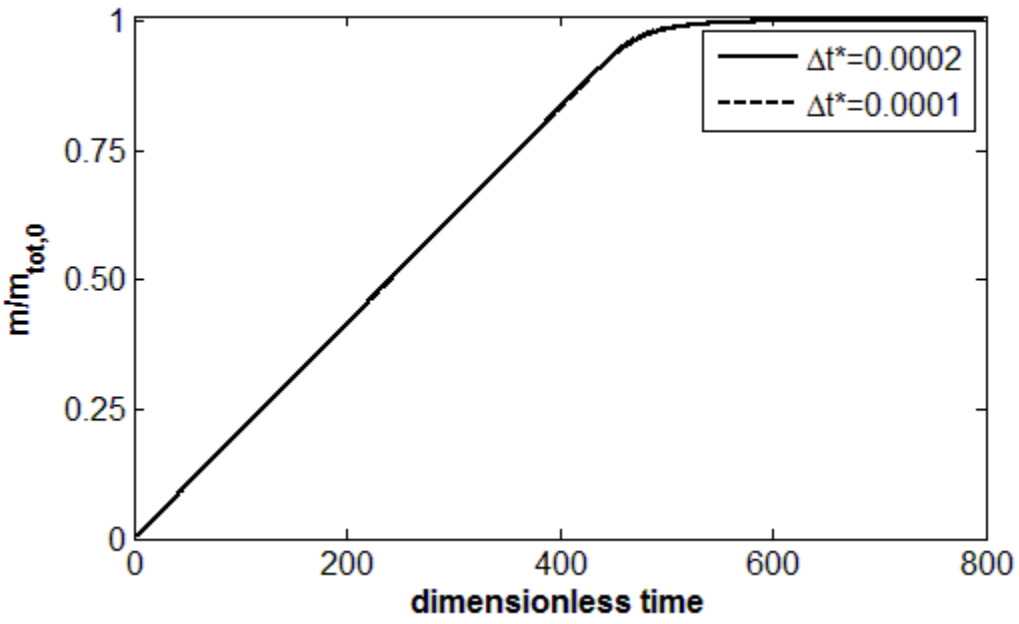

Figure 5.8. The cumulative mass collected at a plate 5 cm deep when dimensionless time step, Δt^* , is reduced to half. The results were obtained by integrating Eq. (30).

5.1.3 Comparison of results of two methods

In order to compare the results obtained from two above-mentioned methods, the settling curves are plotted in one graph (Figure 5.9). As seen, there is no significant discrepancy between the two curves. This is good way to test the accuracy of the methods, as we dealt with the problem by using two different approaches, and we achieved the same results.

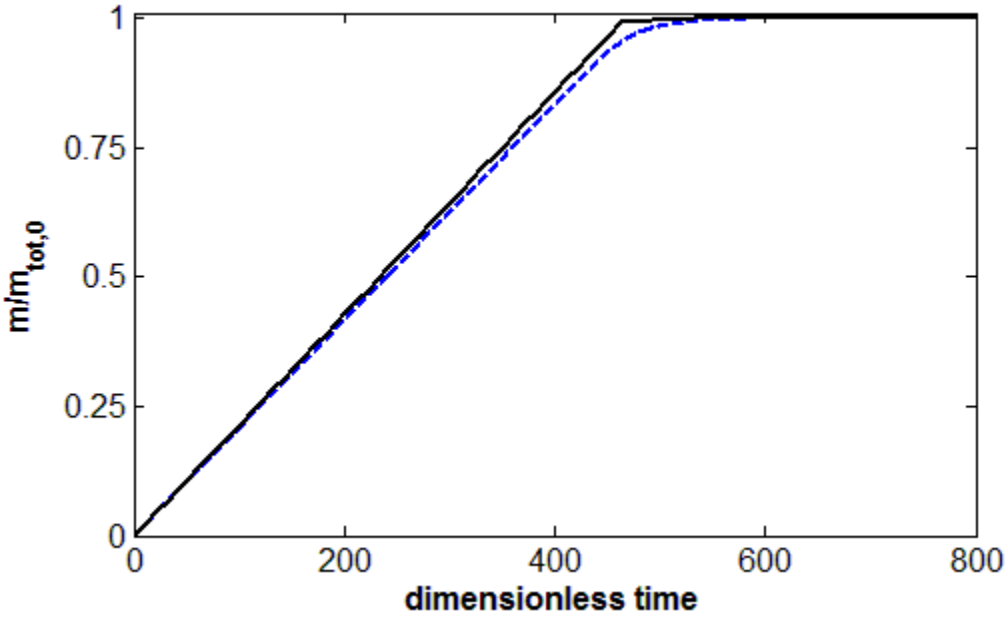

Figure 5.9. The cumulative mass collected at a plate 5 cm deep. Solid line is result of Rosenbrock, and dashed-line is the result obtained from integrating Eq. (30).

5.2 Maximum allowable size of aggregates, *N*

At time $t = 0$, the fluid contains only primary particles that could be in a range of sizes according to the initial PSD, but all are in the form of singlets. However, soon after beginning of aggregation, single particles attach to each other to make larger species, e.g. doublets, triplets, etc. The size of the aggregates grows by adhering to other primary particles and previously created aggregates over time. Consequently, theses particulates settle under the force of gravity. The larger the aggregates, the faster will settling occur. The process continues until all the solids are settled and make a solid layer at the bottom of the vessel. Particles can grow to a certain size depending on the depth of the column and the particle settling velocities.

Let $d_{\max}$ be the largest aggregate that can be produced in a settling column for a given depth. Accordingly we can find the number of primary particles within it as we know each aggregate

consists of only primary particles; this number is called the "maximum allowable number of primary particles," which is denoted by N. It is the number of primary particles within the aggregate with the maximum allowable size, $d_{\max}$. Figure 5.10 shows that the settling curve (i.e. collected mass against time) depends upon N. If the aggregates are able to grow larger, they will settle faster. However, beyond a certain value of N, the aggregates do not have enough time to grow more as they reach the bottom of the vessel. Of course, for an infinite depth and time, the aggregates can grow until all the particles become united to make only one large aggregate. It is worth noting that it is assumed that no breakage takes place, and aggregation is irreversible. The preliminary results were only obtained by assuming $N = 100$. Here, we implemented our model to examine the effect of N.

Suppose that the collecting tray was placed at a depth of 15 mm in a suspension. The suspension consisted of 1 μm silica particles (with density of 2.65 g/cm^3) in *n*-heptane. The mass concentration of particles was 5 wt%, and the collision efficiency was assumed to be 1. Figure 5.10 shows the settling curves (i.e. the amount of mass collected at the tray over time) for several values of N in the range of 100 and 2400. The rate of sedimentation increases by increasing N; however, there is a certain value beyond that the settling rate does not improved by increasing N. It is then assumed to reach the 'saturation' condition.

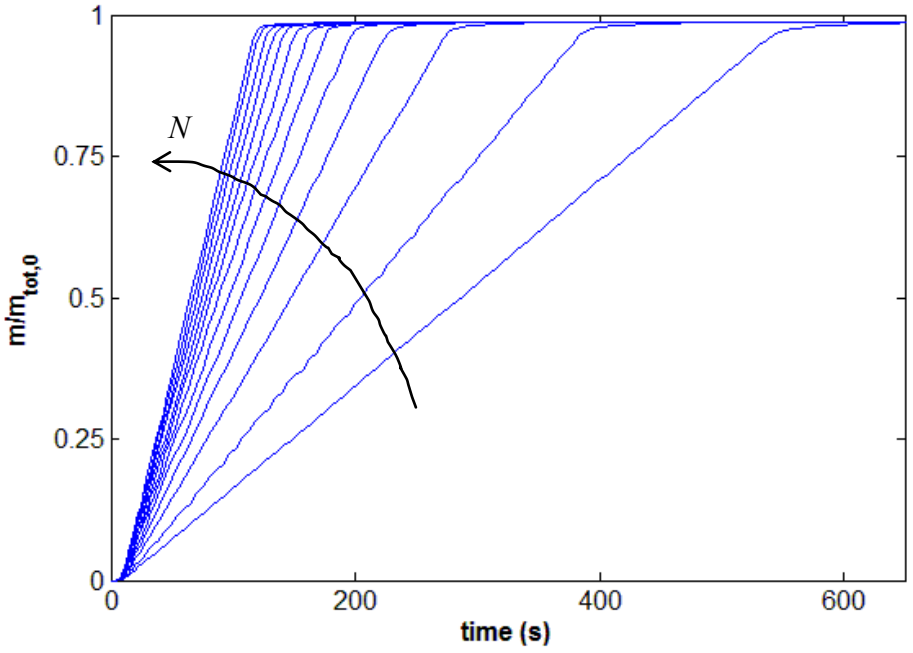

Figure 5.10. The cumulative mass collected at a plate 1.5 cm deep in a suspension which is made of 1μm silica particles in pure heptane. The situation of rapid aggregation was assumed.

In the case of fast aggregation, particles quickly join the others to reach that maximum size, and then travel downward until they get to the bottom of the vessel. In contrast, slow aggregation takes more time for the particles to reach the maximum size so that most of the aggregates reach the bottom without having the chance to reach the maximum size.

By increasing the maximum allowable size for the aggregates, N, the CPU time increases exponentially as it requires a larger number of equations to be solved at each time step. In addition, the set of equations becomes stiffer so that smaller time steps are required to keep the solution stable. Figure 5.11 shows the turn-around time versus N for the above-mentioned system (i.e. 1 μm silica particles at 5wt% concentration in heptane). As shown in the picture,

for small N, it takes only minutes to obtain the results, but the simulation takes longer by increasing N, such that it requires to run the program for weeks for $N > 3000$.

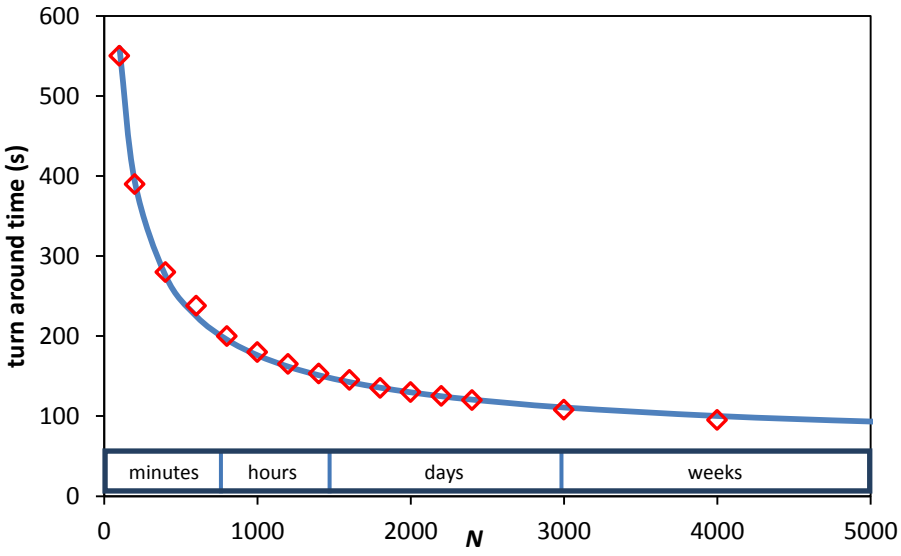

Figure 5.11. The amount of time required to get the results for different values N

5.3 Scaling procedure to calculate the settling behavior

To run the model, a value of N should be assumed; therefore particles can grow only to a certain size. Accordingly, the results are then obtained based on this assumption. The settling curves, however, can be plotted for any value of N by scaling the one that was obtained for a given value of N. The scaling procedure is discussed as follows: First the mass-weighted average size of particles in the entire vessel is calculated as below

$$k_{\mathrm{m,avg}=} \frac{\int k^2 n_k dV}{\int k n_k \, dV} \tag{44}$$

$$d_{\mathrm{avg}} = d_0 \left(k_{\mathrm{avg}}\right)^{\frac{1}{d_f}} \tag{45}$$

In above equation, k_{avg} is the number of primary particles within the aggregate with the average size of d_{avg}; n_k is the number density of k-aggregates (i.e. an aggregate containing k primary particles).

The settling velocity of such an aggregate can then be calculated. The settling velocity for a fractal objects is

$$v_k = \frac{(\rho_p - \rho)\mathrm{g}d_0^2}{18\mu}\left(\frac{d_k}{d_0}\right)^{d_f-1} \tag{9}$$

For a different value of N, the average size and in turn the average settling velocity would be different. However, one may obtain one curve from another by scaling using the ratio of settling velocities of average size of aggregates. The ratio of average settling velocity of aggregates, r_v, is determined as follows. The subscripts 1 and 2 indicate the two simulation cases in which two different values of N were chosen. The ratio of average settling velocity is given by

$$r_v = \frac{v_2}{v_1} = \left(\frac{d_{\text{avg},2}}{d_{\text{avg},1}}\right)^{d_f-1} \tag{46}$$

Or, in terms of k_{avg},

$$r_v = \left(\frac{k_{\text{avg},2}}{k_{\text{avg},1}}\right)^{\frac{d_f-1}{d_f}} \tag{47}$$

By scaling the time axis in one of the settling curves using this ratio, we see an approximately 'universal' trend. Figure 5.12a shows the settling curves for N=200, 500, 800, and 1000. The suspension consisted of 1-μm silica particles in *n*-heptane. The mass concentration of particles was 5 wt%, and the collision efficiency was assumed to be 1. The collecting tray was assumed

to be placed at a depth of 15 mm from free surface. Figure 5.12b shows the scaled settling curves by using the procedure described above. It illustrates that the settling curve for N=1000 can be roughly approximated by other settling curves obtained for smaller N.

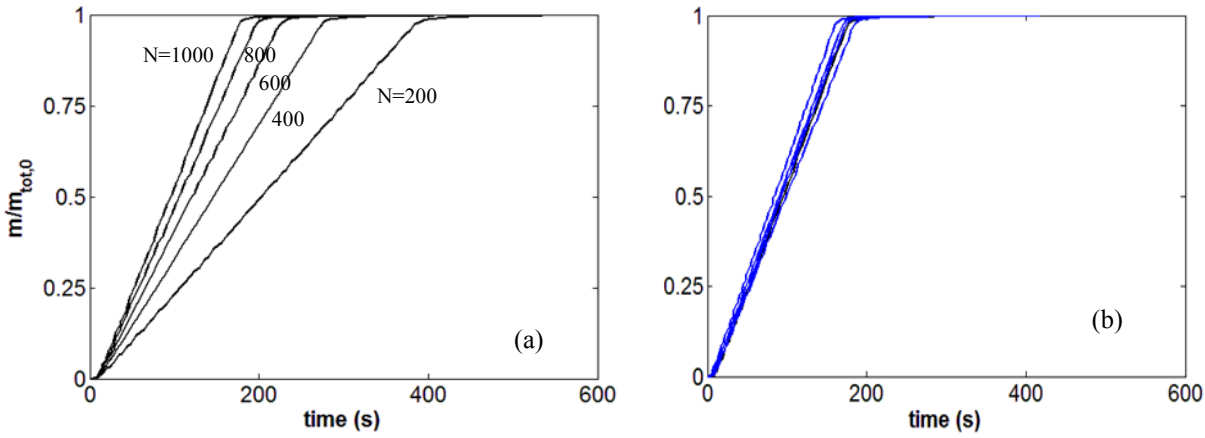

Figure 5.12. a) normal and b) scaled settling curves for N=200, 500, 800, and 1000. The test includes of a suspension of 1 μm silica particles in n-heptane. The collecting tray was assumed to be at 15 mm deep.

5.4 Validation of the numerical model

It is always desirable to have the results of a computer simulation study verified and validated. Although the results of a simulation can only be approximations of the real system, the goal is to produce accurate representation of the system. Simulation results are usually compared to some actual system behavior (e.g. simple experiments that can easily be done in the lab) or previous simulation results that have been already tested and validated. The accuracy should be also examined by mesh refinement to show that the results are independent of mesh size.

In this section, our simulation results are compared to three situations: Cases (1) and (2) are actual experiments involving sedimentation of 1-μm silica particles in two different liquids, and

Case (3) is a theoretical scenario that is well-known in the literature: the universal 'self-preserving' PSD (particle size distribution) involving perikinetic collisions only.

5.4.1 Validation1: Sedimentation of treated silica particles in diluted maltene

A series of settling tests have been conducted using the sedimentation balance in our lab by my colleagues. It is known that bitumen-treated silica particles will adhere strongly to one another in an aliphatic organic liquid, in this case, *n*-heptane with dissolved maltene (i.e. the portion of crude oil that is soluble in *n*-haptane).

The methods and procedures have been discussed earlier. The solid particles were 1-micron bitumen treated silica particles, and the suspending liquid was diluted maltene. The liquid phase was prepared by mixing 5 wt% maltene with *n*-heptane. The solid particles were added at 5 wt% to the suspending liquid. The experiment was repeated three times using the sedimentation balance. The settling curves are shown in Figure 5.13.

The case of diluted maltene with pure heptane was recognized as the rapid coagulation so that we can reasonably assume that the collision efficiency, α, is equal to unity. The turn-around time (i.e. time at which the collected mass on the tray reachs its maximum) was approximately 55 seconds.

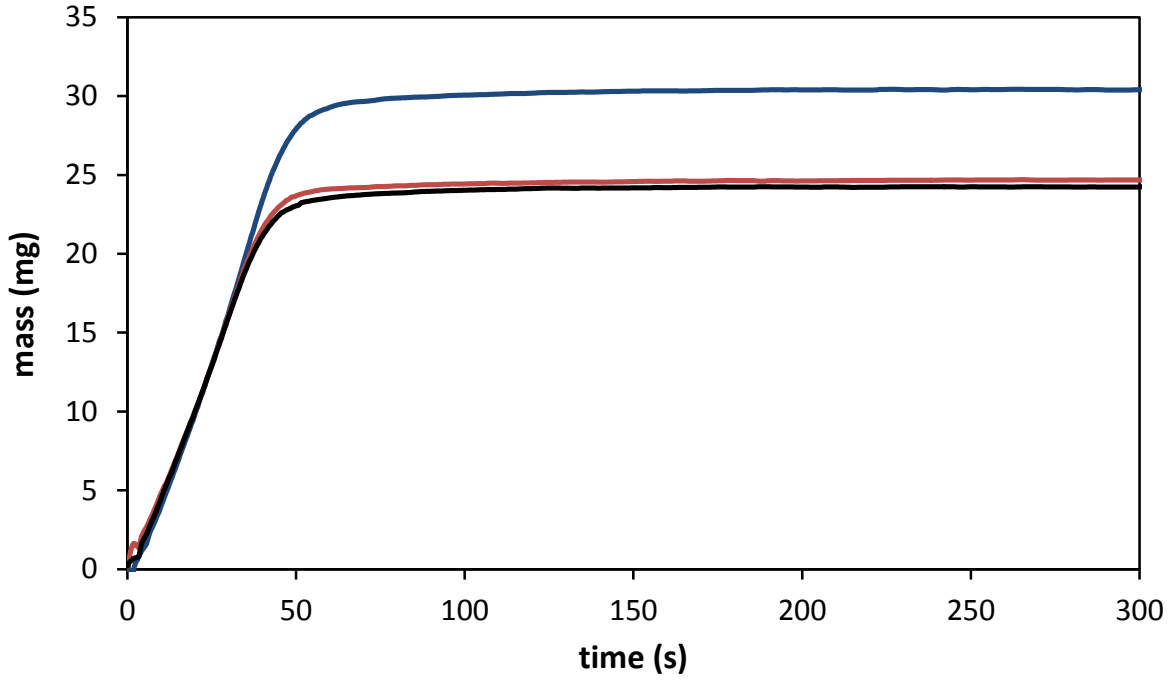

Figure 5.13. The settling curve for bitumen coated silica particles in 5% diluted maltene; collecting tray was located at depth of 15mm

The simulation model was implemented for the same situation and the results are shown in Figure 5.14 as the maximum aggregate size N varies. As the value of *N* increases, the settling time decreases until a certain time after which it does not reduce by increasing N. However, as mentioned earlier, running the simulation for arbitrarily large value of N is impossible using current computing resources; therefore an extrapolation analysis is inevitable. The sedimentation times are plotted versus N in Figure 5.15. The data points were fitted to the equation in the form of below:

$$t = a\, e^{-\left(\frac{N}{b}\right)^{d}} + c \tag{48}$$

where t is the settling time. The parameters a, b, c and d are constants; c indicates the settling time as N is infinitely large. In this case, c was equal to 56. Therefore, the settling time would be 56 seconds from simulation, which is in very good agreement with experimental result (i.e. 55 seconds).

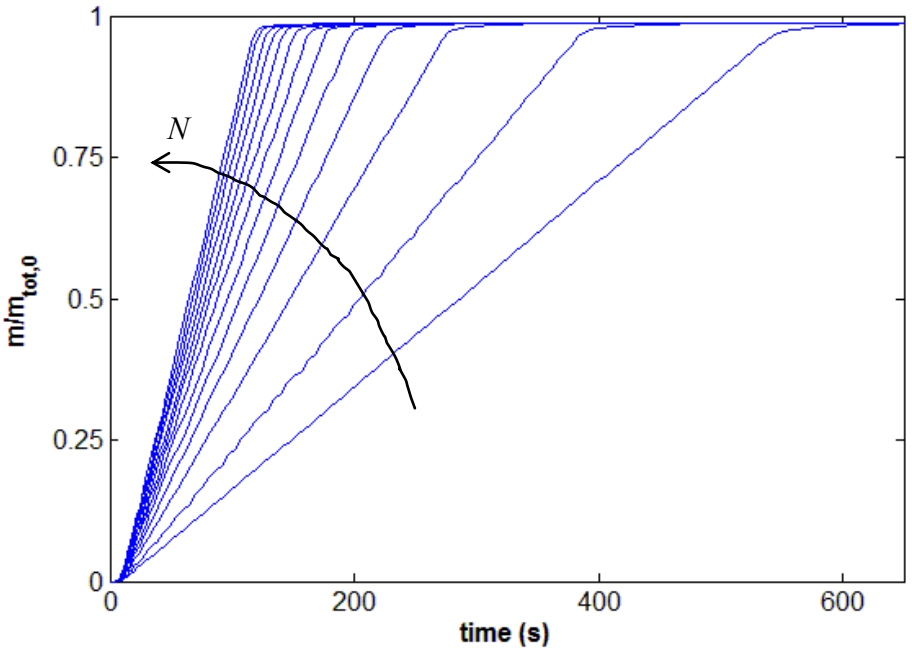

Figure 5.14. The cumulative mass collected at a plate 1.5 cm deep in a suspension which is made of 1μm silica particles in pure heptane. The situation of rapid aggregation ($\alpha = 1$) was assumed.

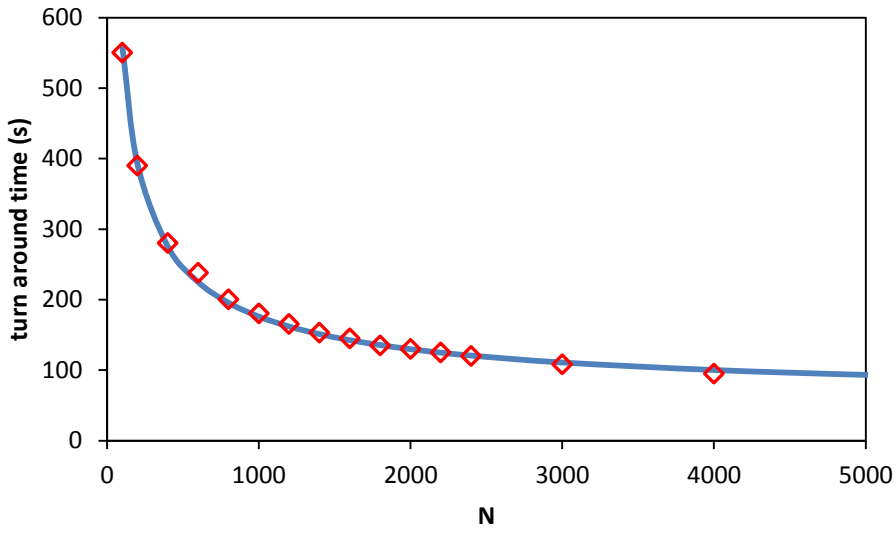

Figure 5.15. Turn-around time versus N (largest allowable number of primary particles in an aggregate) for treated silica particles in diluted maltene; the fitted coefficients are: a =3.921E5, b=2.099E-8, c=56.99, d=0.08508 ($R^2 = 0.9982$).

5.4.2 Validation 2: Sedimentation test of silica particles in water at pH=2

Another sedimentation experiment was conducted, this time concerning the behavior of 1μm silica particles in water. The mass concentration of silica particles was 5% by weight, and the collecting tray was again located at 15 mm depth. If the pH is neutral, the 1-micron particles may take several hours to settle (in accordance with the Stokes velocity of individual spheres) as the particles do not aggregate at pH=7. At this pH, silica particles carry a net negative surface charge; the resulting double layer repulsion prevents any particle-particle adhesion. However, as the pH is lowered to around 2, the pzc (point of zero charge) is reached, and the silica particles readily aggregate due to van der Waals attraction [51]. Such a situation is most likely one of rapid coagulation, with the collision efficiency α being 100%. Figure 5.16 illustrates the settling behavior at pH=2 for 1-micron particles in deionized water. The settling time is about 180 seconds.

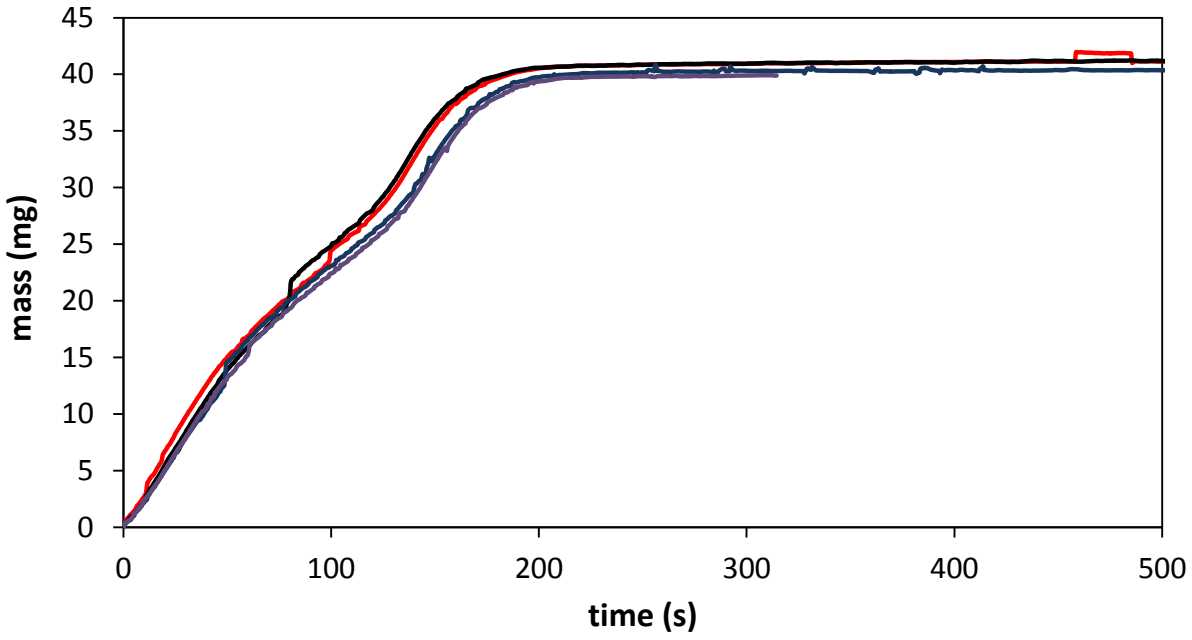

Figure 5.16. Settling curves of 1μm untreated silica particles at 5 wt% concentration in water with pH=2. The sampling tray was at a depth of 15mm.

For the same situation, the settling curve was obtained from simulation model at different values of N (shown in Figure 5.17). Just as in the previous case, in order to find the actual settling time, the turn-around times at various N values are plotted in Figure 5.18, and then fitted to Eq. (48). The coefficient c was obtained equal to 173. Therefore the settling time would be 173 seconds based on numerical simulation. This is once again in good agreement with experiment result (i.e. 180 seconds). Table 5.1 shows a comparison between the numerical results and experimental data for both cases discussed above.

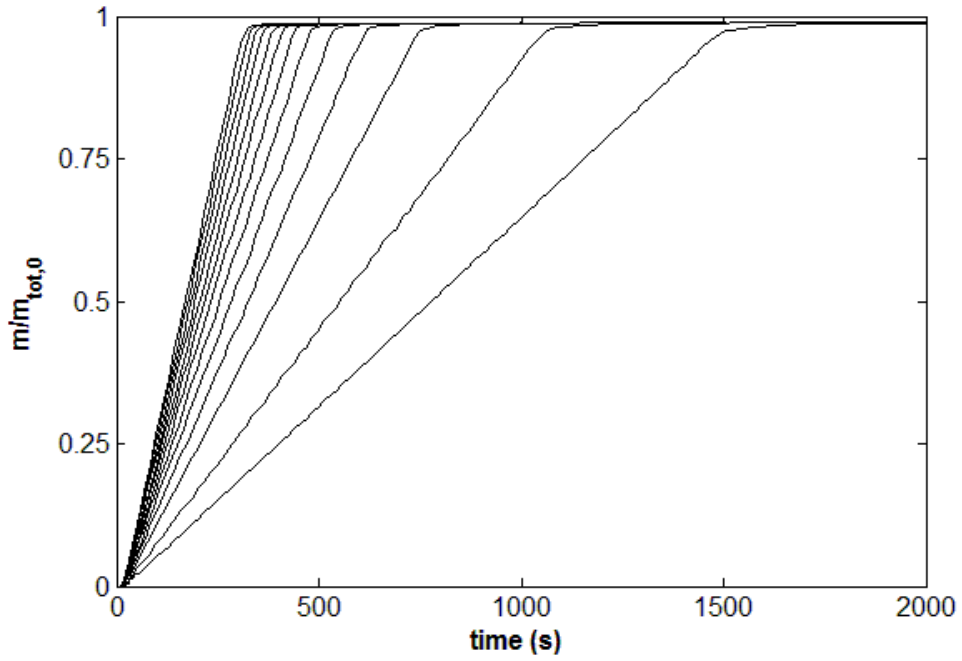

Figure 5.17. The cumulative mass collected by a plate at a depth of 15 mm. The suspension consisted of 1µm silica particles in water of pH 2. Rapid aggregation ($\alpha = 1$) was assumed.

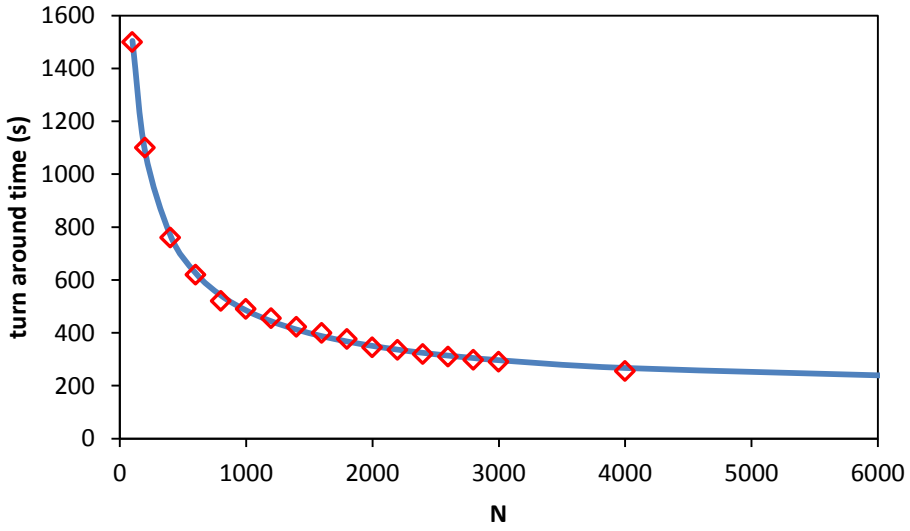

Figure 5.18. Turn-around time versus *N* (largest allowable number of primary particles in an aggregate) for silica particles in water at pH=2; the fitted coefficients are: a =2.545E4, b=0.1977, c=173.2, d=0.1738 ($R^2 = 0.9989$).

Table 5.1. Comparison between modeling and experimental results

Sedimentation test	Settling time (s)	
	Experiment	Modeling
Treated silica in diluted maltene	55	56
Silica in water at pH=2	180	173

5.4.3 Validation 3: Determination of self-preserving PSDs

Here, we choose to use the so-called "self-preserving" particle size distributions (PSDs) as the test. Early investigations of aggregation dynamics often involved seeking solutions to the Smoluchowski equation — in the form of PSDs as functions of time. What was common amongst these studies was the assumption that the number concentrations were independent of spatial position, i.e. the general functions $n_k(\mathbf{r}, t)$ were reduced to $n_k(t)$. Working under this limitation, Friedlander and coworker [9], [72] showed that, by properly scaling the physical parameters, the PSD of a suspension undergoing perikinetic (i.e. Brownian) aggregation would exhibit a "self-preserving" form. Specifically, let the aggregate size k be expressed in its scaled form η according to

$$\eta \equiv \frac{\text{size}}{\text{average size}} = \frac{k}{\langle k \rangle} \tag{49}$$

where $\langle k \rangle$, the average aggregate size, is given by

$$\langle k \rangle = \varphi / n_{\text{tot}} \; ; \tag{50}$$

the quantities φ and n_{tot} are, respectively, the total number of primary particles and the total number of aggregates. For *discrete* particles sizes (i.e. with k having integral values), we have

$$\varphi = \sum_k k n_k \; ; \quad n_{\text{tot}} = \sum_k n_k \, . \tag{51}$$

Finally, the scaled particle size distribution ψ is

$$\psi = \frac{n_k}{n_{\text{tot}}^2/\varphi} \tag{52}$$

For perikinetic transport with 100% collision efficiency, it was shown that plots of ψ versus η (i.e. the scaled PSD) would exhibit, after some initial transience, an asymptotic form that was invariant with time; further, the final $\psi(\eta)$ was independent of the initial PSD. Such asymptotic behaviour is said to be 'self-preserving.' Detailed forms of the self-preserving $\psi(\eta)$ were given by Vemury & Pratsinis [61] and Friedlander & Wang [72] for different fractal dimensions (d_f ranging from 1 to 3). Figure 5.19 shows self-preserving size distribution of aggregates of various fractal dimensions ($d_f = 1 - 3$). The distributions narrow with decreasing d_f because the rate of aggregate growth is larger for lower fractal dimension.

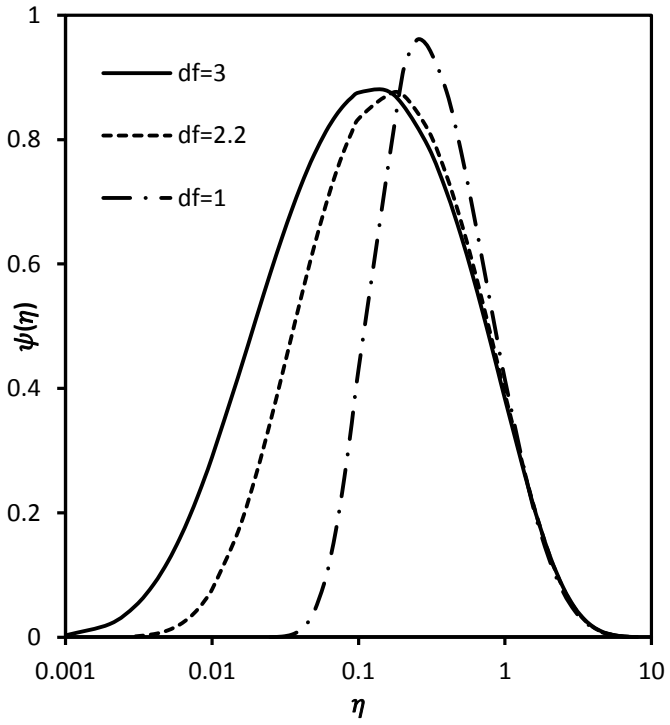

Figure 5.19. Self-preserving size distribution of aggregates of various fractal dimensions [61].

As validation, we will use our numerical scheme (see Section 4) to predict the "literature" self-preserving PSDs. There are two fundamental differences between the analyses of those earlier studies [9], [61], [72] and the current one:

1. The PSDs in the earlier studies were based on a continuous particle size which ranged from 0 to ∞. In this study, the aggregate size k was discrete and, for practical reasons, could not have a maximum value of infinity (k ranged between 1 and N). Our discrete approach can lead to truncation errors which we must ensure, through the present validation process, are negligible.
2. Our numerical scheme is more versatile in that it can account for spatial variations of n_k as well as particle collision by differential settling.

To compare with literature results, we had to suppress spatial variations and differential settling in our numerical simulation; this was done, very simply, by "turning off" gravity (i.e. by setting $g = 0$ in the equations). The maximum aggregate size was chosen to be 1000. Figure 5.20 shows results of our simulations for $d_f = 1$, 2.2 and 3. The contour-like lines represent the transient PSDs as they evolved to the final asymptotic shape [73]. In all three cases, the final PSDs agree very well with what were reported in earlier studies [61], [72] — with differences of less than 1%.

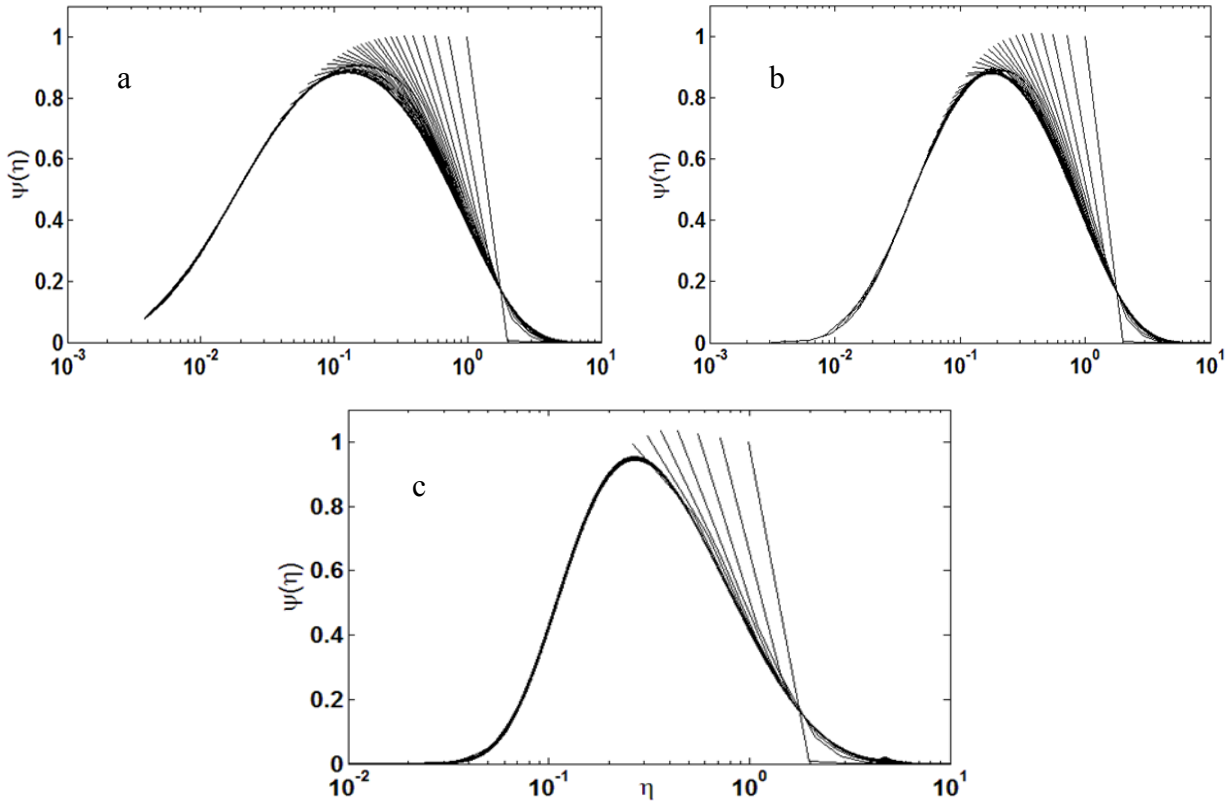

Figure 5.20. Self-preserving PSDs for rapid perikinetic aggregation. The fractal dimensions d_f were (a) 3, (b) 2.2, and (c) 1. The final asymptotic shapes agree very well with those reported by Vemury & Pratsinis [61] and Friedlander & Wang [72].

6 Kinetics of aggregation and sedimentation

6.1 Three stages of settling behavior

In addition to settling velocity, the mechanism of aggregation also depends on the size of primary particles. If the particles are small and/or of equal sizes, Brownian motion will plays a dominant role. As particles aggregate and grow in size, differential settling becomes much more important. Differential settling depends significantly on size. If there is a wider range of aggregates, the rate coefficients will increase dramatically. Hence, in a settling test conducted by using a settling balance (see Section 3.1 for details), one generally expects to see the aggregation of falling particles following three main stages: 1) Growth phase, which begins at $t = 0$ and may last for few seconds or minutes. During this phase, the primary particles begin aggregation to create doublets, triplets, etc. The span at which the settling remains in this stage is determined by the rate of aggregation at the beginning. The faster the aggregation, the shorter will be the growth phase; 2) steady state phase, when aggregation is improved significantly due to birth of larger particles, providing in turn a broader size range; 3) the resting phase. Within the previous two phases, the larger primary particles and a portion of small particles are leaving the suspension (forming a packed bed at the bottom). Towards the end of the process, only a small amount of fine particles will remain. These particles will sediment at a much slower rate. Also, since the number density is reduced significantly during the previous phases, there will not be much aggregation. The resting phase begins when the settling rate slows down significantly and rapidly (corresponding to the 'turn-around' point discussed in the last section). It lasts until it reaches the total mass of particles initially present in the settling column. Figure 6.1 shows a

typical settling curve (i.e. a settling curve resulted from a settling balance) with these three stages.

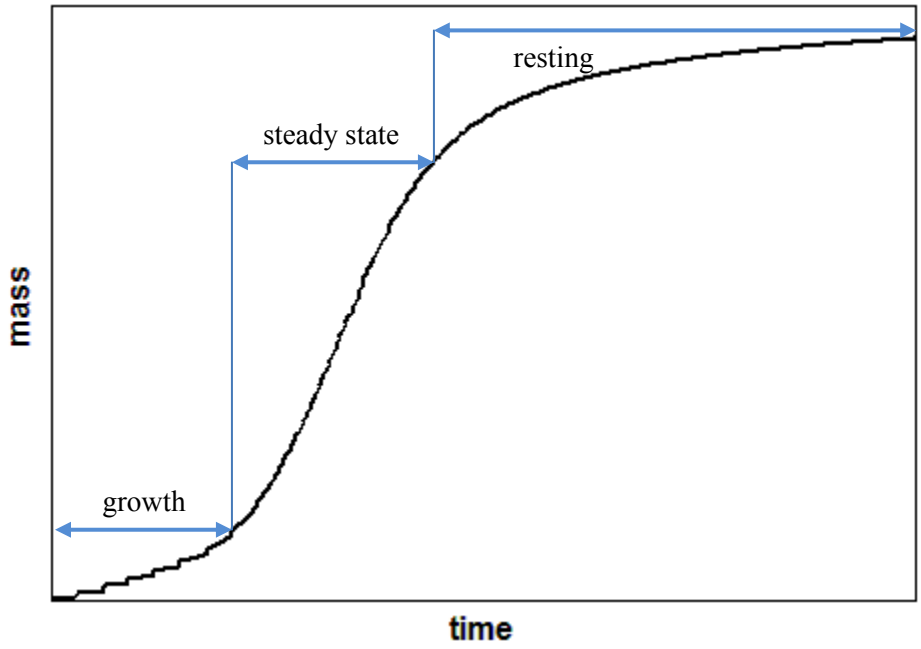

Figure 6.1. A typical settling curve based on data from a settling balance test (see Section 3.2). A collecting tray is placed at a fixed location in a liquid and the mass of collected solids is recorded over time.

The length of each stage, relative to the others, depends on several factors such as the size of primary particles, the attachment probability, etc. In what follows, we discuss a few case studies.

Case Study 1: Short growth period; 1-micron silica particles suspended in heptane

The growth period can be significantly short comparing to the other two stages. Mostly in the case of rapid aggregation (i.e. attachment probability $\alpha = 1$), this growth stage is short. However, it is not necessarily true for large primary particles due to poor aggregation (see discussion in the next section). The growth phase is likely not observed (or missed) when a wide initial size distribution exists. A mixture of different sizes stimulates the aggregation process

due to occurrence of significant differential settling right at the outset. Figure 6.2 shows a cumulative settling curve resulting from a simulation. It represents a process in which the sampling tray was located at a depth of 1.5 cm. The suspension consisted of 5 wt% 1-micron silica particles in heptane. The largest aggregate was allowed to have 1000 primary particles. The fractal dimension was 2, and the collision efficiency was assumed to be unity (i.e. rapid coagulation).

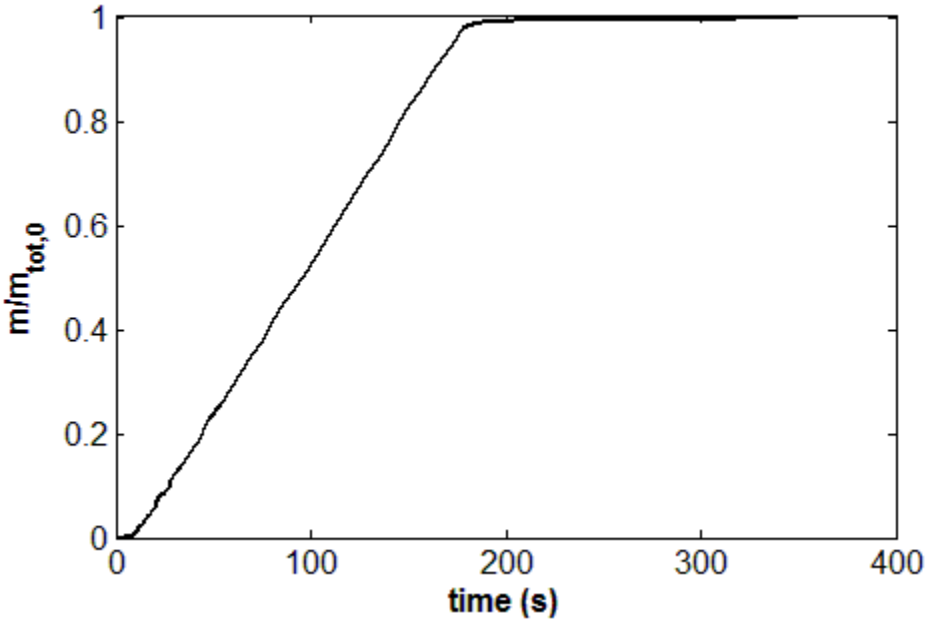

Figure 6.2. The cumulative mass collected by a plate at a depth of 1.5 cm. The amount of mass was divided by total mass at $t = 0$. The primary particles were 1-micron silica spheres at a concentration of 5 wt%. Aggregates were allowed to grow to a maximum size of $k = 1000$.

Case Study 2: Lengthened growth stage; 1-micron silica particles in slow aggregation

Suppose the same test on the same suspension in Case Study 1, except the attachment probability is 0.1. In this case, the particles collide but only one tenth of the collisions are successful in making an aggregate; this results in a slow aggregation. It takes more time to produce larger aggregates in order to enhance the aggregation rate. Figure 6.3 shows how slow aggregation

causes a lengthened growth period. Nonetheless, after creation of enough larger aggregates, when differential settling is improved, a steady sate period begins which lasts for quite some time.

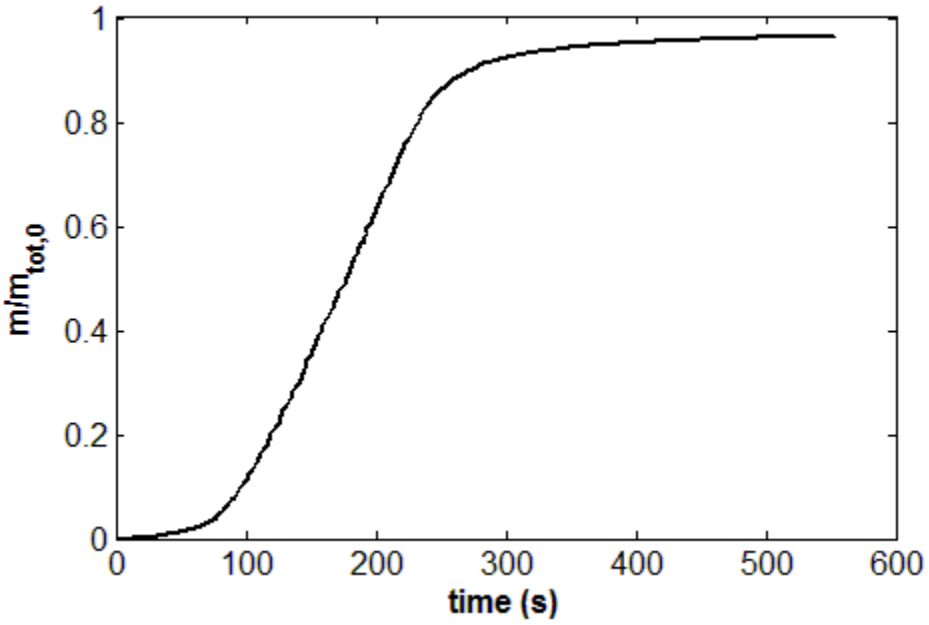

Figure 6.3. The cumulative mass collected at a plate 1.5 cm deep. The amount of mass was divided by total mass at $t = 0$. Aggregates grow up to one containg 1000 primary 1-micron particles. Solid concentration was set to 5% by weight. The attachment probability is 0.1.

Case study 3: Lengthened growth and resting stages; 10-micronsilica particles in heptane

If the primary particles have two specifications: 1) fairly large, and 2) of equal size, the rate of aggregation will be quite low. At the early stages, there is no differential settling (because of the equal sizes). Therefore, aggregation shall be dependent on Brownian motion only, which is insufficient for such large particles to make a great degree of aggregation. In that case, it takes a rather long time to create small amounts of aggregates of different sizes, and this is why the suspension remains longer in the first phase. Figure 6.4 shows the settling curve for a suspension

of mono-size 10-micron silica particles suspended in heptane with a 2 wt% concentration. The measuring tray is at a depth of 2 cm, and the collision efficiency α is one. The aggregates were allowed to grow to a size comprising of 250 primary particles.

Here, the middle phase is short, but the resting period is long. The reason is that, at any instant, the aggregation rate is not the same at different depths along the column. At lower locations, closer to the sampling point, the rate of aggregation is higher because the newly-created aggregates encounter the smaller ones on their downward paths and result in aggregation due to differential settling. However, over time, they meet less number of aggregates which lowers the aggregation rate. As a result, the suspension goes through a longer resting phase after a very short steady state phase.

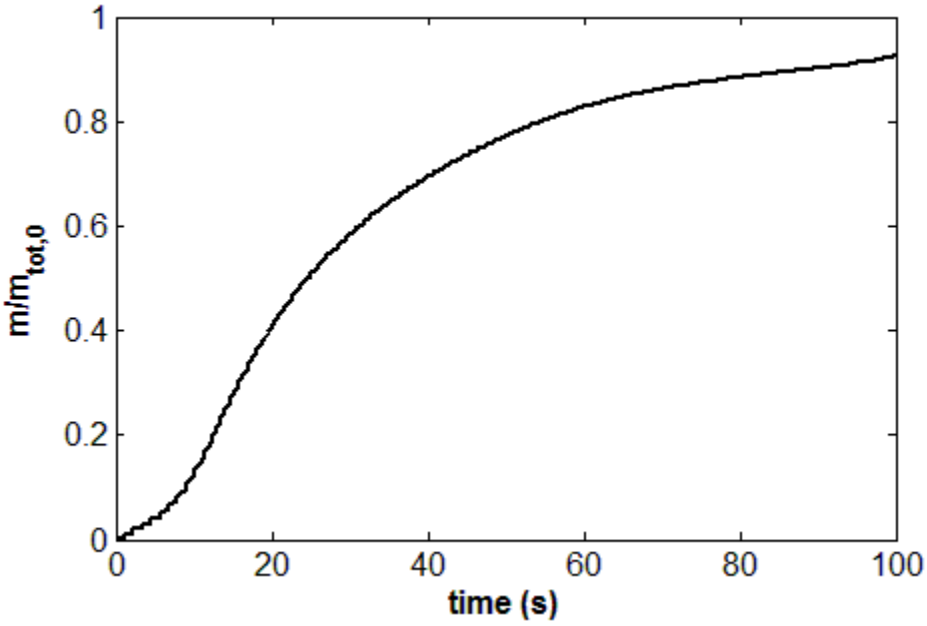

Figure 6.4. The cumulative mass collected at a plate 2 cm deep. The amount of mass was divided by the total mass at $t = 0$. Aggregates grow to one containg 250 primary 10-micron particles. The solids concentration was set to 2% by weight. The attachment probability is 1.

6.2 The role of collision efficiency in settling behavior

As shown above, a mono size dispersion of particles may affect the settling behaviour, especially when the attachment probability is less than 100% (see Case Study 2 in Section 6.1). Here we are interested in examining the impact of collision efficiency on the settling time, rather than the initial growth rate. In industrial applications, the settling time is the most important issue in the design of settling tanks. Settling time is the time that particles take to migrate through some characteristic distance in the vessel (for example, half of the vessel height). The settling time should be less than the 'resident time' of the fluid in the vessel to achieve an acceptable separation efficiency. In our settling curve, the settling time is the point that the curve stops rising and then turns around to level out. It is the time that particles initially located above the measuring tray take to completely settle.

Note that in reality, the particles in a slurry are most likely not of equal size. In the separation of these particles by sedimentation, the poly-dispersity in size will enhance differential settling and reduce the growth period. We will discuss the influence of initial particle size distribution later. Here, let the particles be a mixture of spheres with the size range shown in Table 6.1. This size distribution has been used as the initial condition in the model, and then the settling curve was plotted using the obtained results. The collision efficiency was set to be 1, 0.1 and 0.01. As we discussed in Chapter 2, the collision efficiency is determined by inter-particle forces so by changing the collision efficiency, we actually take the inter-particle forces into account. If there is a strong attractive force between particles, the collision efficiency will be equal to 1; weak forces will results in the lower values of collision efficiency. If repulsive forces exist, particles will not aggregate as collision efficiency is zero. The settling curves are shown in Figure 6.5. The suspension was a mixture of 2 wt% silica particles in a fluid with properties (i.e. density and

viscosity) of heptane. The aggregates were allowed to grow to ones containing 1000 primary particles of 5-micron diameter. The sedimentation probe was assumed to be located at a depth of 2 cm.

Table 6.1. The initial size distribution of particles used to study the role of collision efficiency

size (μm)	wt%
5	0.22
9	0.87
11	2.7
13	6.49
15	12.11
16	17.62
18	19.97
19	17.62
20	12.11
21	6.49
23	2.7
24	0.87
25	0.22

When $\alpha = 1$, the process is quite fast, and the settling time is short. In the other words, the particles are separated very quickly as they adhere to one another to create bigger aggregates that settle faster than the individual particles. In contrast, the settling time is much longer if α is less than one. For $\alpha = 0.1$, a growth period and an extended resting period are observable, as the particles take more collisions to create aggregates. This phenomenon makes a remarkable resting period. It is interesting to note that if α is sufficiently small (e.g. $\alpha = 0.01$), the aggregates do not grow much so that a large portion of the aggregates are the small ones. Under

this condition, there is not a significant amount of large aggregates. This is the reason that the settling curve looks like the one when $\alpha = 1$, except it is much slower.

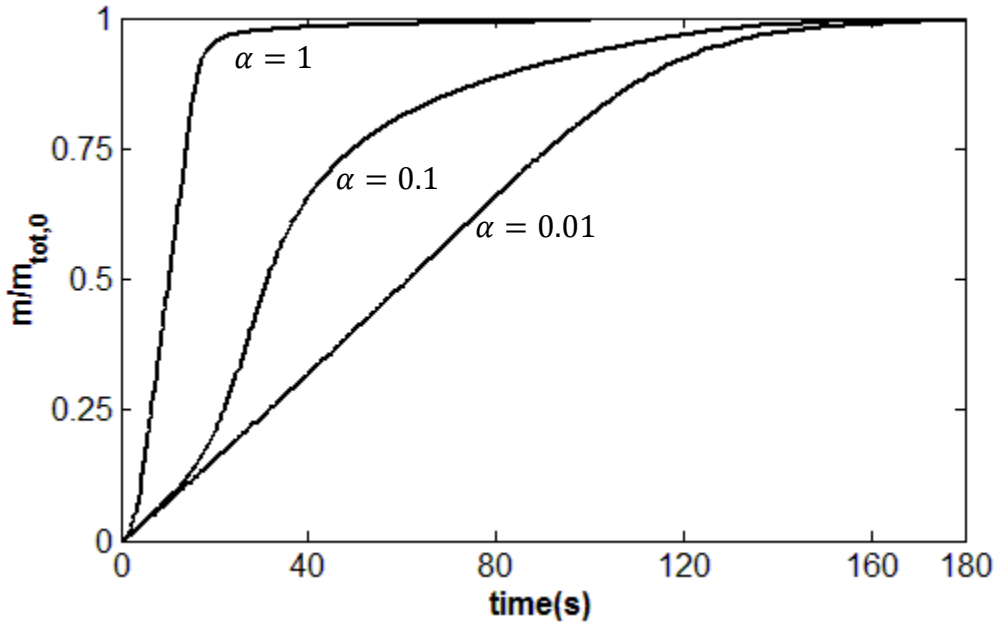

Figure 6.5. The cumulative mass collected on a tray that is 2 cm deep. The settling curves are shown for $\alpha = 1$, 0.1, and 0.01. The collision efficiency is determined by inter-particle forces.

In terms of settling time — which is an important factor in the design of settling tanks — if the conditions were properly chosen so that α is equal to one, the sedimentation would occur much faster and easier, otherwise the settling time would be longer, and therefore a bigger settling vessel is required. The other point is that for the suspensions with $\alpha = 0.1$ or $\alpha = 0.01$, both settling curves reach the maximum at roughly the same time. Therefore, if we aim for 100% separation, we will not be able to decrease the size of the settling vessel by increasing collision efficiency from 0.01 to 0.1. If one, on the other hand, requires only 75% separation, then the situation with $\alpha = 0.1$ will perform better than the one with $\alpha = 0.01$.

6.3 Size distribution over time

One of the best ways to investigate aggregation kinetics is to follow the evolution of the aggregate size distribution as they grow and at the same time settle. In our simulation, no breakage is assumed, so that the population of aggregates may diminish only due to sedimentation. The size of aggregates increases as they adhere together, which consequently accelerates their removal by increasing their sedimentation velocity. As a wide range of aggregate sizes are involved in the process (from a single primary particle to aggregates comprising of thousands primary particles), it is easier to look instead at the average aggregate size.

Consider a suspension of aggregates in a fluid. The size of each aggregate is specified by the number of primary particles within it. Thus, a 'k-aggregate' is one with k primary particles. Let n_k be the number density, and m_k be the mass of the *k*-aggregates.

The number-weighted and mass-weighted average sizes of *k*-aggregates in a settling column, denoted $k_{n,\text{avg}}$, and $k_{m,\text{avg}}$ respectively, are given by the following expressions:

$$k_{n,\text{avg}} = \frac{\int k n_k dV}{\int n_k dV} \; ; \quad k = 1, \dots, N \tag{44}$$

$$k_{m,\text{avg}} = \frac{\int m_k k n_k dV}{\int m_k n_k dV} \; ; \quad k = 1, \dots, N \tag{53}$$

In the above equations, N is the number of primary particles in the largest aggregate. Since

$$m_k = k \times m_\text{p}$$

the mass average is

$$k_{m,\text{avg}=}\frac{\int k^2 n_k dV}{\int k n_k \, dV} \quad k = 1, \ldots, N \tag{54}$$

Each k-aggregate is comprised of k primary particles of diameter d_p and has a fractal dimension d_f; therefore

$$d_\text{avg} = d_\text{p}\left(k_\text{avg}\right)^{1/d_f}$$

In above equation, k_avg is the number of primary particles in an aggregate of average size d_avg.

Recalling Case Studies 1 and 2 in Section 6.1, let us examine the size distribution of aggregates as time progresses. A suspension of 1-micron silica particles, at a concentration of 5 wt% in a liquid, was considered. The largest aggregate was allowed to be made up of 1000 primary particles. The collision efficiency was assumed to be 100% in Case Study 1, while it was 0.1 in Case Study 2. Figure 6.6 and 6.7 show the mass-weighted average size of aggregates for Cases 1 and 2.

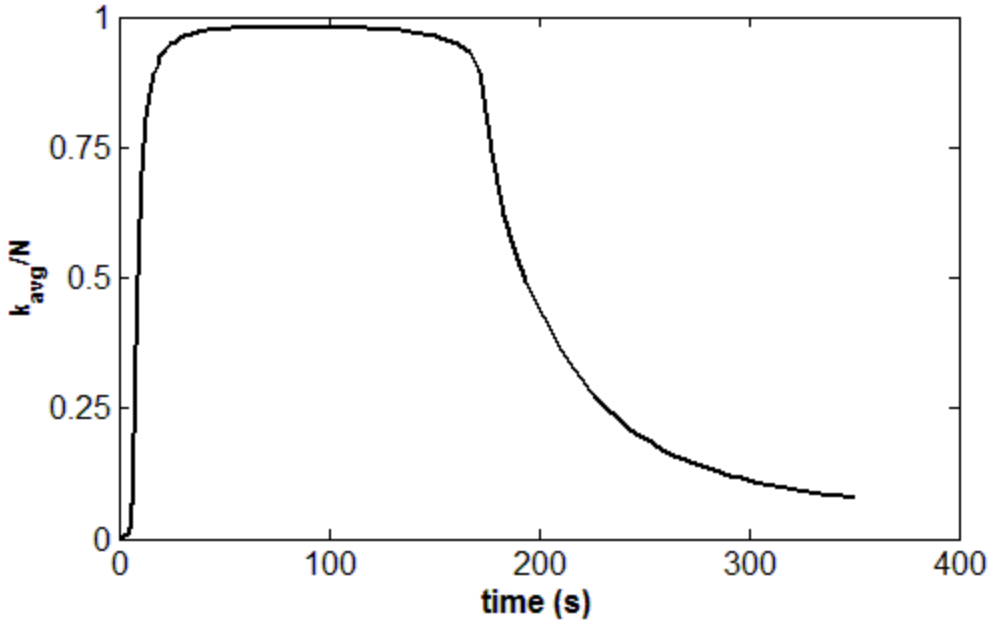

Figure 6.6. Mass-weighted average size of aggregates over time for a suspension of 1-micron silica particles. The collision efficiency was assumed to be 1. N is the number of primary particles in the largest allowable aggregate (here, N =1000).

Figure 6.6 illustrates that in rapid aggregation (i.e. $\alpha = 1$), the aggregates grow promptly so that the average size of the aggregates increases rapidly, and it reaches a value very close to the maximum number, N , in a short time period (N is the number of primary particles in the largest allowable aggregate). Here, the rate of aggregation is larger than the rate of sedimentation as the aggregates that are removed by sedimentation are replaced quickly by production of new aggregates. Therefore, the average size of aggregates remains high for an extended time period, until all the particles are settled and no more smaller particles are left to create large ones. Note that the turn-around time is roughly the same as that in Figure 6.2.

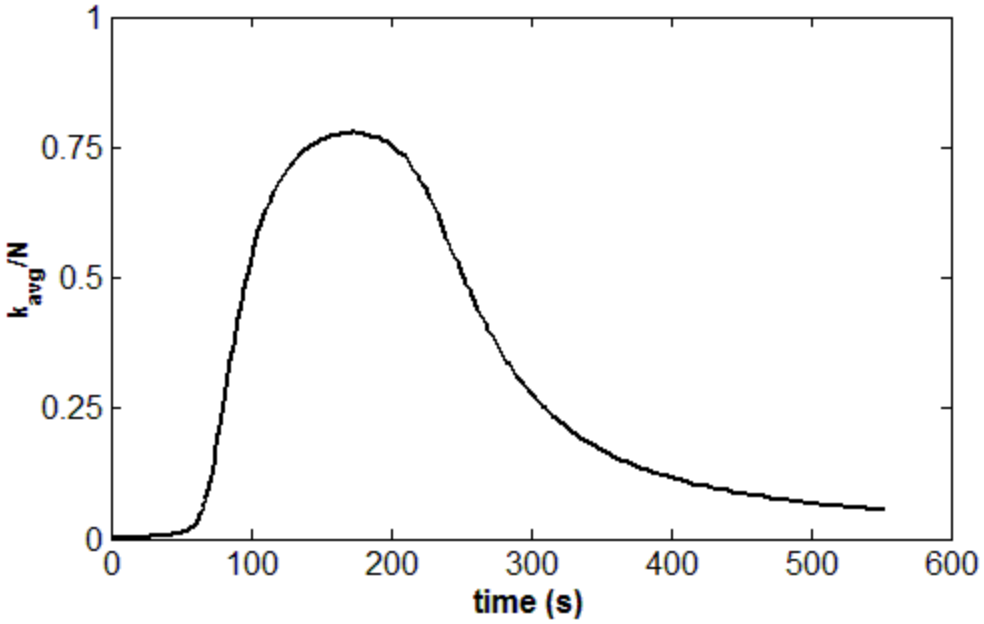

Figure 6.7. Mass-weighted average size of aggregates over time for a suspension of 1-micron silica particles. The collision efficiency was assumed to be 0.1. N is the number of primary particles in the largest allowable aggregate. Here N=1000.

Figure 6.7 shows the average size plotted against time for the case $\alpha = 0.1$. In contrast to $\alpha = 1$, the size of the aggregates do not increase rapidly; it takes some delay to reach a certain time at which an abrupt improvement occurs. The aggregates grow during the growth period, which is about 60 s in this case. There is good agreement between the point here and the one in Figure 6.3, at which great improvement is observed in the settling rate. In addition, it is noted that the average size of the aggregates is not a value close to the maximum allowable size, unlike the situation with $\alpha = 1$. This is because the largest aggregates, which settle the fastest, are not replaced as quickly by aggregation. As the aggregation rate is not as rapid, aggregate replacement is limited to smaller entities.

In addition to mass-weighted average, the number-weighted average was also calculated. Figures 6.8 and 6.9 show the number-weighted average size of aggregates in Cases 1 and 2 (see Section 6.1 for details). The mass-weighted average places more emphasis on the larger aggregates. In other words, the average is closer to the size of larger particles. (One may argue that averaging by mass is more representative of our situation since the experimental settling curves are presented on a mass basis.)

Figure 6.8 shows the number average for Case 1 with $\alpha = 1$. The average size of the aggregates increases after a very short delay time, but unlike the mass-weighted average, it takes more time to reach the maximum value, which is not close to the maximum allowable size. This shows that many smaller particles still exist, even though a large portion of the aggregates are the larger ones.

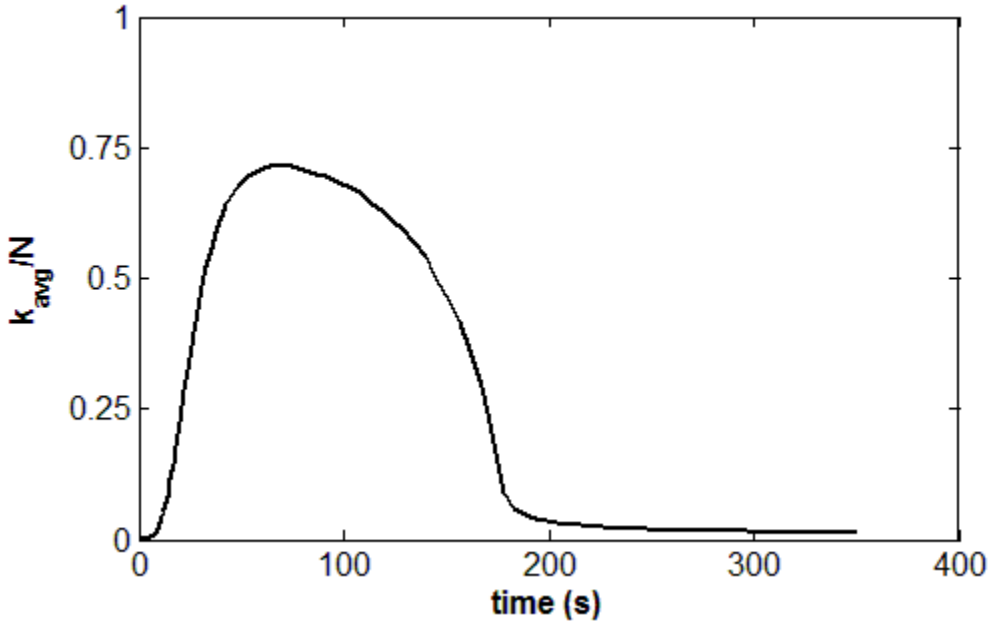

Figure 6.8. Number-weighted average size of aggregates over time for a suspension of 1-micron silica particles. The collision efficiency was 1; the maximum aggregate size N was 1000.

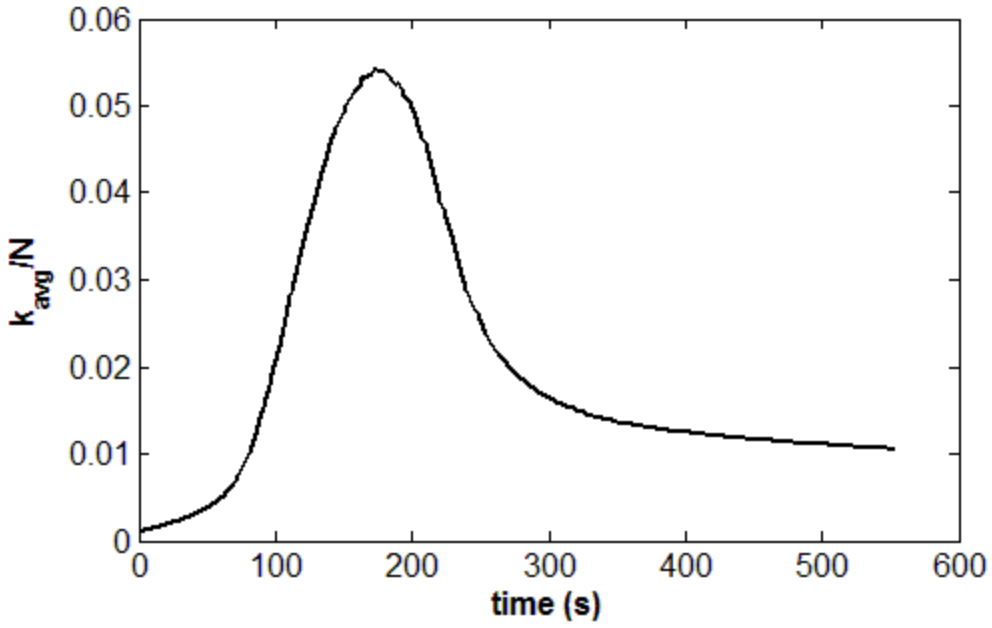

Figure 6.9. Number-weighted average size of aggregates over time for a suspension of 1-micron silica particles. The collision efficiency was 0.1. The maximum aggregate size N was 1000.

As shown in Figure 6.9, the number-weighted average size, when $\alpha = 0.1$, is much less than the largest allowable number N. This illustrates that there are many very fine particles along with some fairly large aggregates. One may compare the mass-weighted average with the number-weighted average, as shown in Figure 6.10, in which dramatic difference is observed between these two parameters. The mass average is seen to increase significantly within the first several seconds; it shows that large aggregates are formed within such a time period. These large aggregates leave the system soon after, owing to their high settling velocities.

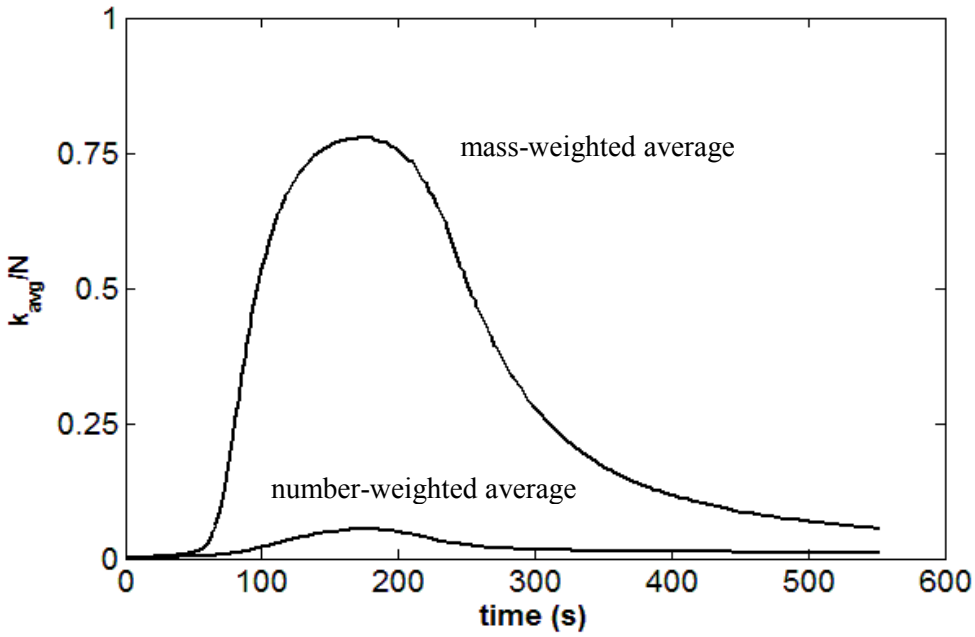

Figure 6.10. Comparison number-weighted average and mass-weighted average size of aggregates over time for a suspension of 1-micron silica particles. The collision efficiency was assumed to be 0.1. (N=1000).

Size distribution at different depths

Thus far, only the average size of the aggregates, determined over the entire settling column, has been investigated. To investigate the effect of depth on size, we calculate the integral in Eq. (54) over two intervals. The first interval was from top (zero depth) to middle of the column; the second interval was from the mid-point to the bottom of the column. Figure 6.11 shows the mass-weighted average size computed over the top and bottom halves of the column, in addition to the entire depth in Case Study 2 (see Section 6.1 for properties of the suspension). As the aggregates grow as they settle, the average size becomes larger in the bottom half compared to that in the top half. The deeper the depth, the higher is the concentration of larger aggregates. It

is interesting to note that the growth periods are the same within all three vertical segments (see Figure 6.11).

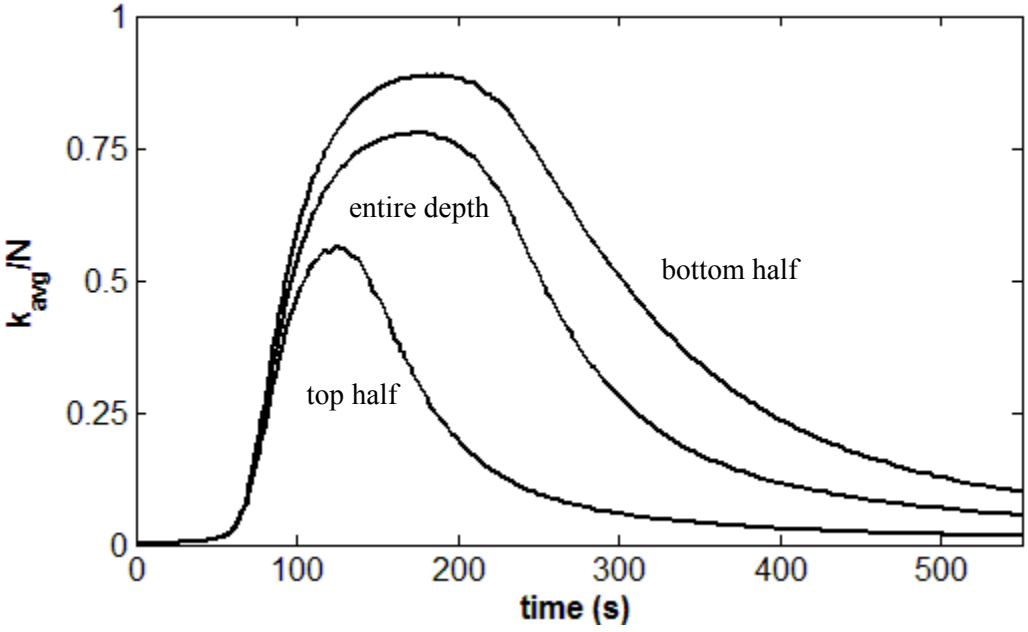

Figure 6.11. Mass-weighted average size of aggregates at different depths (see Section 6.1, Case Study 2 for properties of the suspension).

6.4 The "induction time": mass vs time plot

In Section 3.1, we described a new approach of measuring sedimentation rates in a suspension (tailored for opaque liquids); it involved collecting small samples (0.5 mL) from a fixed location (1 cm below the free surface) and determining the solid masses m within them. The solid mass was measured and plotted in Figure 6.12. From a previous study, it is known that the suspended solids are colloidally stable (i.e. they do not aggregate) in toluene, but become unstable in *n*-heptane [5]. Indeed, as seen in Figures 6.12a and 6.12b, the characteristic settling times in the two solvents differed by orders of magnitude: the solids took over 3 days to traverse a distance of 1 cm in toluene (slightly longer than the time which corresponds to the terminal velocity of

individual particles, as the silica were susceptible also to thermal agitation), but covered the same distance in less than 2 minutes in *n*-heptane. This difference was attributed to the steric repulsion between silica particles in toluene, which left the particles to settle as individual, 0.25-μm spheres. In contrast, there was strong inter-particle attraction in *n*-heptane, giving rise to rapid coagulation and sedimentation [5].

The last set of settling tests was conducted in cyclohexane, following the same procedures. As seen in Figure 6.12c, the settling rate in cyclohexane was somewhat slower than that in *n*-heptane, but was nevertheless of the same order of magnitude. What is noteworthy in Figure 6.12c is the existence of an apparent 'induction time' before which aggregation appeared not to occur. On first reflection, the origin of this 'induction time' is unclear; there does not seem to be any molecular basis for such a phenomenon. To gain further insight into the sedimentation process, we next turned to detailed simulation of the sedimentation process.

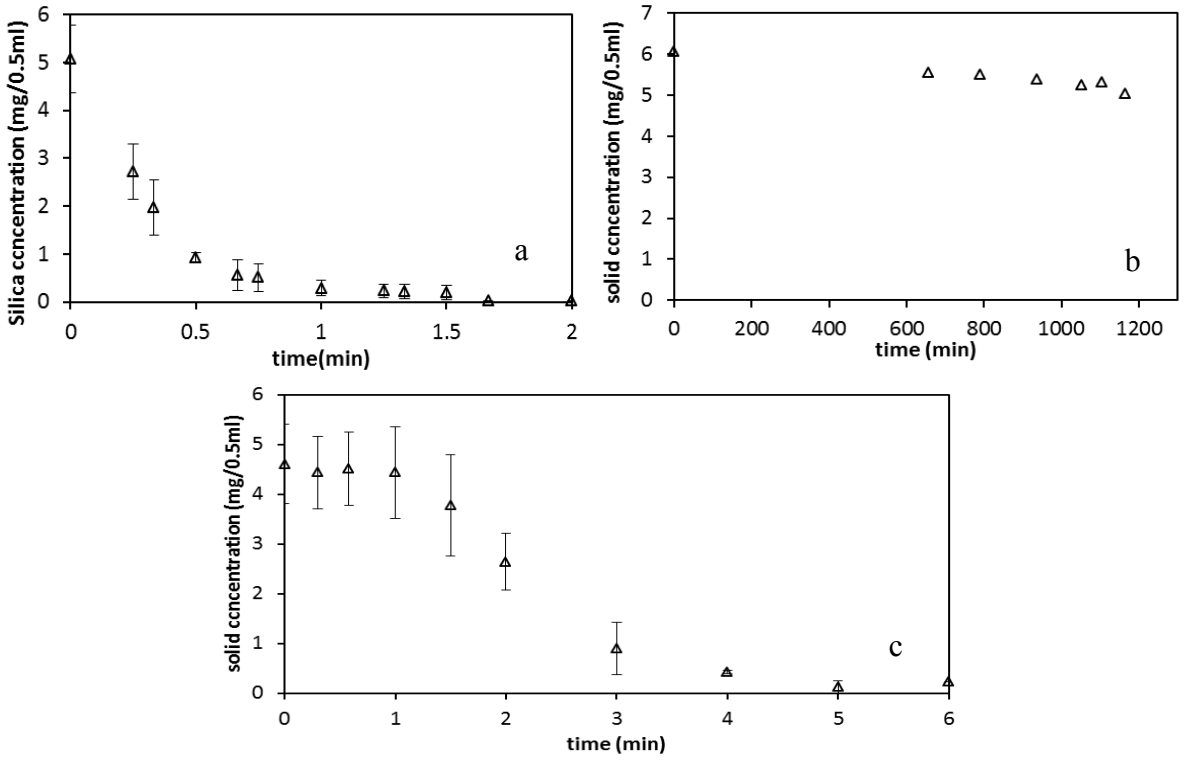

Figure 6.12. Settling behaviours as expressed by plots of m vs. t. The suspending liquids were (a) toluene, (b) *n*-heptane, and (c) cyclohexane. Note that the vertical axes, which are labelled 'solids concentration,' shows the solids mass that were recovered from the 0.5-mL samples.

Simulation results

As seen in Figure 6.12, there were situations when an 'induction time' (i.e. an apparent delay before aggregation commenced) was observed. We show here, from our simulation results, that the apparent induction time may be an artifact resulting from the kinetics of aggregation.

The results obtained from our numerical simulations have been used to provide insights into the experimental results. The suspension was comprised of 1μm silica particles in *n*-heptane. The collision efficiency was assumed to be 0.1. The particles were allowed to grow and make large

aggregates such that the largest one contains 1000 primary particles. The mass m can be easily calculated from the local number concentrations of all aggregates (multiplied by the sample volume to obtain the actual number of particles, then converted to a mass based on ρ_{solid} and d_{p}). Figure 6.13 shows the solids mass at 1 cm below the free surface (cf. Figure 3.1) up to a time of 50 seconds. Note that the mass m on the vertical axis is expressed as a fraction of its maximum value m_0 (i.e. m at $t = 0$).

Figure 6.14 shows the results of another modeling test for the particles with initial size distribution presented in Table 6.1. Again, the particles were assumed to be suspended in heptane; the calculations were done for collision efficiencies α of 1 and 0.1.

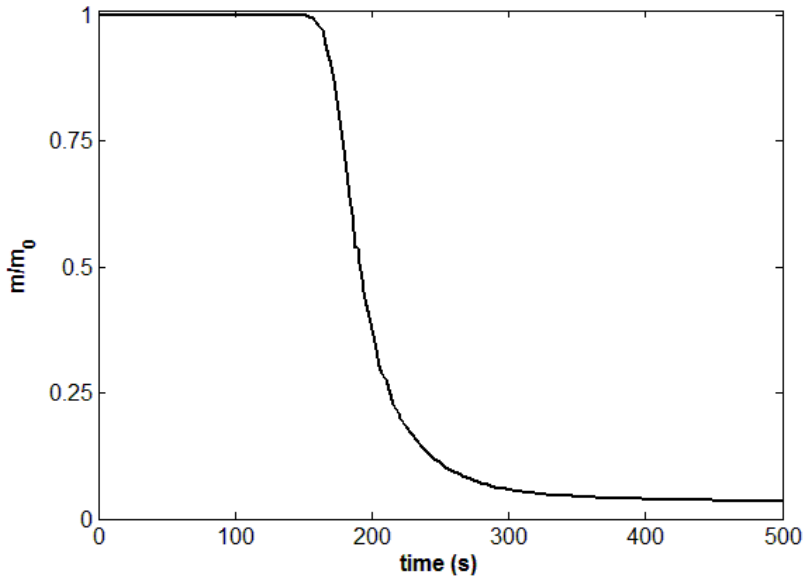

Figure 6.13. The mass concentration of 1-micron silica particles in *n*-heptane at a location that is 1 cm from the free surface; the largest aggregate contains 1000 primary particles ($N = 1000$). The collision efficiency was assumed to be 0.1.

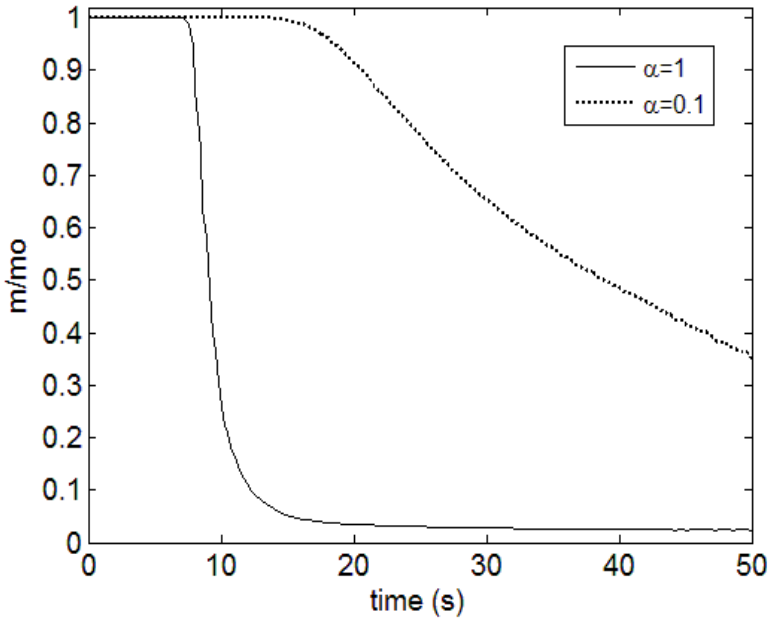

Figure 6.14. Mass concentration of silica particles undergoing aggregation and sedimentation in heptane with two collision efficiencies: $\alpha = 1$ and $\alpha = 0.1$. The initial size distribution was presented in Table 6.1.

As seen from Figure 6.13 and 6.14, there are, at the beginning, flat regions similar to what was observed experimentally (see Figure 6.12). These flat regions appear to suggest periods during which aggregation has yet to take place, thus leading to speculations of 'induction times' (which have no real physical basis). However, in our simulation, particle aggregation commenced immediately at $t = 0$; no delay time was imposed in the calculations. To illustrate this, Figure 6.15 shows the number densities of singlets (i.e. primary particles, with $k = 1$) and doublets ($k = 2$) at a 1-cm depth as functions of time. As expected, the number of singlets decreased monotonically from time $t = 0$ as they combine with others to form larger aggregates; the number of doublets rose momentarily as they were created from singlets, but dropped as they went on to form bigger entities.

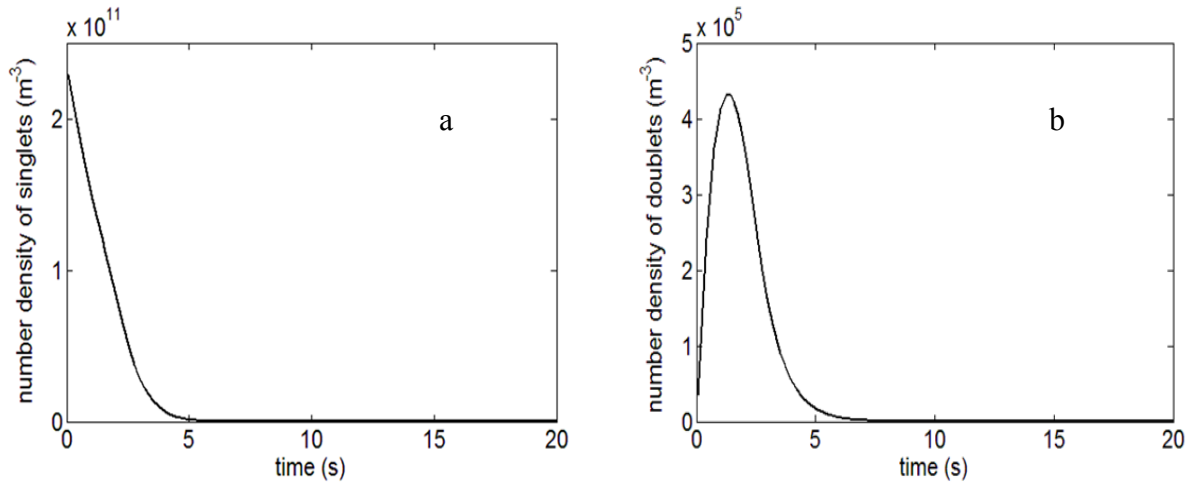

Figure 6.15. Scaled number densities of (a) primary particles, and (b) doublets as functions of time; the time $t = 0$ corresponds to commencement of the settling process.

It is clear from Figure 6.15 that, between the suspended particles (i.e. on the smallest length scales), there was no delay in aggregation. The apparent induction times seen in Figure 6.13 are in fact results of sedimentation kinetics. We propose that sedimentation by differential settling requires some 'lead time' before the phenomenon manifests itself on the macroscopic scale — almost discontinuously as in the case of avalanches.

Figure 6.14 also suggests that the apparent induction time becomes longer as the collision efficiency α decreases. Even for the highest efficiency of $\alpha = 1$, it appears that there would be a finite delay time before sedimentation is seen macroscopically. In reality, however, this delay time may be too short to be observed (as was the case with *n*-heptane in Figure 6.12).

The rate of sedimentation observed in experiments is in fact a function of the rate of aggregation and the rate of settling. The rate of settling, which is essentially the settling velocity, is very low and can be neglected in the early stages of the process. As the aggregates grow, the velocity increases as the settling velocity is proportional to d^{d_f-1}. The rate of aggregation, however,

scales as βn^2 (according to the Smoluchowski theory). The collision frequency, β, is not identical for all particles; indeed, it can be a strong function of aggregate size. On the other hand, the particle number concentrations decrease as they adhere to one another to make bigger aggregates. Thus, as the aggregates grow, the settling velocity increases while the rate of aggregation decreases. Although, the settling velocity is negligible at the beginning, after some time, it will become dominant. That point is the time after which precipitation becomes visible.

6.5 The "induction time": height vs time plot

The traditional method of studying the settling behavior of solids is to monitor the position of the interface between clear liquid and 'cloudy' suspension; the position of this 'mud line' is usually plotted against time. There are some reports in the literature regarding an 'induction time' that was observed experimentally (See Ref [47], [49], and [74]). Here, we demonstrate the capability of our numerical modelling to predict such an 'induction time.' We will evaluate the conditions under that the induction time will be observed.

Figure 6.16 shows the plot of the material density (i.e. mass concentration of material per volume) versus the fluid depth at various times. The material density changes from zero to maximum over a very short vertical distance. This distance is the interface between clear liquid at the top and the suspension at the bottom. The mud line descends over time as aggregation and sedimentation occurs.

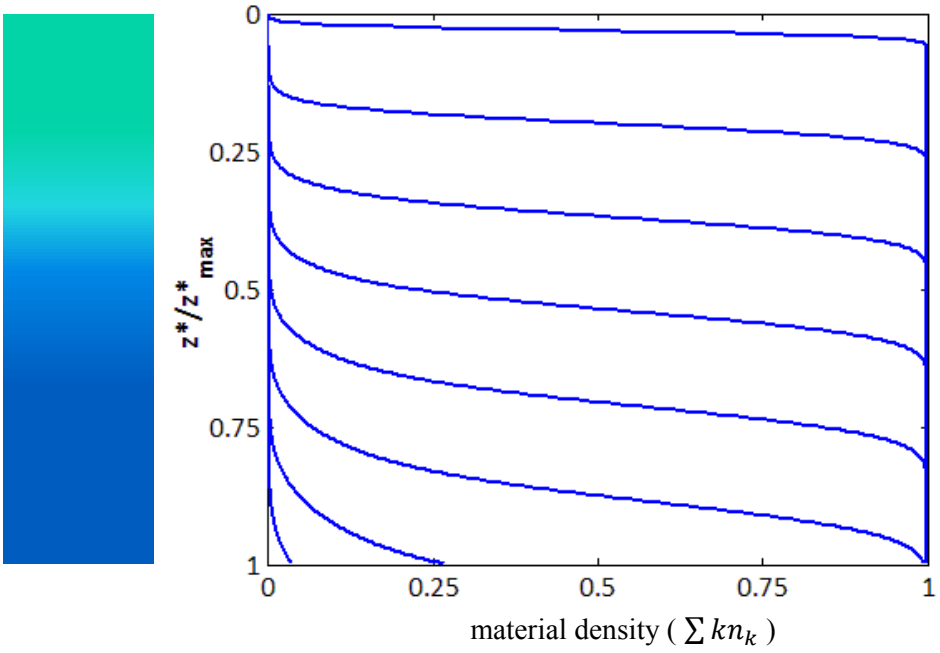

Figure 6.16. Density profiles in a settling column. The curves are obtained from integration of Eq. (30). All quantities are expressed in their non-dimensional forms.

To monitor the location of the mud line over time, the average vertical position was calculated as follows: Writing the material density as $\omega = \sum kn_k$, and recognizing that this density varies rapidly with depth across the mud line, we can define the average mud line position by

$$z_{\text{avg}} = \frac{\int z d\omega}{\int d\omega} \tag{55}$$

The procedure is shown in Figure 6.17: it shows how the location of the mud line (at a given time) was determined. Using this method, the mud line location was approximated and shown in Figure 6.18.

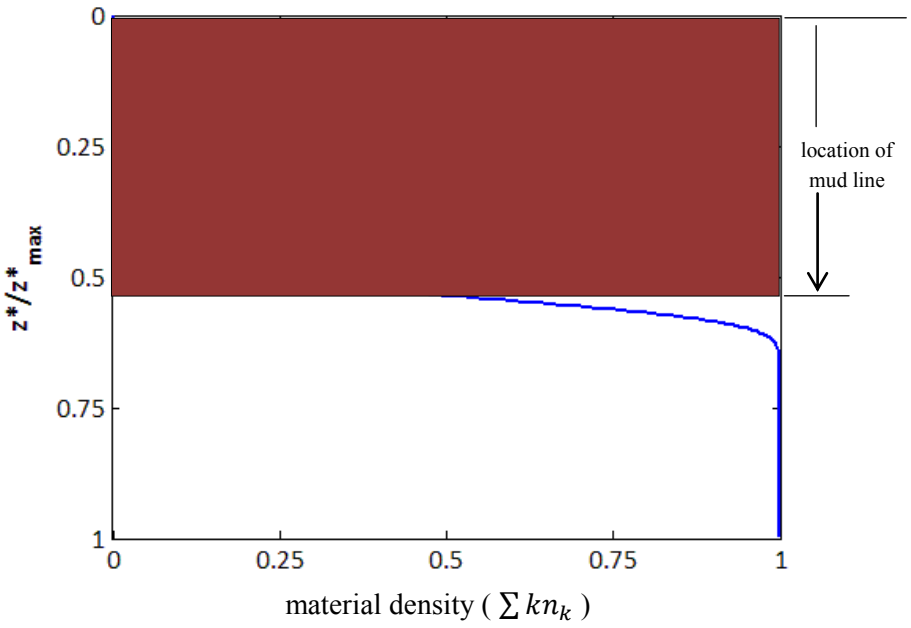

Figure 6.17. Determining location of the mud line

This work has been repeated for various values of collision efficiencies, from $\alpha = 1$ to 0.001. At the maximum aggregation rate, no induction time was observed. However, as the collision efficiency decreases, a perceptible induction time was seen. Although the delay time is rather small from $\alpha = 1$ and $\alpha = 0.01$, it is quite noticeable when $\alpha = 0.001$. The mud line moves slowly at the beginning because not much aggregation occurs. With creation of larger aggregates, the rate of aggregation increases significantly so that an "avalanche" phenomenon occurs, and the mud line descends much faster from that point on.

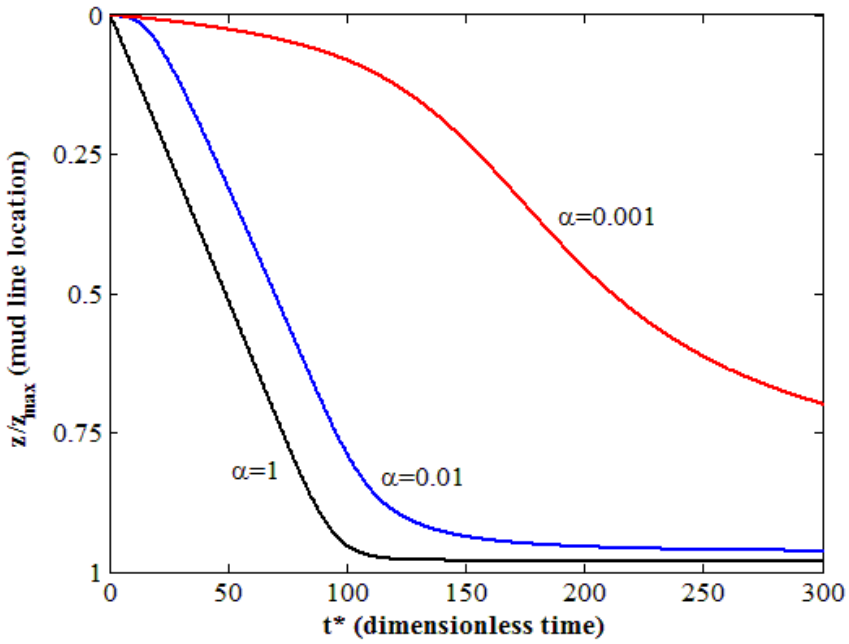

Figure 6.18. Mud line location (calculated using eqn. 55) vs. time. The diameter of the primary particles was 5 µm ($n_0 D_0^3 = 6.25$). The parameter α is the collision efficiency.

Note that the 'induction time' was observed because the initial rate of particle sedimentation and aggregation are relatively slow. However if the rate of sedimentation is higher than the rate of aggregation (e.g. with larger particles), this delay time will not form or will be less visible. Figure 6.19 shows the mud line location for primary particles that are 1.6 times bigger than those in Figure 6.18.

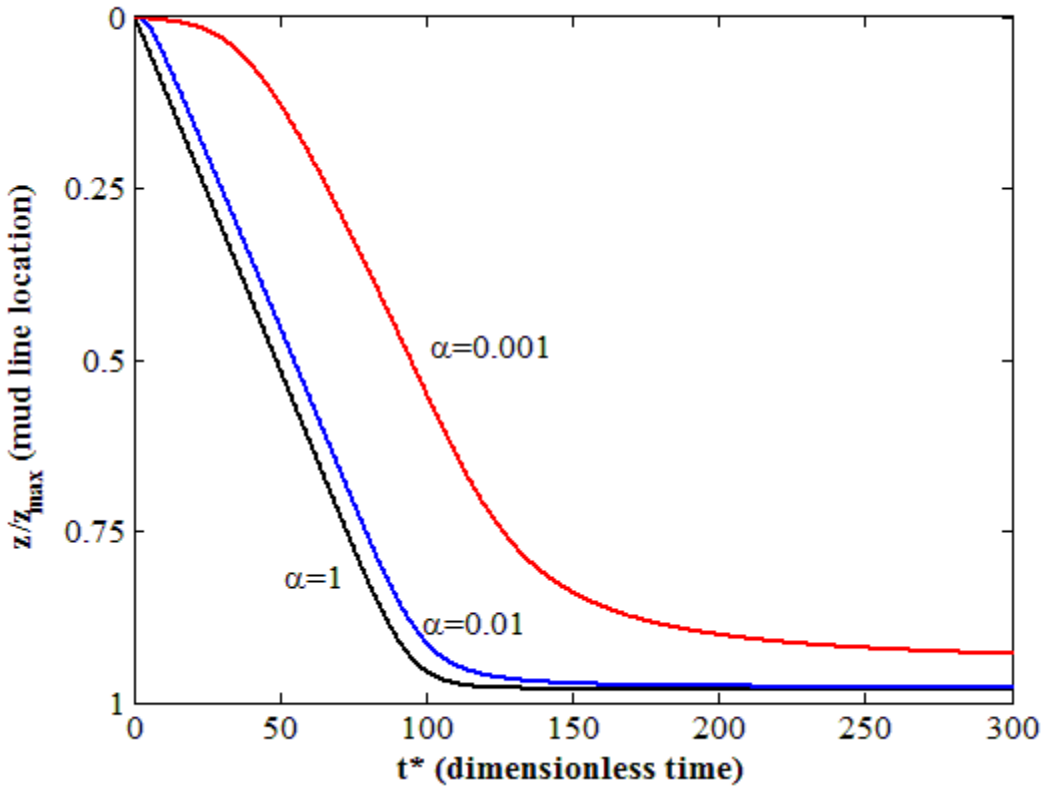

Figure 6.19. Mud line location vs. time. The diameter of the primary particles was 8 μm ($n_0 D_0^3 = 10$). The parameter α is the collision efficiency.

6.6 Diffuse layer

6.6.1 Formation of diffuse layer

As suspended particles and aggregates settle, a layer containing lower concentration of solids begins to form at the top. The population of particles in this layer depends on how quickly the particles aggregate to make larger aggregates and descend faster. This phenomenon results in the formation of an interface between the clear layer and the concentrated layer. The interface travels toward the bottom as displayed in Figure 6.20. The higher degree of aggregation accelerates sedimentation and the interface displacement. However, a sharp interface does not

always exist. Travelling from top toward bottom demonstrates that the mass concentration is gradually decreasing. It begins from a clear liquid ending to a completely cloudy region. The length of transition region (i.e. clear region to dark region) can be expressed as a function of the rate of settling and the time elapsed. A diffuse interface, therefore, is observed which is called the mud line.

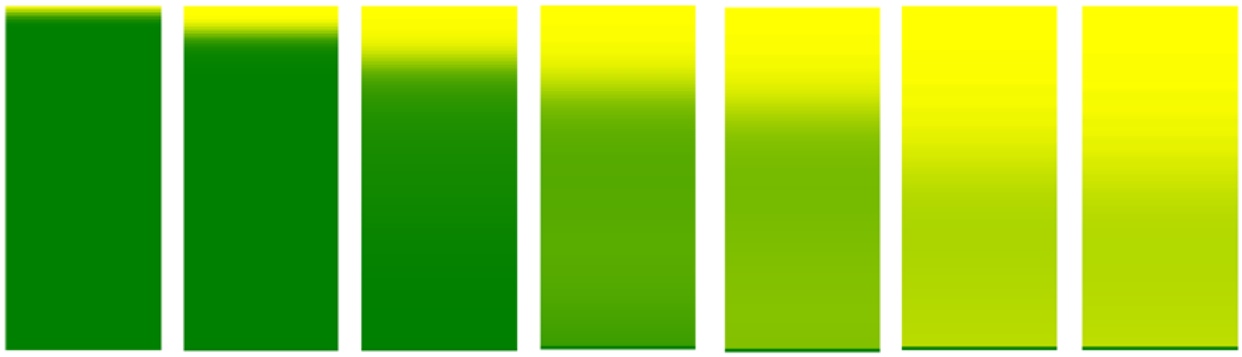

Figure 6.20. Sedimentation of particles and aggregates results in the formation of a diffuse interface between the clear phase and dark region.

6.6.2 The thickness of diffuse layer

A sharp interface is likely to be observed under two conditions during the settling process: either where the particles are all mono-size or when the particles do not aggregate. If particles are neither mono-size nor having a certain tendency to aggregate, a diffuse layer will develop at the interface. It is, therefore, not easy to keep track of the interface in most experiments. However, it is helpful if one looked at the mass concentration of particulate solids in the transition area instead. Mud line, thus was defined as the area where solid content varies between a typical number (e.g. 90% of initial value) and the current maximum concentration, as illustrated in Figure 6.21. At time $(t = 0)$ the ratio of mass concentration to its initial value is unity at all locations, but this ratio decreases as time proceeds. The large particles (even without

aggregation) settle quickly, leaving the concentration ratio less than unity. Furthermore, aggregation, followed by sedimentation, will remove more solids.

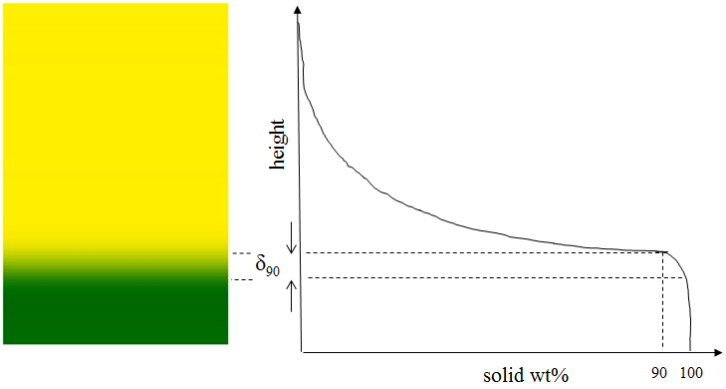

Figure 6.21. The mudline thickness ss defined as the height in which the solid concentration varies between 90% of initial value and maximum value.

According to this definition, the thickness of the diffuse layer was measured over time using the simulation results. Figure 6.22 shows the thickness for collision efficiencies of 0.1, 0.04 and 0.01. The diffuse layer initially expanded until it reached a maximum value after a certain time, then it decreases to a constant value. It remained constant until the diffuse layer (as defined) touched the bottom of the vessel where the thickness began to reduce. In other words, three regimes could be identified: an expansion, constant and ground contact. The slope of the curve at the last section determines the rate at which the interface layer is lowering toward the bottom of the vessel.

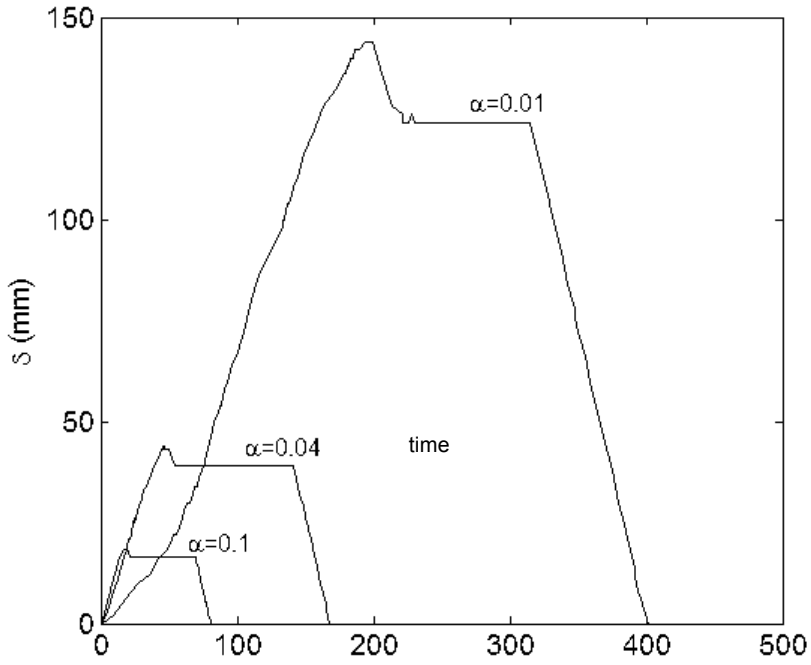

Figure 6.22. The mud line thickness over time

The thickness of the constant section was plotted against collision efficiency in a log-log plot in Figure 6.23. Also shown in the figure is a case where the mud line is defined for the region where the solids content varies between 80% of initial value and the maximum concentration (open symbols), compared with 90% of initial value and the maximum concentration (closed symbols). As seen, there is not a big difference if the arbitrary number of 90% is replaced by 80%.

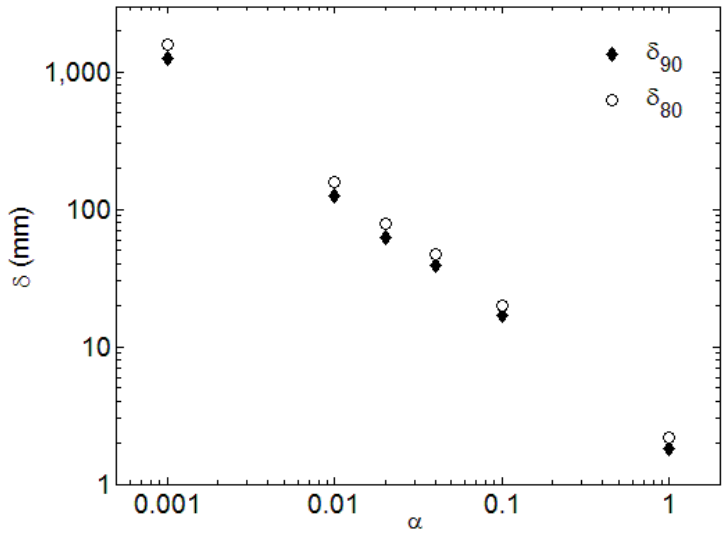

Figure 6.23. The mud line thickness once it becomes constant against the collision efficiency α. δ_{80} is similar to δ_{90}, except the lower range was taken as 80% of the initial mass concentration.

6.6.3 Multiple diffuse layer

It is well-known that an interface (i.e. the mud line), which can be somewhat diffuse, is developed when particulates settle in a fluid. The interface divides the fluid in two parts: a clear liquid and a solids suspension. The concentration of the particulates varies across the interface — from zero to some finite value that is equal to the concentration of the suspension. How the diffuse layer is formed was discussed at length in the previous sections. Note that it is often assumed that *only one* interface is formed, and therefore it is this interface that is tracked in order to quantify the rate of settling. However, it is possible that multiple layers are developed instead of only one. In such a case, the concentration of materials would not increase monotonically with depth. The reason only one interface is observed is likely because the other layer(s), if they exist, are visually difficult to detect; as will be shown here, the particle concentrations around these 'secondary layers' do not vary as dramatically. However, if one measures the turbidity

very carefully and with enough resolution, multiple interfaces can sometimes be observed. Here in this section, the underlying mechanism that causes the formation of several diffuse layers will be discussed.

6.6.3.1 Experiments

Let us assume one is doing a settling test by using the sedimentation balance (see Figure 3.2); the detailed procedures have been described earlier. If only one interface exists in a settling column, one expects to see the amount of collected mass increases more or less linearly over time. This continues until the collected mass reaches a maximum value, at which point the curve levels off. If the initial particle size distribution (PSD) includes some smaller particles, the settling curve will continue increasing but at a much reduced rate. This is because the larger particles settle first with higher velocities along with smaller particles, and when they are all settled, the small particles will be still received by the collecting tray (these small particles do not aggregate easily as their number concentrations would be very low at this point).

It is unusual to see the slope of the settling curve increase after it has already reduced — it looks like the rate of settling improves after it was about to reach zero. However, this behavior was sometimes observed with the settling balance. Figure 6.24 shows the settling curve for a suspension of 5 wt% of 1.5 micron silica particles (claimed by vendor to be 1.5 μm mono-size particles) in water at pH=2. (Recall pH 2 is the point of zero charge; the silica particles will aggregate via van der Waals attraction, giving rise effectively to a collision efficiency of 100%.) The collecting probe was placed 15 mm below the surface. The rate of the mass received by the probe is quite large at the beginning. Soon after that, the rate decreased, and then again increased until it stops rising and levels off. Again at the end, it increased until it reaches the maximum amount.

If the primary particles were all of the same size, the settling curve was expected to rise at a constant slope until it levels off. The observed behavior is attributed to the formation of *multiple diffuse layers*. At the sampling point, a large number of bigger aggregates are received first.

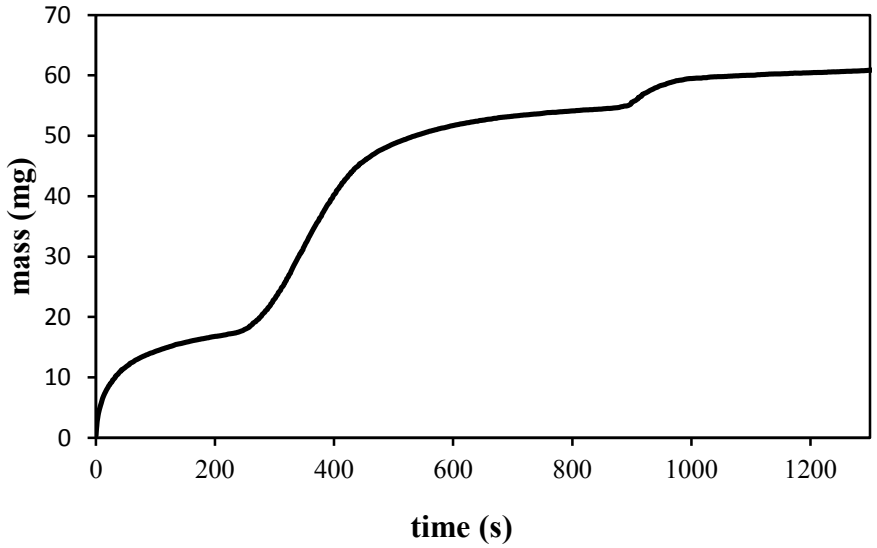

Figure 6.24. Experimental settling curve of a suspension of 5 wt% of 1.5 micron silica particles (claimed by vendor to be 1.5 μm mono-size particles) in water at pH=2. The collecting tray was placed 15 mm below the surface.

How multiple layers are formed

Larger particles settle at a higher rate so that on their way to the bottom they catch the smaller particles and bring them along. This is the main mechanism which occurs in sedimentation systems, as was discussed earlier (i.e. differential settling). As a result, the rate of aggregation is much higher in the mid-layers, because particles grow to even larger aggregates on their way to the bottom, and then they catch the particles in the mid layers at high collision rates. This results in more particle aggregation, and therefore faster sedimentation in the middle zones. Smaller particles at the top, however, do not have any chance to meet larger primary particles. They do not aggregate as much as the particles in the mid-layers, hence they settle at a lower speed. As

time progresses, a clear zone with lowered solids concentration will be developed in the middle, while a layer of suspension still remains at the top. Figure 6.25 is a sketch which illustrates such a phenomenon.

It is speculated that the 1.5 μm silica particles were not actually mono-size. A size distribution measurement that was done in our group has verified this suspicion.

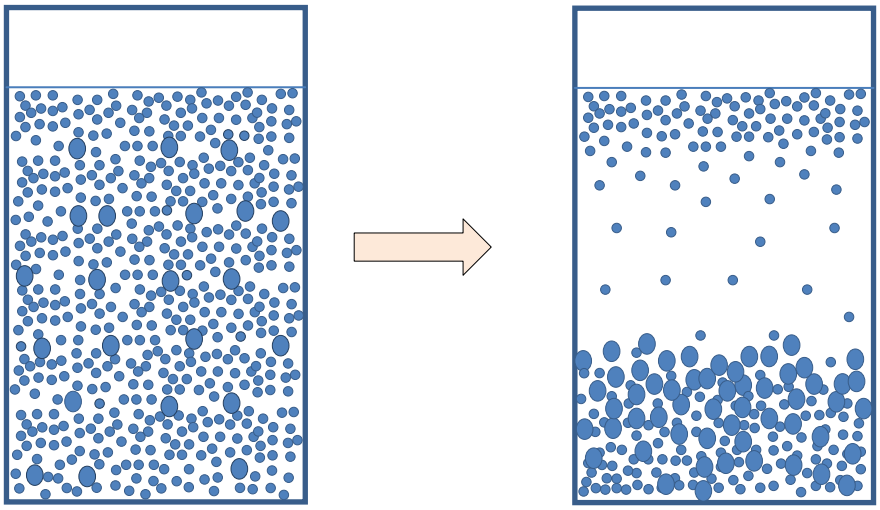

Figure 6.25. Smaller particles are caught by larger ones due to differential settling, so the concentration of particles is much lower in the middle region than at the top.

6.6.3.2 Modeling

Experimentally, it is not always easy to observe the phenomenon of a multiple diffuse layers, especially when the suspending liquid is opaque. Conversely, modeling can provide enough detailed information to demonstrate such an effect. Figure 6.26 shows a settling curve from a numerical study. Here, the primary particles consisted of 5 and 35 μm (90 wt% and 10 wt% respectively) spherical particles in water (1 % by weight concentration). The collection tray is

placed 1.5 cm below the surface, and the collision efficiency is equal to unity. Due to poly-dispersity in size, the rate of sedimentation goes through several inflection points.

Simulation results have been used to show the mass concentration of solids material in the vessel as time progresses. Figure 6.27 shows the mass concentration of solids at different heights in a settling column by colour. The yellow colour corresponds to clear liquid or zero concentration. The dark green colour denotes the initial concentration of the solids; this turns to lighter green as the concentration decreases. A mud line is developed and descends as time progresses. However, a layer of concentrated particles remains at the top. The primary mud line reaches the bottom after a certain time, but the column still contains a cloudy suspension at a lower concentration. Here, a layer of concentrated particles exists above the low concentration region. This is the situation of an 'inversion phenomenon' which occurs sometimes in sedimentation systems. The second mud line descends at a lower speed. It will leave a clear liquid at the end.

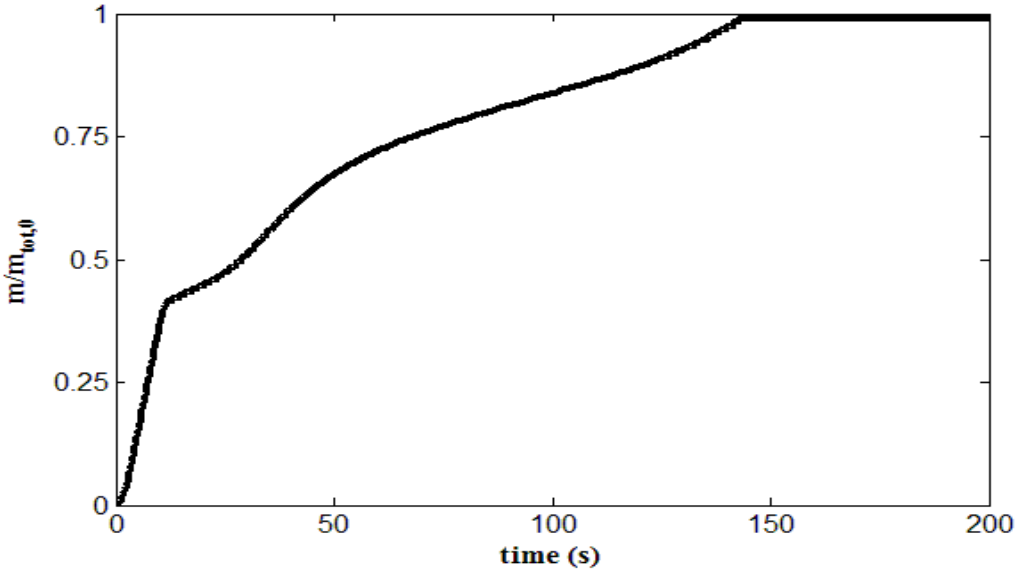

Figure 6.26. Theoretical settling curve of a suspension of 1 wt% of 5 and 35 micron silica particles in water. The collecting tray was placed 15 mm below the surface, and the collision efficiency α was 1.

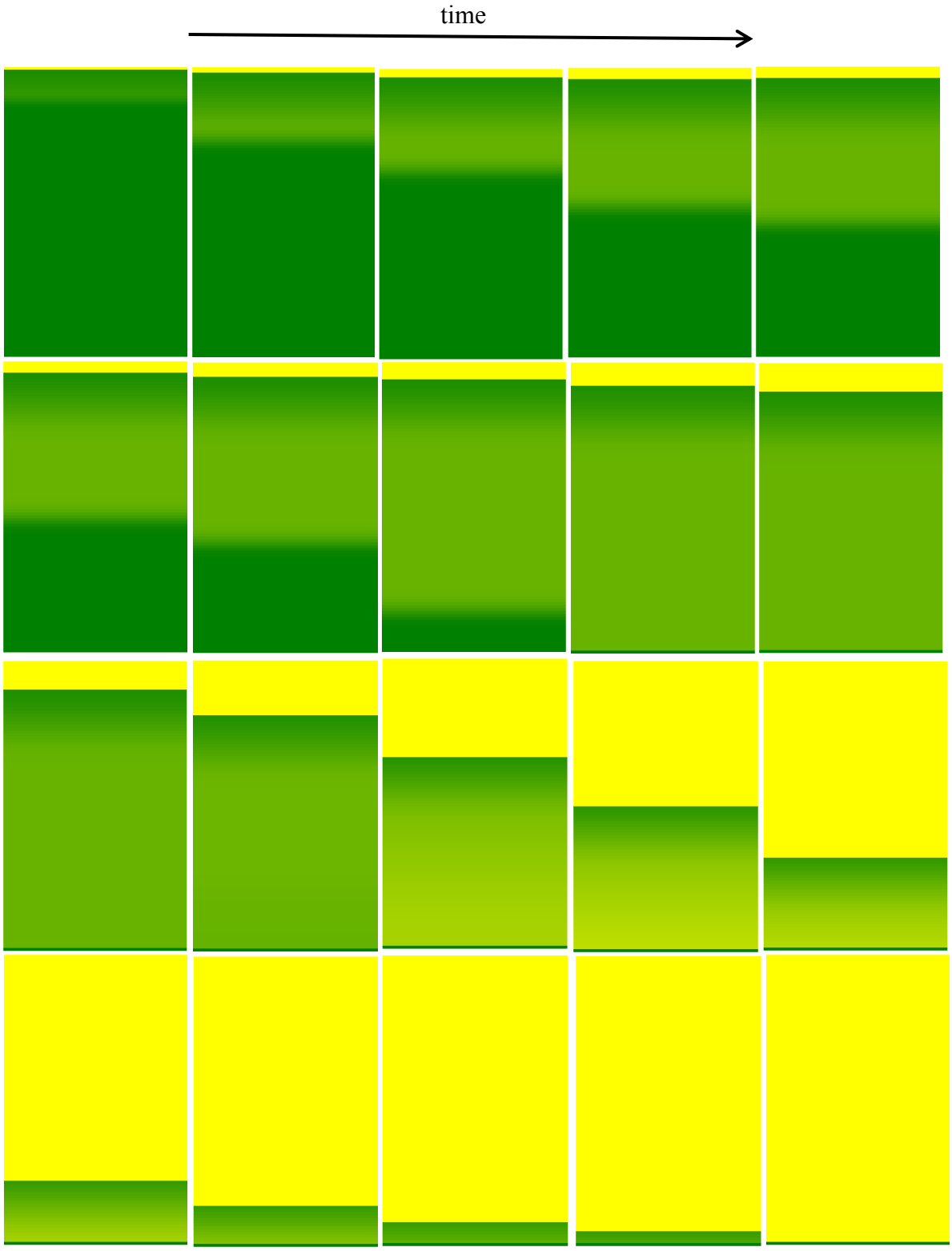

Figure 6.27. Simulation results showing the sedimentation of particulates in a suspension. The yellow colour indicates clear liquid while dark green denotes the highest particle concentration. Multiple diffuse layers are seen in the concentration profiles.

7 Effect of initial size distribution

The particle size is of great importance in many industrial processes; for example, it plays a central role in the design of settling tanks. Smaller particles have lower settling velocities, which in turn require larger settling equipment. If the particles individually settle (i.e. according to Stokes' law), the settling velocity is proportional to the third power of the characteristic length *L* (i.e. $v \sim L^3$). This means when the particle size doubles, it will settle eight times faster. However, when aggregation comes into effect, the size of the particles will not remain constant and therefore the above rule will no longer apply. The primary particles will combine and make aggregates of various sizes as time proceeds; before long, the initial particle size distribution (PSD) may be 'forgotten.' In this section, the effect of initial PSD on the overall kinetics of aggregation and sedimentation will be examined.

Note that in the study of size distribution, a single number (such as the average size) cannot describe the distribution of the sample. Usually, a central point of the distribution, along with one or more values which characterize the width of the PSD, are reported. Therefore, one should distinguish between two equally important descriptor of a distribution: (1) central point, and (2) width describing how much the distribution is spread out. We deal with these two quantities separately in the following sections. We first focus on the second parameter assuming that the central size value is the same; only the width of the PSD is different. In all cases, it is assumed that the primary particles are, at time $t = 0$, distributed uniformly in a settling column.

7.1 The width of distribution

Different PSDs can share the same peak (e.g. the value of highest probability), but their widths can be quite different from one another; Figure 7.1 illustrates some of such distributions. Almost all real particle samples exist as a distribution of sizes. In industrial applications, the real particles to be separated in settling tanks are not mono-sized, although the tanks are often designed with only one average size in mind. It is thus desirable to investigate the effect of PSD width on the settling behaviour.

Numerical simulation is used here to predict the behaviour of situations with different initial PSDs (shown in Figure 7.1). The suspension is assumed to consist of silica particles in heptane, and a sedimentation balance (Figure 3.2) is used to characterize settling process. The sampling point is 1 cm below the free surface. The simulation results (scaled mass versus time at a fixed location) were plotted in Figure 7.2. The only difference between four cases is the initial PSDs; the other properties have been kept unchanged. Interestingly, all the curves fell on top of each other, indicating that the settling behaviour is insensitive to initial PSD under certain condition (i.e. here in this case the width of distribution is different, but they share the same peak).

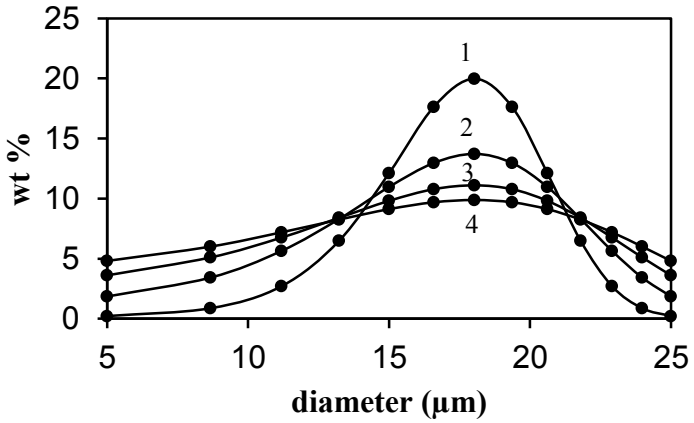

Figure 7.1. A mixture of spherical particles of various diameters was used to mimic the initial particle size distribution (PSD). In the mixtures, the amount of each size could be different.

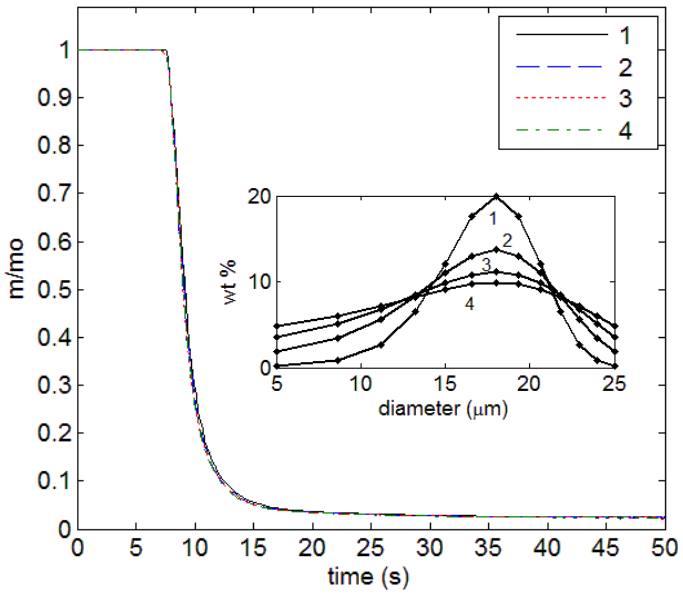

Figure 7.2. Theoretical settling curves (scaled mass concentration at a fixed location) against time for four different initial PSDs. The results suggest that, given a common average size, the width of the initial PSD does not influence the settling behaviour.

With regards to experiments, a series of tests was also conducted to study the effect of PSD. Two mixtures of silica particles (A and B), as shown in Figure 7.3, were used to carry out settling tests using the sedimentation balance (see Section 3.2 for details). These two samples were mixtures of 0.25, 0.5, and 1μm silica particles at different mass ratios. The peaks occur at the same size, but the compositions were different. The particles were suspended in water at pH 2 (point of zero charge, which leads to rapid coagulation). The settling curves (amount of mass collected on the tray) were plotted in Figure 7.4. The tray was located at a depth of 15 mm in the suspension. The settling curves were close enough to conclude that the settling curves were insensitive to the initial PSDs (while sharing a common peak size).

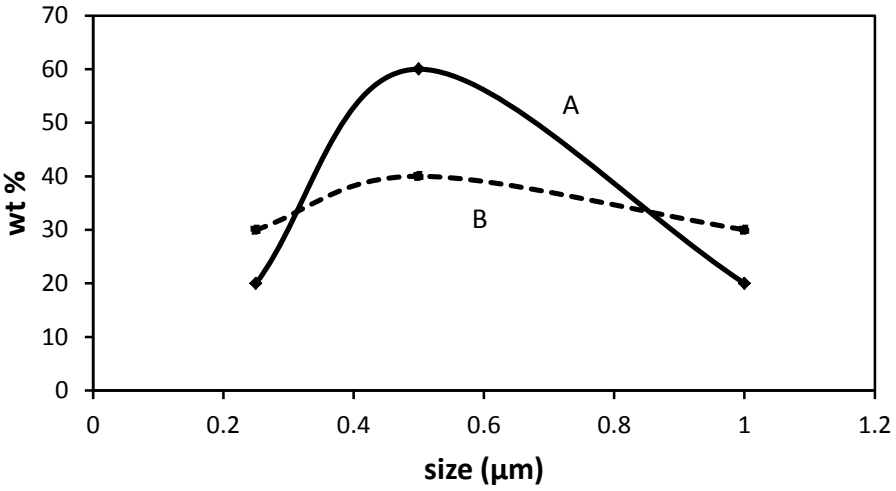

Figure 7.3. Two mixtures of silica particles comprising 0.25, 0.5 and 1µm beads at different mass fractions. The mass fractions were adjusted so that the two mixtures share a common average size.

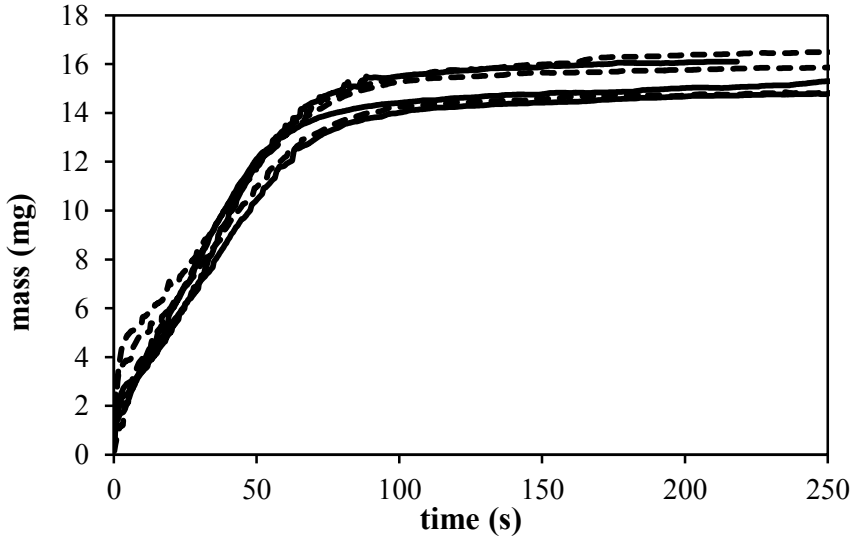

Figure 7.4. Experimental settling curves for a suspension of two mixtures of silica particles (Mixtures A and B, as indicated in Figure 7.3) in water at pH 2. The solid lines are the results for Mixture A, and the dashed line for Mixture B.

The above theoretical and experimental results indicate that, for PSDs of the same average size (weighted by mass), the settling behaviours are insensitive to the width of the size distribution. However, the settling behaviour might be influenced if the initial PSDs were significantly

dissimilar (i.e. in a case where the initial PSDs have different peaks). Further simulations were carried out to investigate such a conjecture. Figure 7.5 shows two size distributions with slightly different peaks.

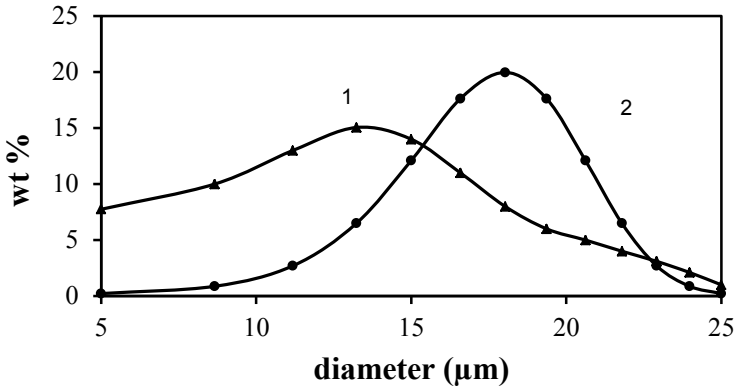

Figure 7.5. Two significantly different initial PSDs applied to the model to study effect of its dissimilarity on the settling behaviour.

These new initial PSDs were then applied as the initial condition to solve the simulation equations. The resulting settling curves were compared in Figure 7.6. It is remarkable that, given the different PSDs shown in Figure 7.5, the settling curves were practically overlapped.

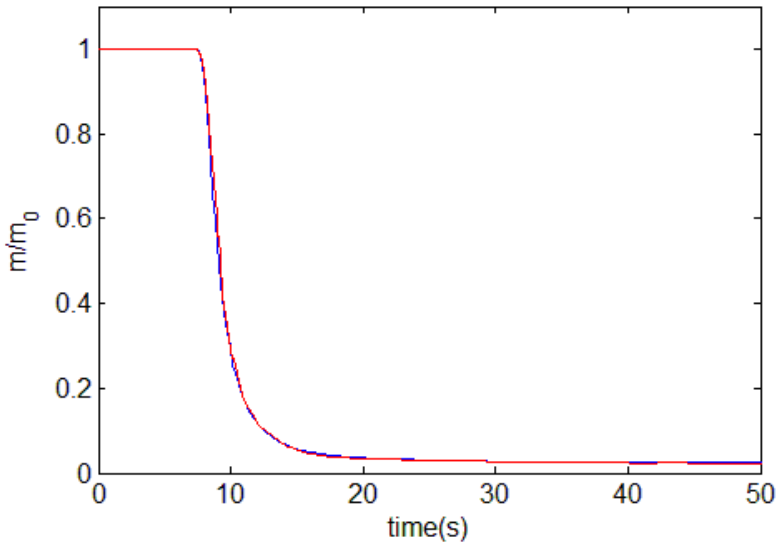

Figure 7.6. Theoretical settling curves (plotted in red and blue) resulting from the two initial PSDs shown in Figure7.5.

For another two mixtures shown in Figure 7.7, the collected mass at the tray (i.e. similar to a sedimentation balance experimental test) was plotted. Again, our numerical simulation shows that in this case the settling curves are insensitive to the initial PSD.

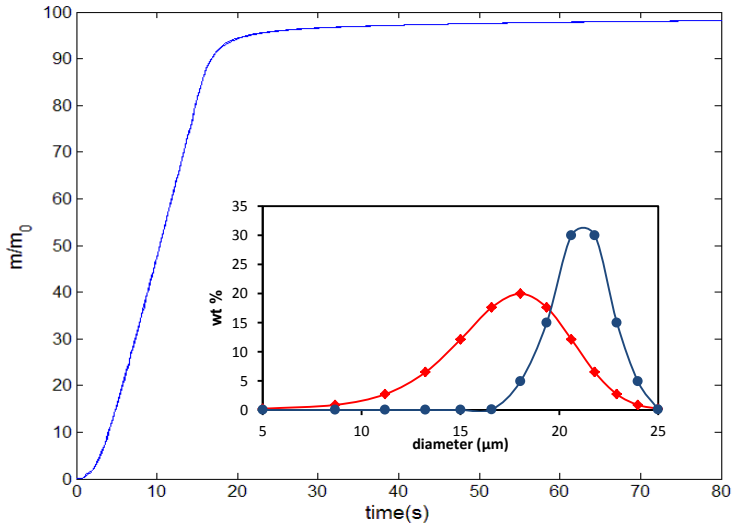

Figure 7.7. Numerical simulation of the cumulative mass collected by a plate at a depth of 2 cm. The primary particles, 1 micron in diameter, were allowed to grow to a size of 1000. The solids concentration was set at 5 wt%.

Nonetheless, one may expect to see variations in the settling rate if the initial PSDs were vastly different. (The settling rate of a 1-micron particle would be quite different from that of a 10-micron particle, for example.) In order to model such a scenario, the initial PSDs were selected in such a way that the initial size distributions are very different. The peaks were located further from each other as displayed in Figure 7.8.

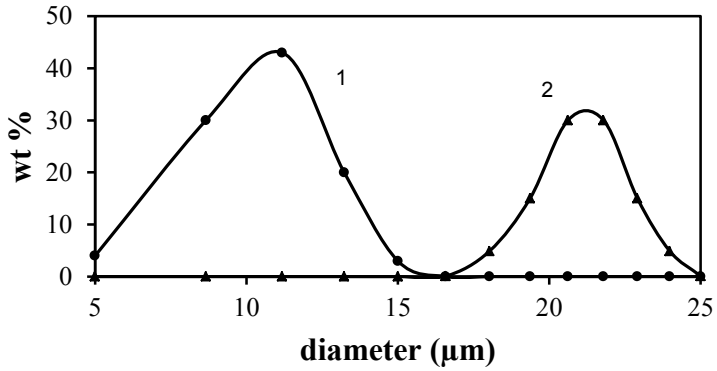

Figure 7.8. Initial PSDs for the case of vastly different mixtures of primary particles

Figure 7.9 presents the results of a study carried out for these initial PSDs. It shows that if the initial conditions were sufficiently dissimilar, the settling curves would no longer overlap. Similar to a buffer solution, the settling behaviour of a mixture of fine particles shows insensitivity to the initial PSD; however, this 'buffering effect' breaks down when the initial perturbation becomes too large.

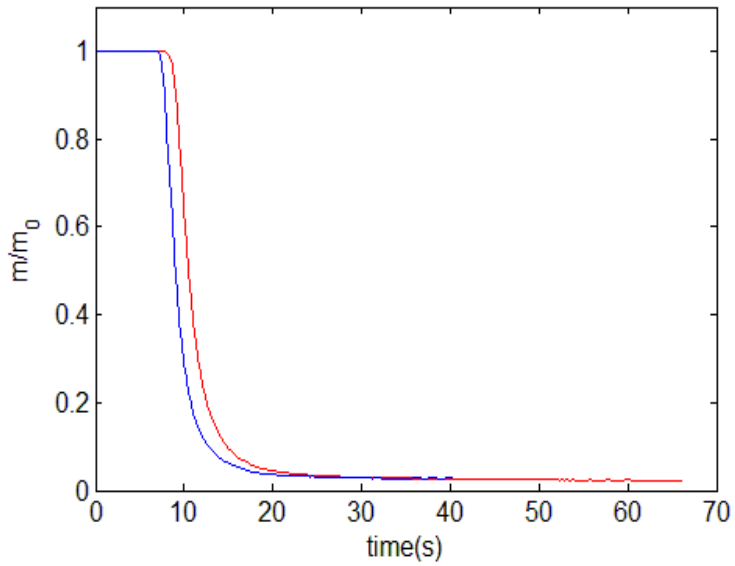

Figure 7.9. Theoretical settling curves resulting from initial PSDs in Figure 7.8.

The commutative mass collected at the tray was also plotted in Figure 7.10. The tray was located at a depth of 2 cm.

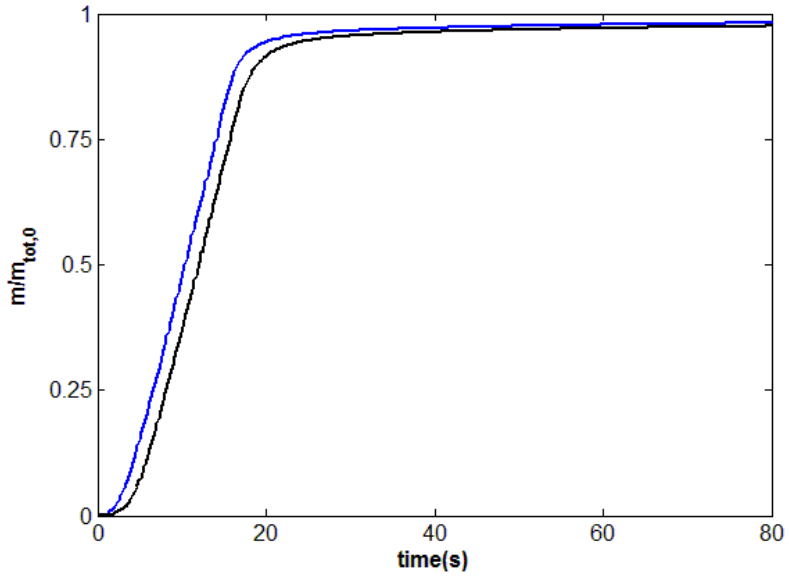

Figure 7.10. Cumulative mass collected on a plate at a depth of 2 cm. The two samples have initial PSDs specified in Figure 7.8.

7.2 The central value of distribution

It is believed that large particles always fall faster than small particles of the same material. For example, suppose that two spherical glass beads are allowed to settle in water: it is clear that the larger bead will settle faster than the smaller one; it is because the larger bead has a higher Stokes velocity. This obvious result, however, may not be easily extended to aggregating particles. When it comes to a large number of particles, aggregation may turn all predictions 'upside down.' The question arises here is whether a suspension of large particles still settle faster than smaller ones, if they aggregate at the same time.

Let us compare two samples of particles of the same material and same weight suspended in a given amount of liquid in two separate containers. One sample consists of particles with smaller

size than the other. If the particles do not aggregate, assuming they are spherical, their settling velocity (terminal velocity) will follow Stokes' law; their velocity will not change as they move downwards. On the contrary, when aggregation comes into play, the particles attach to the others on their way to the bottom; this process will make larger objects (aggregates) which settle faster. The settling velocity of these entities, then, constantly increases as they travel more distances.

At $t = 0$, all particles — in the form of singlets — begin aggregating. Both initially large and small particles aggregate, but the rate of aggregation is higher among small particles than large particles (not due to size but because at the same mass concentration, there would be larger number of small particles suspended in the fluid). After a while, when the particles travel a certain depth, initially small particles are now large enough that they can settle at the same rate of the initially large particles.

If there is still large amounts of particles suspended in the fluid, aggregation continues so that one may see that at a deeper location, initially smaller particles settle even faster than initially large particles. Note that when we compare two suspensions (i.e. small size against large size) with the *same mass concentration*, this phenomenon will be observed only if two following conditions are met:

1. The mass concentration of particles should be above a certain amount. The availability of enough amounts of particles to participate in the aggregation is necessary to obtain the desired result.
2. If one lets the aggregation occur, then after enough time (corresponding to a certain depth), the rate of settling of initially small particles will catch up to the rate of settling of

initially large particles; therefore, larger particles will not necessary settle faster than smaller particles.

To verify this hypothesis, we use a simple model: we compare two suspensions in two separate containers. Sample a contains $1\,\mu m$ particles, and sample b contains $0.5\,\mu m$ diameter; both samples are suspended in water. The mass concentrations of samples a and b in suspension is kept identical; therefore, the number concentration of particles in suspension b is eight times the number concentration of sample a; (at $t = 0$, we assume that the number concentration of particles in suspension a is $10 \times 10^{17} m^{-3}$). We let the particles in both suspensions aggregate according to Smoluchowski equation of balance (see Eq.(5)). For simplicity, we assume the particles coalesce upon collision (i.e. $d_f = 3$), and the collision efficiency is 100%. Differential settling was considered as the dominant collision mechanism (Eq.(3)). Since aggregation by differential settling will not start if all particles are of the same size, we introduce a small amount of doublets in the suspensions (about 4 wt% doublets). As time proceeds, the average size of the aggregates in both suspensions is determined according to Eq. (44); the results are shown in Figure 7.11.

At $t = 0$, suspension a contains larger particles ($1\,\mu m$) while suspension b includes smaller ones ($0.5\,\mu m$). The average size increases over time; the only difference is that particles in suspension b grow much faster so that their average size will become equal and even greater than that in suspension a. This will cause the particles in suspension b settle faster than the ones in suspension a.

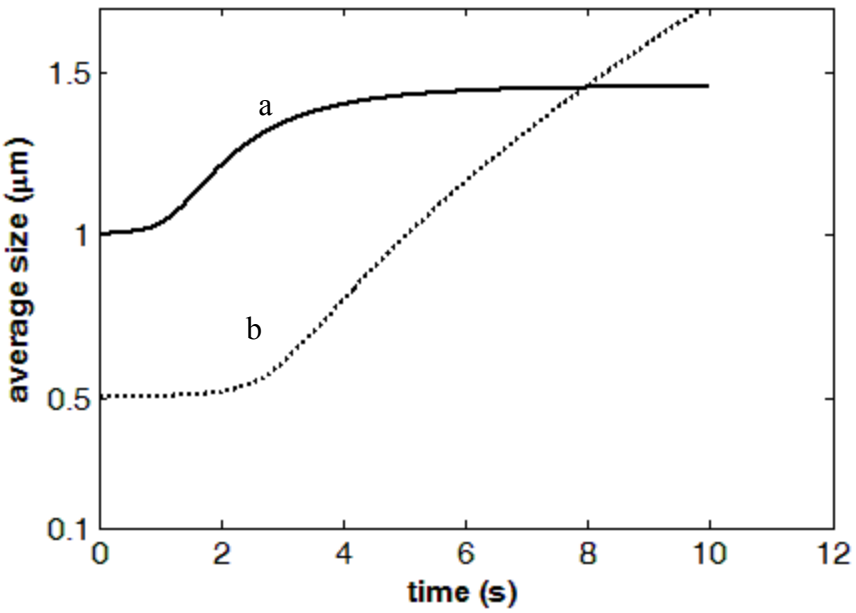

Figure 7.11. The average size of aggregates against time in suspension a and b. Number concentration of particles in suspension a is equal to $10 \times 10^{17} m^{-3}$, and is $80 \times 10^{17} m^{-3}$ in suspension b.

Note that this phenomenon is observed only if the initial concentration of materials in the suspension is large. We reduced the concentration to half of what it was in the above trial (let number concentration of sample a be equal to $5\times 10^{17}\mathrm{m}^{-3}$). The average size of aggregates over time is shown in Figure 7.12. Contrary to what was observed earlier, within the same time period, the average size of aggregates in suspension b remains less than that in suspension a. Therefore, one observes that particles in suspension b settle at a lower velocity comparing to suspension a.

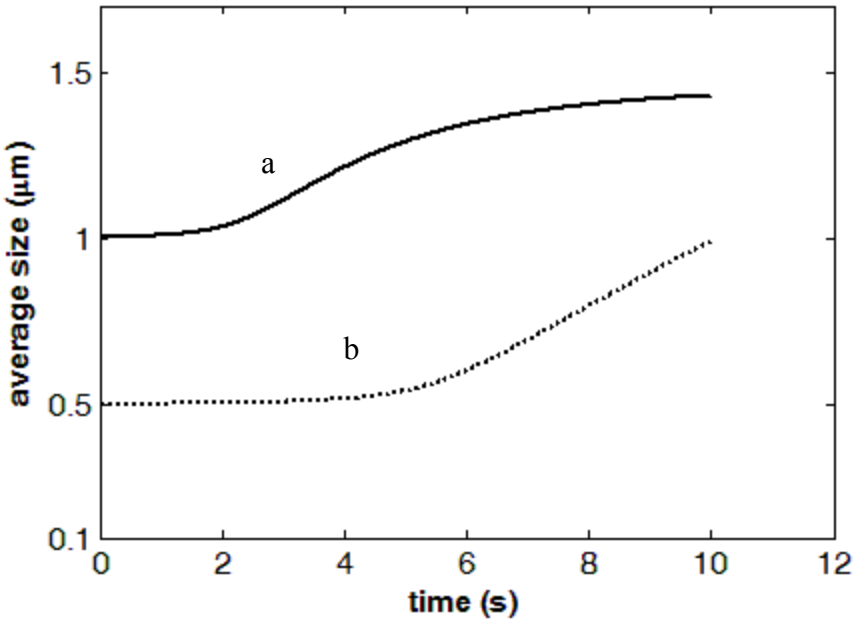

Figure 7.12. The average size of aggregates against time in suspension a and b. Number concentration of particles in suspension a is equal to $5 \times 10^{17} m^{-3}$, and that for suspension b is $40 \times 10^{17} m^{-3}$

Experimental observations

To examine the above theory experimentally, a series of sedimentation tests was conducted by using the sedimentation balance. Three separate suspensions of silica beads with different sizes ($0.25\ \mu m, 0.5\ \mu m,$ and $1\ \mu m$) were prepared in three containers. The mass density of the particles was set to 1.5wt%, and they were fully suspended in deionized water at pH=2. A collecting tray was placed at 10 mm below the surface (see Section 3.2 for details of procedure). At time $t = 0$, the particles were allowed to settle. We knew previously that silica particles aggregate at pH=2, therefore aggregation and sedimentation occur together. The amount of mass collected on the tray was measured over time; the results are shown in Figure 7.13.

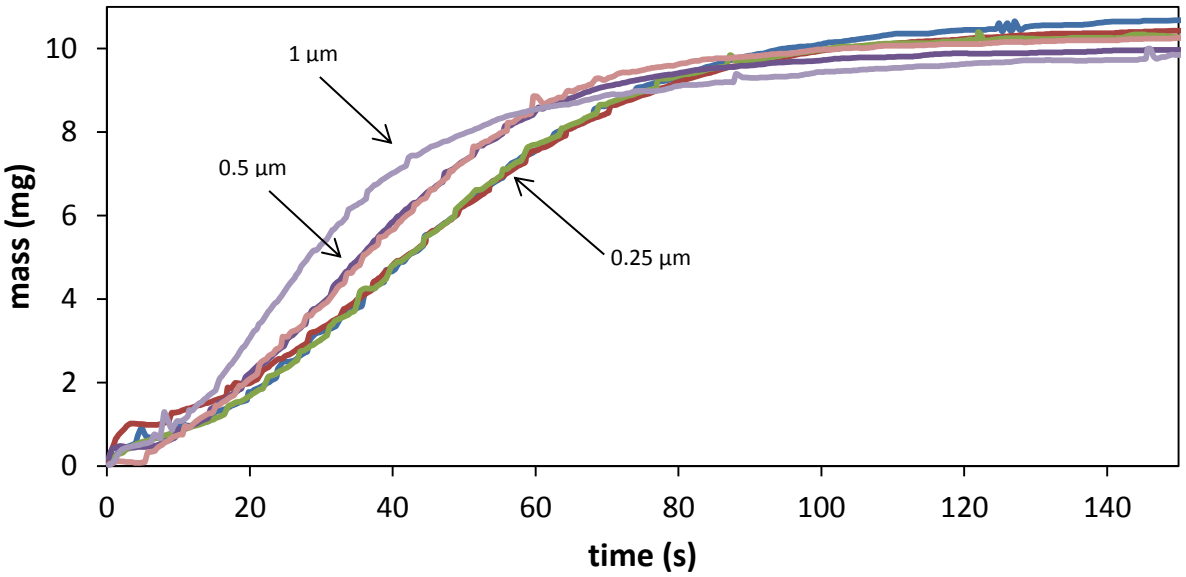

Figure 7.13. The settling curves of 1.5 wt% silica particles (0.25, 0.5 and 1 µm) in water at pH=2. The settling probe was at 10 mm below surface.

As it was generally expected, Figure 7.13 shows that 1 µm particles settled faster so that the corresponding curve took less time to turn around and level out. The 0.25-micron particles were the slowest particles to settle. This is in agreement with the general belief that larger particles settle faster than small ones. However, we showed earlier that if the concentration of particles increases, aggregation may produce larger aggregates from small particles that settle faster; the question is whether a higher concentration (e.g. 3wt% instead of 1.5 wt%) of particles will contain enough amounts of particles for a required degree of aggregation? Is Condition 1 met by increasing the concentration from 1.5 wt% to 3 wt% ?

Examination of Condition 1, concentration:

To answer the question, another series of experiments were conducted with 3 wt% of materials in water. All other properties were kept similar. Figure 7.14 presents the settling curves. It shows that the 1-micron particles settled faster than the other two; however, the 0.25-micron particles

seem to settle at the same rate as the 0.5-micron particles. It shows that aggregation of 0.25-micron particles has created large entities that settle at a rate equal to settling rate of initially 0.5-micron particles. Nonetheless, the concentration of primary particles (i.e. 3 wt%) was only enough to make particles of 0.25 µm settle at about the same rate for particles of 0.5 µm in size. Therefore, if we increase the concentration again, we would expect to see the 0.25-micron particles settle even faster than before. To test this situation, experiments were repeated with a greater value of concentration (the mass concentration of silica particles in samples were increased to 5 wt%). The settling curves are shown in Figure 7.15.

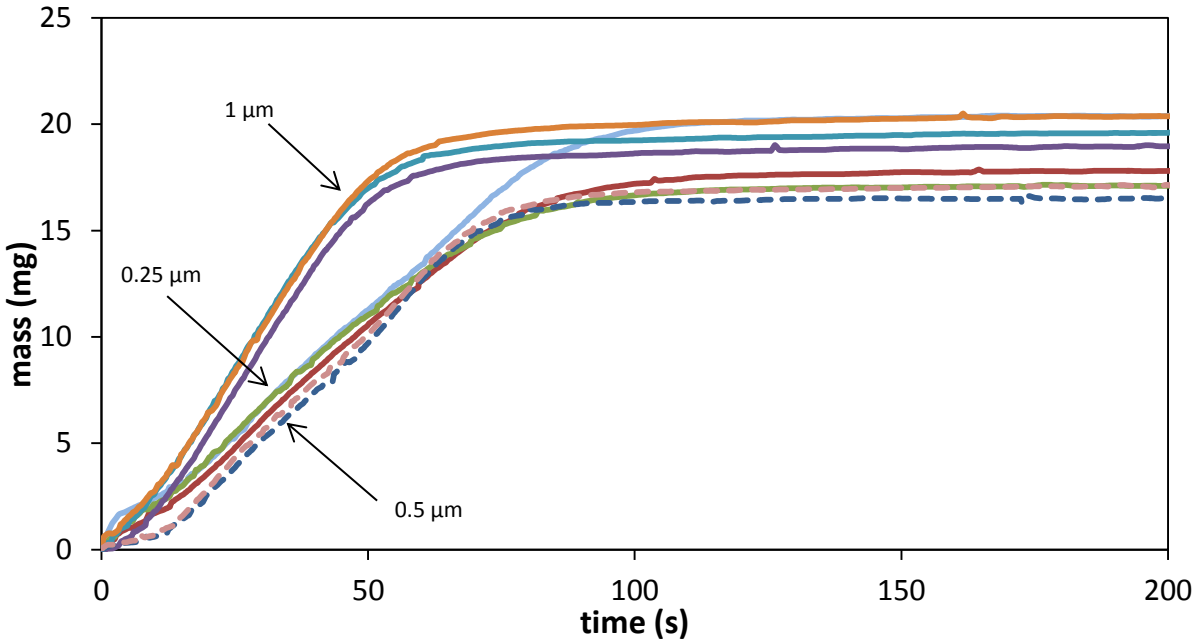

Figure 7.14. The settling curves of 3 wt% silica particles (0.25, 0.5 and 1 µm) in water at pH=2. The settling probe was at 10 mm below surface.

Figure 7.15 shows that by increasing the mass concentration, the rate of aggregation has been increased significantly so that the 0.25-micron particles settle even faster than 0.5-micron particles. The settling curve has passed the settling curve of 0.5-micron particles, although it was still slower than 1-micron particles.

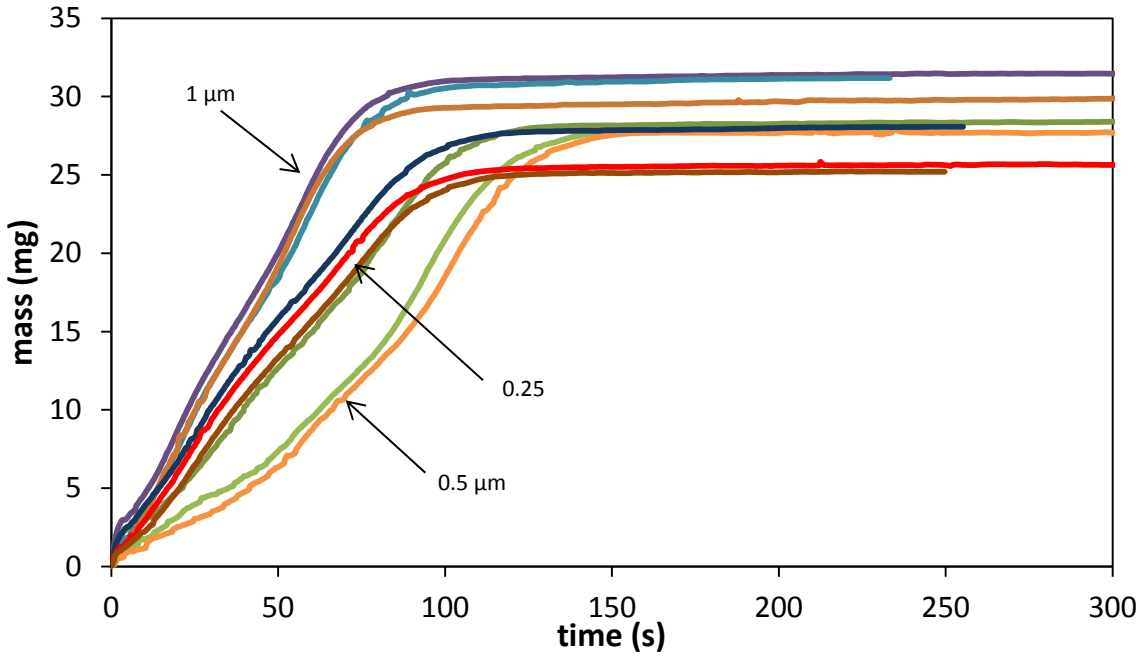

Figure 7.15. The settling curves of 5 wt% silica particles (0.25, 0.5 and 1 µm) in water at pH=2. The settling probe was at 10 mm below surface.

Examination of Condition 2, time:

The second condition mentioned in the theory was that the particles should aggregate for a long enough time. To examine this condition experimentally, another series of experiments was conducted with similar mass concentration (i.e. 5 wt%), but this time the collecting tray was placed at 15mm below the free surface. A longer time period, in order to provide more aggregation time, would be achieved by relocating the collecting point to a deeper place. The settling curves are shown in Figure 7.16. It seems that the 0.25-micron particles settled at about the same rate as the 1-micron particles. This evidence proves that the aggregation time is a key parameter affecting the settling behavior. We can therefore conclude that there is a certain time (accordingly, a certain sampling depth) at which small particles settle at the same rate as large particles. It is the point after which the particles 'forget their history' (re: their initial PSD).

We tried another series of experiments by placing the collecting tray 30 mm below the free surface. At a deeper location, the 0.25-micron particles settle much faster; in this case even the settling rate of 0.5-micron particles could catch up to the settling rate of 1-micron particles (Figure 7.17) so that they settle almost at the same rate as the settling rate of the 1-micron particles.

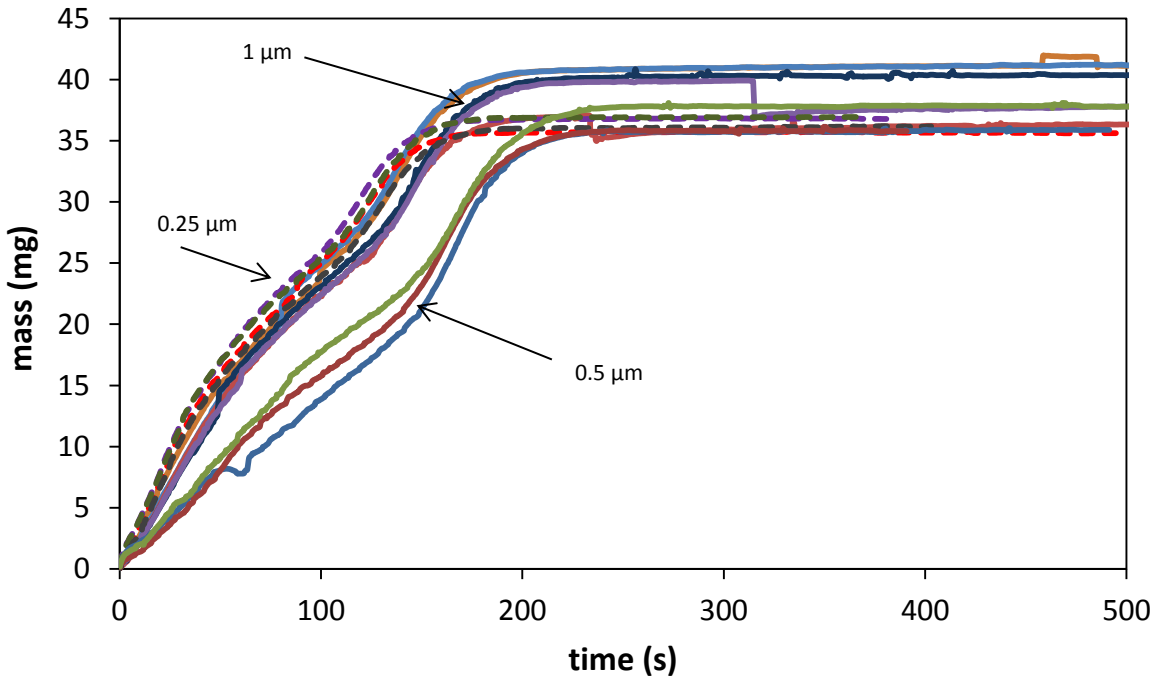

Figure 7.16. The settling curves of 5 wt% silica particles (0.25, 0.5 and 1 µm) in water at pH=2. The settling probe was at 15 mm below surface.

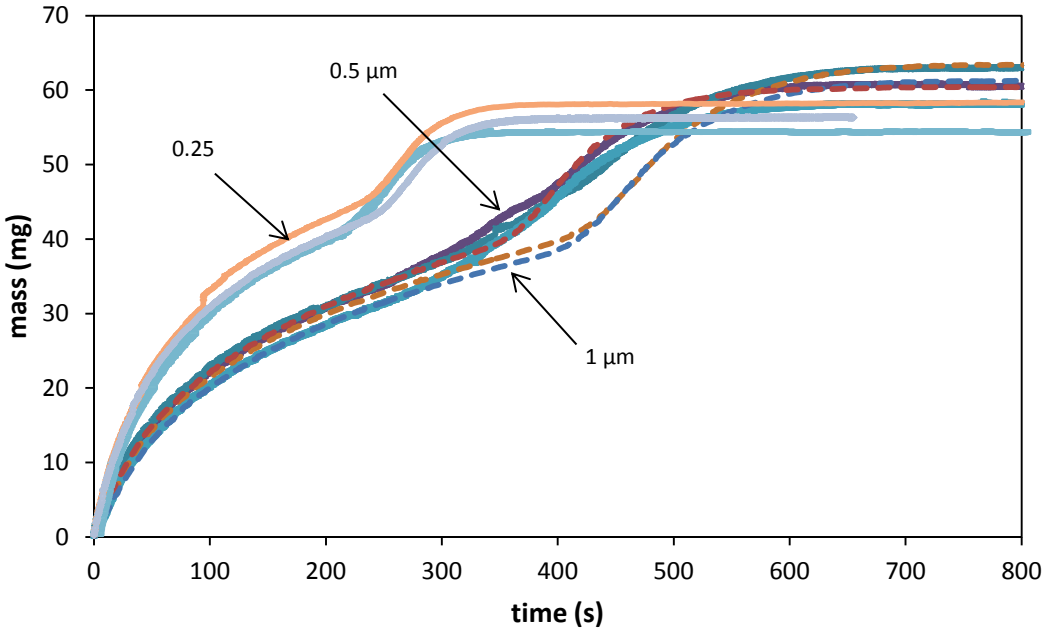

Figure 7.17. The settling curves of 5 wt% silica particles (0.25, 0.5 and 1 µm) in water at pH=2. The settling probe was at 30 mm below surface.

8 Conclusion remarks

The aggregation and sedimentation of fine particles in a liquid was studied both theoretically (with development of a detailed model) and experimentally. Our model accounts for spatial variations in particle densities, which is a new and important extension to all current theories. Moreover, our model is capable of predicting the overall dynamics which results from two simultaneously occurring effects, namely, aggregation and sedimentation. In the design of settling tanks in which both aggregation and sedimentation take place, it is not sufficient to only consider a cut off size; the underlying kinetics is much more complicated and requires deeper insights into the overall process. The results of this study provide just such information (e.g. in the explanation of an 'induction time,' and the relation between settling rate and initial particle size distribution). Although this is a general study of the sedimentation process, its major motivation is the separation of unwanted fine particulates from diluted bitumen. In the process of bitumen extraction from the Canadian oil sands, a new approach has been proposed that uses an organic solvent instead of water to liberate bitumen from oil sands ores. One of the main challenges of such a technology has been the removal of suspended fine solids in hydrocarbon. The results of this research will contribute to the solution of this problem, in particular, the elimination of the unwanted fines by gravity settling.

The following are highlights of this research:

- A detailed numerical model of aggregation and sedimentation was developed which applies to situations that have *non-uniform* particle distributions. All previous studies in

the literature were limited to either macromolecular structures (50 nm or smaller) or applications involving vigorous (i.e. turbulent) mixing; there was also no treatment of non-uniform particle distributions in those studies due to the complexity of the phenomena. Here, all main issues of aggregation and sedimentation, including fractal properties of the aggregates, were taken into account. Solutions to the equations were discussed, and the model was successfully solved through two different approaches and then validated against the experimental results.

- The model provides deeper insights into the performance of settling units through prediction of detailed dynamics of aggregation and sedimentation.
- The model revealed valuable information regarding the formation of a 'mud line,' which is the interface between clear liquid at the top and a 'cloudy' suspension at the bottom. This is an important issue as most experiments on sedimentation are based on following the location of this mud line over time. Our model showed how the various mud lines are formed and predicted the thickness of such lines.
- One of the most important issues in the design of sedimentation units is the size distribution of particles. Although the settler is designed for a specific size range of particulates, the feed that is sent to the equipment may not be always be of the appropriate size distribution. This study resulted in two main conclusions: (a) The settling behaviour will remain insensitive to the initial size distribution if the median size remains unchanged. Distribution of sizes around a common median, and even moderate changes of the median value, will not affect the settling behaviour. (b) If aggregation continues for sufficiently long time, the initial size distribution may be 'forgotten'; this

means that a suspension of initially smaller particles may settle faster than a suspension containing initially larger particles.

- The kinetics of the sedimentation process was studied through experiments and numerical modeling. There were situations when an "induction time" (i.e. an apparent delay before aggregation began) was observed. We showed here, from our simulation results, that the apparent induction time may be an artifact resulting from the unique kinetics of aggregation.

Recommendations and future work

The aggregates can grow to large species (e.g. as big as 1mm) if they remain in the liquid for a long enough time period. When these aggregates reach the bottom of the vessel, they join the others to make a packed bed. We suppose that aggregation continues until the aggregates arrive at the bed. If the primary particles are very small (i.e. in the sub-micron range), thousands and thousands may attach to each other. Therefore, the suspension contains thousands of aggregate sizes. The model should keep track of these thousands of aggregates at each time step, which is not practical with current computing capabilities. However, in the future, the code developed in this study can be used to study such large systems.

Particles make fractal objects when they aggregate. In this study, it was assumed that the fractal dimension d_f of all aggregates were equal. Actual aggregates, however, may become restructured as time progresses so that some aggregates may not have the same fractal dimension as the others. Therefore, a single value of the fractal dimension may not represent the entire range of aggregate sizes. With enhanced computational powers in the future, it may be possible to take this phenomenon into account. This will require storing more information of the

aggregates when they coagulate and settle. It is also recommended that the fractal dimension of the particles be measured experimentally. With this new information, the values of d_f in the model can then be adjusted accordingly.

By combining experimental and modeling results (i.e. by fitting theoretical predictions to empirical data), it is possible to predict the collision efficiency α of any situation, especially for the case of fine clays in diluted bitumen. This is important as the collision efficiency is the primary parameter which affects the kinetics of aggregation.

The numerical and experimental studies in this research were focused exclusively on situations with low concentration of suspended materials, as fine particles are usually at low concentrations in our bitumen-related applications. However, our theoretical model can be extended to examine the effects of particle concentration on sedimentation kinetics, especially in the regime of hindered settling.

References

[1] E. G. Kelly and D. J. Spottiswood, *Introduction to mineral processing*. New York: Wiley, 1982.

[2] B. A. Wills, *Mineral processing technology : an introduction to the practical aspects of ore treatment and mineral recovery*, Seventh Ed. Butterworth-Heinemann, 2006, p. 16.

[3] M. C. Fuerstenau and K. N. Han, Eds., *Principles of mineral processing*. Society for Mining, Metallurgy, and Exploration, Inc., 2003.

[4] D. Lesueur, "The colloidal structure of bitumen: consequences on the rheology and on the mechanisms of bitumen modification.," *Adv. Colloid Interface Sci.*, vol. 145, no. 1–2, pp. 42–82, Jan. 2009.

[5] Y. Jin, W. Liu, Q. Liu, and A. Yeung, "Aggregation of silica particles in non-aqueous media," *Fuel*, vol. 90, no. 8, pp. 2592–2597, Aug. 2011.

[6] R. J. Hunter, *Foundations of collloid science*, Second Edi. New York: Oxford University Press, 2001.

[7] J. Richardson, J. Harker, and J. Backhurst, *Coulson and Richardson's Chemical Engineering*, Fifth Edit., vol. 2. Oxford: Boston- Butterworth-Heinemann, 2002.

[8] M. Elimelech, J. Gregory, X. Jia, and R. Williams, *Particle deposition and aggregation: measurement, modelling and simulation*. Elsevier, 1995.

[9] S. Friedlander, *Smoke, dust, and haze Fundamentals of aerosol dynamics*, 2nd ed. Oxford University Press, 2000.

[10] J. Israelachvili, *Intermolecular and surface forces*, Third Edit. Elsevier, 2011.

[11] P. Van der Hoeven and J. Lyklema, "Electrostatic stabilization in non-aqueous media," *Adv. Colloid Interface Sci.*, vol. 42, pp. 205–277, 1992.

[12] J. Gregory and C. R. O'Melia, "Fundamentals of flocculation," *Crit. Rev. Environ. Control*, vol. 19, no. 3, pp. 185–230, Jan. 1989.

[13] A. Alldredge and P. McGillivary, "The attachment probabilities of marine snow and their implications for particle coagulation in the ocean," *Deep Sea Res. Part A. Oceanogr. ...*, vol. 38, no. 4, pp. 431–443, 1991.

[14] R. L. Zollars and S. I. Ali, "Shear coagulation in the presence of repulsive interparticle forces," *J. Colloid Interface Sci.*, vol. 114, no. 1, pp. 149–166, Nov. 1986.

[15] C. P. Johnson, X. Li, and B. E. Logan, "Settling Velocities of Fractal Aggregates," *Environ. Sci. Technol.*, vol. 30, no. 6, pp. 1911–1918, Jan. 1996.

[16] P. Meakin, "Fractal aggregates," *Adv. Colloid Interface Sci.*, vol. 28, pp. 249–331, 1988.

[17] M. Tence, J. P. Chevalier, and R. Jullien, “On the measurement of the fractal dimension of aggregated particles by electron microscopy: experimental method, corrections and comparison with numerical models,” *J. Phys.*, vol. 47, no. 11, pp. 1989–1998, 1986.

[18] P. Tang and J. Raper, “Modelling the settling behaviour of fractal aggregates–a review,” *Powder Technol.*, pp. 114–125, 2002.

[19] J. R. Kilps, B. E. Logan, and A. L. Alldredge, “Fractal dimensions of marine snow determined from image analysis of in situ photographs,” *Deep Sea Res. Part I Oceanogr. Res. Pap.*, vol. 41, no. 8, pp. 1159–1169, Aug. 1994.

[20] R. K. Chakraborti, J. F. Atkinson, and J. E. Van Benschoten, “Characterization of Alum Floc by Image Analysis,” *Environ. Sci. Technol.*, vol. 34, no. 18, pp. 3969–3976, Sep. 2000.

[21] A. Thill, S. Veerapaneni, B. Simon, M. Wiesner, J. Bottero, and D. Snidaro, “Determination of Structure of Aggregates by Confocal Scanning Laser Microscopy.,” *J. Colloid Interface Sci.*, vol. 204, no. 2, pp. 357–62, Aug. 1998.

[22] W. Lick, H. Huang, and R. Jepsen, “Flocculation of fine-grained sediments due to differential settling,” *J. Geophys. Res.*, vol. 98, no. 4, pp. 279–288, 1993.

[23] P. Tang, J. Greenwood, and J. a Raper, “A model to describe the settling behavior of fractal aggregates.,” *J. Colloid Interface Sci.*, vol. 247, no. 1, pp. 210–9, Mar. 2002.

[24] D. Schaefer, J. Martin, P. Wiltzius, and D. Cannell, “Fractal geometry of colloidal aggregates,” *Phys. Rev. Lett.*, vol. 52, no. 26, pp. 2371–2375, 1984.

[25] G. C. Bushell, Y. D. Yan, D. Woodfield, J. Raper, and R. Amal, "On techniques for the measurement of the mass fractal dimension of aggregates.," *Adv. Colloid Interface Sci.*, vol. 95, no. 1, pp. 1–50, Jan. 2002.

[26] Q. Jiang and B. Logan, "Fractal dimensions of aggregates determined from steady-state size distributions," *Environ. Sci. Technol.*, vol. 25, no. 12, pp. 2031–2038, 1991.

[27] J. Martin, J. Wilcoxon, D. Schaefer, and J. Odinek, "Fast aggregation of colloidal silica," *Phys. Rev. A*, vol. 41, no. 8, pp. 4379–4391, 1990.

[28] M. Lin, H. Lindsay, D. Weitz, and R. Ball, "Universal reaction-limited colloid aggregation," *Phys. Rev. A*, vol. 41, no. 4, pp. 2005–2020, 1990.

[29] D. Thomas, S. Judd, and N. Fawcett, "Flocculation modelling: a review," *Water Res.*, vol. 33, no. 7, pp. 1579–1592, 1999.

[30] P. Sandkühler, M. Lattuada, H. Wu, J. Sefcik, and M. Morbidelli, "Further insights into the universality of colloidal aggregation.," *Adv. Colloid Interface Sci.*, vol. 113, no. 2–3, pp. 65–83, May 2005.

[31] P. Somasundaran and V. Runkana, "Modeling flocculation of colloidal mineral suspensions using population balances," *Int. J. Miner. Process.*, vol. 72, no. 1–4, pp. 33–55, Sep. 2003.

[32] T. Matsoukas and S. Friedlander, "Dynamics of aerosol agglomerate formation," *J. Colloid Interface Sci.*, vol. 146, no. 2, pp. 495–506, 1991.

[33] C. Cametti, P. Codastefano, and P. Tartaglia, “Aggregation kinetics in model colloidal systems: a light scattering study,” *J. Colloid Interface Sci.*, vol. 131, no. 2, pp. 409–422, 1989.

[34] F. Concha and R. Burger, “A century of research in sedimentation and thickening,” *Kona*, vol. 20, no. 20, pp. 38–70, 2002.

[35] A. S. Dukhin, S. S. Dukhin, and P. J. Goetz, “Gravity as a factor of aggregative stability and coagulation.,” *Adv. Colloid Interface Sci.*, vol. 134–135, pp. 35–71, Oct. 2007.

[36] S. B. Grant, J. H. Kim, and C. Poor, “Kinetic Theories for the Coagulation and Sedimentation of Particles.,” *J. Colloid Interface Sci.*, vol. 238, no. 2, pp. 238–250, Jun. 2001.

[37] A. S. Kim and K. D. Stolzenbach, “Aggregate formation and collision efficiency in differential settling,” *J. Colloid Interface Sci.*, vol. 271, no. 1, pp. 110–119, Mar. 2004.

[38] C. Wen, L. Zhang, and H. Lin, “The rate of coagulation of particles in a sedimenting dispersion at large Péclet number,” *J. Colloid Interface Sci.*, vol. 142, no. 1, pp. 257–265, 1991.

[39] X. Jia, D. J. Wedlock, and R. a. Williams, “Simulation of simultaneous aggregation and sedimentation,” *Miner. Eng.*, vol. 13, no. 13, pp. 1349–1360, Nov. 2000.

[40] M. Smoluchowski, “Versuch einer mathematischen Theorie der Koagulationskinetic koloider Lösungen,” *Z. Phys. Chem.*, vol. 92, pp. 129–168, 1917.

[41] G. M. Fair and R. S. Geramell, “A mathematical model of coagulation,” *J. Colloid Sci.*, vol. 19, no. 4, pp. 360–372, 1964.

[42] P. Horvai, S. V. Nazarenko, and T. H. M. Stein, “Coalescence of Particles by Differential Sedimentation,” *J. Stat. Phys.*, vol. 130, no. 6, pp. 1177–1195, Dec. 2007.

[43] M. Filella and J. Buffle, “Factors controlling the stability of submicron colloids in natural waters,” *Colloids Surfaces A Physicochem. ...*, vol. 73, pp. 255–273, 1993.

[44] B. Krishnappan, “Modelling of settling and flocculation of fine sediments in still water,” *Can. J. Civ. Eng.*, vol. 17, pp. 763–770, 1990.

[45] K. H. Gardner, T. L. Theis, and T. C. Young, “Colloid aggregation: numerical solution and measurements,” *Colloids Surfaces A Physicochem. Eng. Asp.*, vol. 141, no. 2, pp. 237–252, Nov. 1998.

[46] D. G. Lee, J. Bonner, and L. Garton, “Modeling coagulation kinetics incorporating fractal theories: a fractal rectilinear approach,” *Water Res.*, vol. 34, no. 7, pp. 1987–2000, 2000.

[47] A. Vanderhasselt, “Estimation of sludge sedimentation parameters from single batch settling curves,” *Water Res.*, vol. 34, no. 2, pp. 395–406, Feb. 2000.

[48] A. Zahabi, M. R. Gray, J. Czarnecki, and T. Dabros, “Flocculation of Silica Particles from a Model Oil Solution: Effect of Adsorbed Asphaltenes,” *Energy & Fuels*, vol. 24, no. 6, pp. 3616–3623, Jun. 2010.

[49] M. Balastre, J. . Argillier, C. Allain, and a Foissy, “Role of polyelectrolyte dispersant in the settling behaviour of barium sulphate suspension,” *Colloids Surfaces A Physicochem. Eng. Asp.*, vol. 211, no. 2–3, pp. 145–156, Dec. 2002.

[50] J.-W. Kim and F. Nestmann, “Settling behavior of fine-grained materials in flocs,” *J. Hydraul. Res.*, vol. 47, no. 4, pp. 492–502, 2009.

[51] J. K. Gupta and S. Basu, “Simultaneous aggregation and sedimentation of silica particles in the presence of surfactants,” *Colloids Surfaces A Physicochem. Eng. Asp.*, vol. 255, no. 1–3, pp. 139–143, Mar. 2005.

[52] E. A. Gonzalez and P. S. Hill, “A method for estimating the flocculation time of monodispersed sediment suspensions,” *Deep Sea Res. Part I Oceanogr. Res. Pap.*, vol. 45, no. 11, pp. 1931–1954, Nov. 1998.

[53] C. Allain, M. Cloitre, and F. Parisse, “Settling by cluster deposition in aggregating colloidal suspensions,” *J. Colloid Interface Sci.*, vol. 416, pp. 411–416, 1996.

[54] U. Weilenmann, C. O’Melia, and W. Stumm, “Particle transport in lakes: Models and measurements,” *Limnol. Oceanogr.*, vol. 34, no. 1, pp. 1–18, 1989.

[55] M. C. Sterling, J. S. Bonner, A. N. S. Ernest, C. a Page, and R. L. Autenrieth, “Application of fractal flocculation and vertical transport model to aquatic sol-sediment systems.,” *Water Res.*, vol. 39, no. 9, pp. 1818–30, May 2005.

[56] D. Thomas, S. Judd, and N. Fawcett, “Flocculation modelling: a review,” *Water Res.*, vol. 33, no. 7, pp. 1579–1592, 1999.

[57] M. J. Hounslow, H. S. Mumtaz, A. P. Collier, J. P. Barrick, and A. S. Bramley, "A micro-mechanical model for the rate of aggregation during precipitation from solution," *Chem. Eng. Sci.*, vol. 56, no. 7, pp. 2543–2552, Apr. 2001.

[58] P. Koh, J. Andrews, and P. Uhlherr, "Modelling shear-flocculation by population balances," *Chem. Eng. Sci.*, vol. 42, no. 2, pp. 353–362, 1987.

[59] H. Mumtaz, M. Hounslow, N. Seaton, and W. Paterson, "Orthokinetic aggregation during precipitation: A computational model for calcium oxalate monohydrate," *Chem. Eng. Res. Des.*, vol. 75, no. 2, pp. 152–159, 1997.

[60] K. Mannistu, H. Yarranton, and J. Masliyah, "Solubility modeling of asphaltenes in organic solvents," *Energy & fuels*, vol. 11, no. 3, pp. 615–622, 1997.

[61] S. Vemury and S. Pratsinis, "Self-preserving size distributions of agglomerates," *J. Aerosol Sci.*, vol. 26, no. 2, pp. 175–185, 1995.

[62] J. T. G.Overbeek, *Colloid Science, Vol. I*. New York: Elsevier, 1952.

[63] D. G. Lee, J. S. Bonner, L. S. Garton, A. N. S. Ernest, and R. L. Autenrieth, "Modeling coagulation kinetics incorporating fractal theories: comparison with observed data," *Water Res.*, vol. 36, no. 4, pp. 1056–66, Feb. 2002.

[64] R. Clift, J. R. Grace, and M. E. Weber, *Bubbles, Drops and Particles*. New York: Academic Press, 1978.

[65] J. Gregory, “Monitoring particle aggregation processes.,” *Adv. Colloid Interface Sci.*, vol. 147–148, pp. 109–23, 2009.

[66] D. Ramkrishna, *Population balances, theory and applications to particulate systems in engineering*. Academic Press, 2002.

[67] S. Kumar and D. Ramkrishna, “On the solution of population balance equations by discretization—III. Nucleation, growth and aggregation of particles,” *Chem. Eng. Sci.*, vol. 52, no. 24, pp. 4659–4679, 1997.

[68] W. Press, S. Teukolsky, W. Vetterling, and B. Flannery, *Numerical recipes in Fortran: the art of scientific computing*, 2nd ed. New Tork: Cambridge University Press, 1992.

[69] C. Lin and L. Snyder, *Principles of parallel programming*. Addison Wesley, 2009.

[70] K. M. Chandy and S. Taylor, *An introduction to parallel programming*. Boston: Jones and Bartlett Publishers, 1992.

[71] R. Chandra, L. Dagum, D. Kohler, D. Maydan, J. McDonald, and R. Menon, *Parallel programming in OpenMP*. Morgan Kaufmann, 2001.

[72] S. Friedlander and C. Wang, “The self-preserving particle size distribution for coagulation by Brownian motion,” *J. Colloid Interface Sci.*, vol. 22, no. 2, pp. 126–132, 1966.

[73] S. Vemury, K. Kusters, and S. Pratsinis, “Time-lag for attainment of the self-preserving particle size distribution by coagulation,” *J. Colloid Interface Sci.*, vol. 165, no. 1, pp. 53–59, 1994.

[74] K. Cacossa and D. Vaccari, “Calibration of a compressive gravity thickening model from a single batch settling curve,” *Water Sci. Technol.*, vol. 30, no. 8, pp. 107–116, 1994.

Appendix A

Here, a brief description of Rosenbrock method is given. The solution is obtained using this equation (fourth-order method):

$$n(k,i_z)|_{t+\Delta t} = n(k,i_z)|_t + B_1u_1(k,i_z) + B_2u_2(k,i_z) + B_3u_3(k,i_z) + B_4u_4(k,i_z) \quad \text{(A1)}$$

where B_1, B_2, B_3 and B_4 are constants:

$$B_1 = \frac{19}{9};\ B_2 = \frac{1}{2};\ B_3 = \frac{25}{108};\ B_4 = \frac{125}{108}$$

$u_1(k,i_z)$, $u_2(k,i_z)$, $u_3(k,i_z)$, $u_4(k,i_z)$ are some coefficients. Let $\boldsymbol{u}_1$ be a vector that its components are $u_1(k,i_z)$ for $= 1, \dots, N$. Therefore $\boldsymbol{u}_1$ has N components. $\boldsymbol{u}_1$ is determined by solving the equation below:

$$(\mathbf{1}/\gamma\Delta t - \boldsymbol{f}') \cdot \boldsymbol{u}_1 = \boldsymbol{f}(\boldsymbol{n}|_t) \quad \text{(A2)}$$

Note that $\boldsymbol{n}|_t$ is a vector that its components are $n(k,i_z)|_t$. On the right side $\boldsymbol{f}(\boldsymbol{n}|_t)$ is a vector that its components are calculated as below:

$$f_1 = \frac{dn_1}{dt};\ f_2 = \frac{dn_2}{dt}, \dots, f_k = \frac{dn_k}{dt}.$$

In above equation $\boldsymbol{f}'$ is the Jacobian matrix; the elements of the N-by-N Jacobian matrix in this case have been calculated by analytical differentiation (shown in Table A1). $\gamma = 0.5$.

Let $\boldsymbol{u}_2$, $\boldsymbol{u}_3, and\ \boldsymbol{u}_4$ be the other coefficients $u_2(k, i_z)$, $u_3(k, i_z)$, and $u_4(k, i_z)$. They are determined as follows

$$(\mathbf{1}/\gamma\,\Delta t - \boldsymbol{f}') \cdot \boldsymbol{u}_2 = f(\boldsymbol{n}|_t + a_{21}\boldsymbol{u}_1) + c_{21}\boldsymbol{u}_1/\Delta t \tag{A3}$$

$$(\mathbf{1}/\gamma\,\Delta t - \boldsymbol{f}') \cdot \boldsymbol{u}_3 = f(\boldsymbol{n}|_t + a_{31}\boldsymbol{u}_1 + a_{32}\boldsymbol{u}_2) + (c_{31}\boldsymbol{u}_1 + c_{32}\boldsymbol{u}_2)/\Delta t \tag{A4}$$

$$(\mathbf{1}/\gamma\,\Delta t - \boldsymbol{f}') \cdot \boldsymbol{u}_4 = f(\boldsymbol{n}|_t + a_{41}\boldsymbol{u}_1 + a_{42}\boldsymbol{u}_2 + a_{43}\boldsymbol{u}_3) + (c_{41}\boldsymbol{u}_1 + c_{42}\boldsymbol{u}_2 + c_{43}\boldsymbol{u}_3)/\Delta t \tag{A5}$$

In above equations the coefficients a_{ij}, and c_{ij} are constants:

Table A1. The Jacobian matrix to be used in Rosenbrock method

$-\sum_{i=1}^{N-1}\beta_{1,i}n_i$	$-\beta_{1,2}n_1$	…	$-\beta_{1,N-2}n_1$	$-\beta_{1,N-1}n_1$	0
$\frac{1}{2}\beta_{1,1}n_1$ $-\beta_{2,1}n_2$	$-\sum_{i=1}^{N-2}\beta_{2,i}n_i$	…	$-\beta_{2,N-2}n_2$	0	0
$\beta_{1,2}n_2$ $-\beta_{3,1}n_3$	$\beta_{1,2}n_1$ $-\beta_{3,2}n_3$	…	0	0	0
⋮	⋮	⋱	⋮	⋮	⋮
$\beta_{1,N-2}n_{N-2}$ $-\beta_{N-1,1}n_{N-1}$	$\beta_{2,N-3}n_{N-3}$	…	$\beta_{N-2,1}n_1$ $-\beta_{N-2,2}n_2$	$-\sum_{i=1}^{N-(N-1)}\beta_{N-1,i}n_i$	0
$\beta_{1,N-1}n_{N-1}$	$\beta_{2,N-2}n_{N-2}$	…	$\beta_{N-2,2}n_2$	$\beta_{N-1,1}n_1$	0

The method here exerts an adaptive step size control. Implementation of this algorithm by adjusting the step-size results in minimum computational efforts while the desired accuracy of the solution is preserved. A few greater step sizes may results in a faster computation. The truncation error in this method is estimated for any step size, and then compared with required

tolerance. If the error is larger than the desired one, we should decrease the step-size; and if the error is smaller, the step-size is increased. The size of next step, Δt_{next} is adjusted as below

$$\Delta t_{next} = \begin{cases} S\Delta t \left|\frac{\in}{\in_0}\right|^{-1/4} & \in \geq \in_0 \\ S\Delta t \left|\frac{\in}{\in_0}\right|^{-1/3} & \in < \in_0 \end{cases} \tag{A6}$$

In above equation S is a safety factor which is a number close to unity, and $\in$ and $\in_0$ are the truncation error and required tolerance, respectively.

The error is estimated as below:

$$\in (k) = E_1 u_1(k) + E_2 u_2(k) + E_3 u_3(k) + E_4 u_4(k) \tag{A7}$$

E_1, E_2, E_3 and E_4 are coefficients. The maximum value of error is compared with required tolerance.

Appendix B

The FORTRAN code is presented here. Note that variables N and alpha, number of primary particles in the largest aggregates, and the collision efficiency respectively, should be set in the body and subroutines as well.

```
PROGRAM Sedimentation_aggregation _test
IMPLICIT NONE
include "omp_lib.h"
INTEGER :: i,j, p
INTEGER :: h
INTEGER :: m,r
INTEGER :: condition
INTEGER N
INTEGER :: plot_counter
INTEGER :: time_counter, max_time_counter
DOUBLE PRECISION :: Df,D0,particle_wt_percent
DOUBLE PRECISION :: height,sampling_location
DOUBLE PRECISION :: delta_t,delta_h,alpha,final_time
DOUBLE PRECISION :: k, T,g
DOUBLE PRECISION :: liquid_density, liquid_viscosity
DOUBLE PRECISION :: particle_density

PARAMETER (N=28000) ! number of primary particles in the largest aggregate
PARAMETER (Df=2.0)   ! fractal dimension
PARAMETER (D0=1.E-6) ! (m) Diameter of primary particles
PARAMETER (particle_wt_percent=5.0)  ! mass concentration of particles
PARAMETER (height=0.05) ! (m) height of the settling column
PARAMETER (final_time=200) ! time set up
PARAMETER (sampling_location=0.001) !(m)
PARAMETER (delta_h=0.001)
PARAMETER (h=(1.0/delta_h)) ! h is the number of bins

PARAMETER (alpha=0.001) ! collision efficiency
PARAMETER (k=1.38e-16) ! (g cm2 / s2 K) Boltzman constant
PARAMETER (T=298.0) ! (K) temperature
PARAMETER (g=9.80665)
PARAMETER (liquid_density=0.98) !(g/cm3) water
PARAMETER (liquid_viscosity=0.9) !(cp) water
PARAMETER (particle_density=2.65) ! (g/cm3) silica
DOUBLE PRECISION :: Progress
DOUBLE PRECISION , EXTERNAL :: derivs
```

```
!-------------------------------------------------------------
! The place we decide to switch on or off the differential settling
      LOGICAL:: differential_settling
      PARAMETER (differential_settling=.TRUE.)
!-------------------------------------------------------------
DOUBLE PRECISION :: real_final_time, time(h)
DOUBLE PRECISION :: real_time
DOUBLE PRECISION :: w_bin, w_bin_samp
DOUBLE PRECISION ::  htry, eps, hdid(h), hnext, time1(h)
DOUBLE PRECISION :: D(N)
DOUBLE PRECISION :: s(h,N),yscal(N)
DOUBLE PRECISION :: nold(N)
DOUBLE PRECISION :: ds1(N), ds2(N)
DOUBLE PRECISION :: sumpart1, sumpart2
DOUBLE PRECISION :: beta(N-1,N-1), y(N),dydx(N)
DOUBLE PRECISION :: No_bin_travelled(N)
DOUBLE PRECISION :: settlling_velocity(N)
DOUBLE PRECISION :: No_bin_travelled_modify(N)

DOUBLE PRECISION :: single_particle_weight
DOUBLE PRECISION :: w,wt1, wt2, wt5, wt7, wt9, wt11, wt13, wt15
DOUBLE PRECISION :: wt17, wt19, wt21, wt23, wt25
DOUBLE PRECISION :: liquid_volume
DOUBLE PRECISION :: particle_volume
DOUBLE PRECISION :: mixture_volume
DOUBLE PRECISION :: particle_initial_conc
DOUBLE PRECISION :: nT0
DOUBLE PRECISION :: pco1, pco2
DOUBLE PRECISION :: settlling_velocity1

DOUBLE PRECISION :: phi_bin, nt_bin
DOUBLE PRECISION :: eta_bin(50,N), psi_bin(50,N)
DOUBLE PRECISION :: phi_t, nt_t, mass_t
DOUBLE PRECISION :: eta_t(50,N), psi_t(50,N)
DOUBLE PRECISION :: ni(N), hmin,hmax, timefake
      common /coeff/ beta

! ****************************************************************
!  particle concentration calculation
! ****************************************************************

      single_particle_weight=4.0/3.0*3.14*(D0/2.0)**3.0*
     *   (particle_density*1000.0)*1000.0 !(g/particle)
      liquid_volume=(100.0-particle_wt_percent)/liquid_density ! (cm3)
      particle_volume=particle_wt_percent/particle_density ! (cm3)
      mixture_volume=liquid_volume+particle_volume
      particle_initial_conc=particle_wt_percent/
     *    single_particle_weight/mixture_volume ! (# of particles/cm3)
      nT0=particle_initial_conc
      ! PSD (1)
      wt1=80.0
```

```
      wt2=20.0
      wt5=0.0  ! % wt
      wt7=0.0  ! % wt
      wt9=0.0
      wt11=0.0
      wt13=0.0  ! % wt
      wt15=0.0
      wt17=0.0
      wt19=0.0
      wt21=0.0  ! % wt
      wt23=0.0  ! % wt
      wt25=0.0
!$omp parallel do
      DO i = 1,h
               DO j=2,N
                        s(i,j)=0.0
               END DO
            s(i,1) = wt1/100.*1.
            s(i,2) = wt2/100.*1./2.
            s(i,5)=wt5/100.*1./5.
            s(i,7)=wt7/100.*1./7.
            s(i,9)= wt9/100.*1./9.
            s(i,11)= wt11/100.*1./11.
            s(i,13)=wt13/100.*1./13.
            s(i,15)=wt15/100.*1./15.
            s(i,17)= wt17/100.*1./17.
            s(i,19)= wt19/100.*1./19.
            s(i,21)=wt21/100.*1./21.
            s(i,23)=wt23/100.*1./23.
            s(i,25)=wt25/100.*1./25.
       End DO
!$omp end parallel do
!-------------------------------------------------------------------------------
      settlling_velocity1=g*D0*D0*(particle_density-liquid_density)*
     *    1000.0/18.0/(liquid_viscosity*0.001)
!$omp parallel do
      DO i = 1,N
         D(i) = i**(1.0/Df)*D0
         settlling_velocity(i)=g*D(i)*D0*
     *       (particle_density-liquid_density)*1000.0/18.0/
     *        (liquid_viscosity*0.001)/settlling_velocity1
!    m/s
         No_bin_travelled_modify(i)=0.0
      END DO
!$omp end parallel do

      pco1=2.0*k*T/3.0/(liquid_viscosity*0.01)
      pco2=(D0*3.14*g/18.0/liquid_viscosity/0.01)*
     *    (particle_density-liquid_density)
!$omp parallel do
      DO i=1,N-1
```

```
          DO j=1, N-1
            beta(i,j)=pco1*((D(i)+D(j))**2.0/(D(i)*D(j)))
          ! cm3/s
            IF (differential_settling) THEN
               beta(i,j)=beta(i,j)+pco2*ABS(D(i)-D(j))*(D(j)+
     *            D(i))**2.0/4.0*1.0e10;
               ! cm3/s
            END IF
          END DO
        END DO
!$omp end parallel do
!$omp parallel do
        DO i=1, N-1
          DO j=1, N-1
                beta(i,j)=beta(i,j)*nT0*height/settlling_velocity1
          END DO
        END DO
!$omp end parallel do

!-------------------------------------------------------------------------------
        OPEN(UNIT=1, FILE='time.dat') ! recording time
        OPEN(UNIT=2, FILE='OUTn.dat') ! number density of aggregates
        OPEN(UNIT=3, FILE='OUTwbin.dat') ! mass density
        OPEN(UNIT=4, FILE='mass.dat') ! total mass
        OPEN(UNIT=8, FILE='n_before_arrange.dat') ! number densities before rearrangements
        OPEN(UNIT=9, FILE='OUTwbin_samp.dat') ! mass density at only one bin
        OPEN(UNIT=7, FILE='No_bin_travelled.dat')
!-------------------------------------------------------------------------------

        max_time_counter=INT(final_time/delta_t)
        plot_counter=0
        do i=1,h
        time(i)=0.
        time1(i)=0.
        enddo
        htry=0.0001
        eps=0.00001

        DO
          hmax=-1000.
          hmin=1000.

!$omp parallel do private (y)
!$omp+ shared (/coeff/,eps)
          DO i=1,h
            DO j=1,N
              y(j)=s(i,j)
              yscal(j)=1.
            END DO

            call stiff(y,N,timefake,htry,eps,yscal,hdid(i),hnext,derivs)
```

```
          if (hdid(i)<hmin) hmin=hdid(i)
          if (hdid(i)>hmax) hmax=hdid(i)
          htry=hnext

       END DO !i
!$omp end parallel do
!$omp parallel do private (y)
!$omp+ shared (/coeff/,eps)
       DO i=1,h
          DO j=1,N
            y(j)=s(i,j)
            yscal(j)=1.
          END DO
          If (hmin>0.001) hmin=0.001       ! delta_t
         call stiff2(y,N,time(i),hmin,eps,yscal,hdid(i),hnext,derivs)
          DO j=1,N
            s(i,j)=y(j)
          END DO

       END DO !i
!$omp end parallel do
           real_time=time(9)*(height/settlling_velocity1)
           WRITE (8,*) real_time                              !
            DO i=1,h-1
               DO j=1,N
                 w=s(i,j)
                 WRITE (8,*) w
            END DO
          END DO

!   ***REARRANGEMENT_SETTLING***
          DO j=1, N
             No_bin_travelled(j)=INT(settlling_velocity(j)*hmin/
     *       delta_h)

             No_bin_travelled_modify(j)=No_bin_travelled_modify(j)+
     *         ((settlling_velocity(j)*hmin/delta_h-
     *          No_bin_travelled(j)))
          END DO

          DO j=1,N
           IF (No_bin_travelled_modify(j)>1.) THEN
                          No_bin_travelled(j)=No_bin_travelled(j)+1
                  No_bin_travelled_modify(j)=No_bin_travelled_modify(j)
     *            -1.0
           END IF
           WRITE (7,*) real_time,j, No_bin_travelled(j)            !

          END DO
!
              DO i=1, N
```

```
                    DO p=h, No_bin_travelled(i)+1, -1
                        DO j=1 ,No_bin_travelled(i)
                            s(p,i)=s(p,i)+s(p-j,i)
                            s(p-j,i)=0.0
                    END DO

            END DO
          END DO

         mass_t=0.0
          DO i=1,h
              w_bin=0. ! w=m/m0
            DO j=1,N
              w_bin=w_bin+j*s(i,j)
              mass_t=mass_t+j*s(i,j) ! nT0*single_particle_weight;
            END DO
               WRITE (3,*) real_time, i, w_bin
             END DO
         WRITE (4,*) real_time, mass_t

         w_bin_samp=0. ! w=m/m0
         DO j=1,N
        w_bin_samp=w_bin_samp+j*s(NINT(sampling_location*h/height),j)
!nT0*single_particle_weight;
         END DO
             WRITE (9,*) real_time, w_bin_samp
             WRITE (1,*) real_time, h,N
         WRITE (2,*) real_time
             DO i=1,h
               DO j=1,N
                 w=s(i,j)
              WRITE (2,*) w
            END DO
         END DO
    IF (real_time> final_time) EXIT    ! time check
    END DO !time_counter

    CLOSE(1)
    CLOSE(2)
    CLOSE(3)
    CLOSE(4)
    close(9)
    CLOSE(8)
    CLOSE(7)
         stop
    END PROGRAM p

    SUBROUTINE stiff(y,n,x,htry,eps,yscal,hdid,hnext,derivs)
    INTEGER n,NMAX,MAXTRY
    DOUBLE PRECISION eps,hdid,hnext,htry,x,xx,dydx(n),y(n),yscal(n),
   * SAFETY,GROW,PGROW,SHRNK,PSHRNK,ERRCON,GAM,A21,A31,A32,A2X,A3X,
```

```
     * C21,C31,C32,C41,C42,C43,B1,B2,B3,B4,E1,E2,E3,E4,C1X,C2X,C3X,
     * C4X
      EXTERNAL derivs
      PARAMETER (NMAX=2800,SAFETY=0.9,GROW=1.5,PGROW=-.25,
     * SHRNK=0.5,PSHRNK=-1./3.,ERRCON=.1296,MAXTRY=1000)
      PARAMETER (GAM=1./2.,A21=2.,A31=48./25.,A32=6./25.,C21=-8.,
     * C31=372./25.,C32=12./5.,C41=-112./125.,C42=-54./125.,
     * C43=-2./5.,B1=19./9.,B2=1./2.,B3=25./108.,B4=125./108.,
     * E1=17./54.,E2=7./36.,E3=0.,E4=125./108.,C1X=1./2.,
     * C2X=-3./2.,C3X=121./50.,C4X=29./250.,A2X=1.,A3X=3./5.)

C    USES derivs,jacobn,lubksb,ludcmp

      INTEGER i,j,jtry,indx(NMAX)
      DOUBLE PRECISION d,errmax,h,xsav,a(NMAX,NMAX),dfdx(NMAX),
     * dfdy(NMAX,NMAX),dysav(NMAX),err(NMAX),g1(NMAX),g2(NMAX),g3(NMAX),
     * g4(NMAX),ysav(NMAX)
      xsav=x !Save initial values.
      call derivs(x,y,dydx)
      do i=1,n
        ysav(i)=y(i)
        dysav(i)=dydx(i)
      enddo !11
      call jacobn(xsav,ysav,dfdx,dfdy,n,NMAX)
      h=htry !Set stepsize to the initial trial value.
      do jtry=1,MAXTRY  !23
        do i=1,n !Set up the matrix 1 -    !13
          do j=1,n !12
            a(i,j)=-dfdy(i,j)
          enddo !12
          a(i,i)=1./(GAM*h)+a(i,i)
        enddo !13
        call ludcmp(a,n,NMAX,indx,d) !LU decomposition of the matrix.
        do i=1,n !Set up right-hand side for g1.  !14
          g1(i)=dysav(i)+h*C1X*dfdx(i)
        enddo !14
        call lubksb(a,n,NMAX,indx,g1) !Solve for g1.
        do i=1,n !Compute intermediate values of y and x. !15
          y(i)=ysav(i)+A21*g1(i)
        enddo !15
        x=xsav+A2X*h
        call derivs(x,y,dydx) !Compute dydx at the intermediate values.
        do i=1,n !Set up right-hand side for g2.    !16
          g2(i)=dydx(i)+h*C2X*dfdx(i)+C21*g1(i)/h
        enddo !16
        call lubksb(a,n,NMAX,indx,g2) !Solve for g2.
        do i=1,n !Compute intermediate values of y and x.  !17
          y(i)=ysav(i)+A31*g1(i)+A32*g2(i)
        enddo !17
        x=xsav+A3X*h
        call derivs(x,y,dydx) !Compute dydx at the intermediate values.
```

```
   do i=1,n !Set up right-hand side for g3. !18
   g3(i)=dydx(i)+h*C3X*dfdx(i)+(C31*g1(i)+
*     C32*g2(i))/h
   enddo !18
   call lubksb(a,n,NMAX,indx,g3) !Solve for g3.
   do i=1,n !Set up right-hand side for g4.  !19
    g4(i)=dydx(i)+h*C4X*dfdx(i)+(C41*g1(i)+
*      C42*g2(i)+C43*g3(i))/h
   enddo !19
   call lubksb(a,n,NMAX,indx,g4) !Solve for g4.
   do i=1,n !Get fourth-order estimate of y and error estimate. !21
     y(i)=ysav(i)+B1*g1(i)+B2*g2(i)+B3*g3(i)+B4*g4(i)
     err(i)=E1*g1(i)+E2*g2(i)+E3*g3(i)+E4*g4(i)
   enddo !21
   x=xsav+h

 !if(x.eq.xsav)pause 'stepsize not significant in stiff'
   errmax=0. !Evaluate accuracy.
   do i=1,n      !22
     errmax=max(errmax,abs(err(i)/yscal(i)))
   enddo !22
   errmax=errmax/eps !Scale relative to required tolerance.
   if(errmax.le.1.)then !Step succeeded. Compute size of next step and rehdid=
        hdid=h                          !turn.
        if(errmax.gt.ERRCON)then
             hnext=SAFETY*h*errmax**PGROW
        else
             hnext=GROW*h
        endif
        return
   else !Truncation error too large, reduce stepsize.
         hnext=SAFETY*h*errmax**PSHRNK
         h=sign(max(abs(hnext),SHRNK*abs(h)),h)
   endif
enddo !23 !Go back and re-try step.
pause 'exceeded MAXTRY in stiff'
END
SUBROUTINE jacobn(x,y,dfdx,dfdy,nn,nmax)
INTEGER nn,nmax,i,j
DOUBLE PRECISION x,y(*),dfdx(*),dfdy(nmax,nmax)
DOUBLE PRECISION alpha

parameter (alpha=1.0)
INTEGER N
parameter (N=2800)
DOUBLE PRECISION beta(N-1, N-1)
common /coeff/ beta
do i=1,nmax  ! 11
  dfdx(i)=0.
enddo !11
do i=1,nmax
```

```
      do j=1,nmax
        dfdy(i,j)=0.0
      enddo
    enddo

    do i=2, nmax-1
      do j=1,nmax-i
        dfdy(i,j)=alpha*(-y(i)*beta(i,j))
      enddo
    enddo
    do i=2,nmax
      do j=1,i-1
        dfdy(i,j)=dfdy(i,j)+alpha*beta(i-j,j)*y(i-j)
      enddo
    enddo

    do i=1,nmax
      dfdy(i,i)=0.0
      do j=1,nmax-i
        dfdy(i,i)=dfdy(i,i)-alpha*beta(j,i)*y(j)
      enddo
    enddo


    return
    END
    SUBROUTINE derivs(x,y,dydx)
    DOUBLE PRECISION x,y(*),dydx(*)
    DOUBLE PRECISION sumpart1,sumpart2
    INTEGER N
    DOUBLE PRECISION alpha
    parameter (N=2800)
    parameter (alpha=1.0)
    DOUBLE PRECISION beta(N-1, N-1)
    common /coeff/ beta
    INTEGER r,j,m

    DO j=1, N
          sumpart1=0.
          DO m=1, j-1
            r=j-m
            sumpart1=sumpart1+beta(m,r)*y(m)*y(r)
       END DO
       sumpart2=0.
       DO m=1, N-j
         sumpart2=sumpart2+beta(j,m)*y(m)*y(j)
           END DO
!
       dydx(j)=alpha*(0.5*sumpart1-sumpart2)

           END DO ! j
```

```
return
END
SUBROUTINE lubksb(a,n,np,indx,b)
INTEGER n,np,indx(n)
DOUBLE PRECISION a(np,np),b(n)
INTEGER i,ii,j,ll
DOUBLE PRECISION sum
ii=0
do i=1,n !12
  ll=indx(i)
  sum=b(ll)
  b(ll)=b(i)
  if (ii.ne.0)then
    do j=ii,i-1 !11
      sum=sum-a(i,j)*b(j)
    enddo !11
  else if (sum.ne.0.) then
       ii=i
  endif
  b(i)=sum
enddo !12
do i=n,1,-1    !14
  sum=b(i)
  do j=i+1,n  !13
    sum=sum-a(i,j)*b(j)
  enddo !13
  b(i)=sum/a(i,i) !Store a component of the solution vector X.
enddo !14
return !All done!
END

SUBROUTINE ludcmp(a,n,np,indx,d)
INTEGER n,np,indx(n),NMAX
DOUBLE PRECISION d,a(np,np),TINY
PARAMETER (NMAX=2800,TINY=1.0e-20) !Largest expected n, and a small number.
!Given a matrix a(1:n,1:n), with physical dimension np by np, this routine replaces it by
!the LU decomposition of a rowwise permutation of itself. a and n are input. a is output,
!arranged as in equation (2.3.14) above; indx(1:n) is an output vector that records the
!row permutation eected by the partial pivoting; d is output as 1 depending on whether
!the number of row interchanges was even or odd, respectively. This routine is used in
!combination with lubksb to solve linear equations or invert a matrix.
INTEGER i,imax,j,k
DOUBLE PRECISION aamax,dum,sum,vv(NMAX) !vv stores the implicit scaling of each row.

d=1.                        !d=1. No row interchanges yet.
do i=1,n ! 12          Loop over rows to get the implicit scaling informaaamax=
                              !0. tion.
    aamax=0.
    do j=1,n !11
      if (abs(a(i,j)).gt.aamax) aamax=abs(a(i,j))
    enddo !11
```

```
      if (aamax.eq.0.) pause 'singular matrix in ludcmp' !No nonzero largest element.
    vv(i)=1./aamax !Save the scaling.
    enddo !12
    do j=1,n ! 19   This is the loop over columns of Crout's method.
      do i=1,j-1 ! 14 This is equation (2.3.12) except for i = j.
        sum=a(i,j)
        do k=1,i-1 !13
          sum=sum-a(i,k)*a(k,j)
        enddo !13
        a(i,j)=sum
      enddo !14
      aamax=0.
      do i=j,n !16
      sum=a(i,j)
         do k=1,j-1 !15
           sum=sum-a(i,k)*a(k,j)
         enddo !15
         a(i,j)=sum
         dum=vv(i)*abs(sum) !Figure of merit for the pivot.
         if (dum.ge.aamax) then !Is it better than the best so far?
           imax=i
           aamax=dum
         endif
      enddo !16
      if (j.ne.imax)then !Do we need to interchange rows?
        do k=1,n !  17       Yes, do so...
          dum=a(imax,k)
          a(imax,k)=a(j,k)
          a(j,k)=dum
        enddo !17
        d=-d !...and change the parity of d.
        vv(imax)=vv(j) !Also interchange the scale factor.
      endif
      indx(j)=imax
      if(a(j,j).eq.0.)a(j,j)=TINY
           if(j.ne.n)then !Now, ally, divide by the pivot element.
             dum=1./a(j,j)
             do i=j+1,n !18
               a(i,j)=a(i,j)*dum
             enddo !18
           endif
    enddo !19 Go back for the next column in the reduction.
    return
    END
    SUBROUTINE stiff2(y,n,x,htry,eps,yscal,hdid,hnext,derivs)
    INTEGER n,NMAX,MAXTRY
    DOUBLE PRECISION eps,hdid,hnext,htry,x,xx,dydx(n),y(n),yscal(n),
   * SAFETY,GROW,PGROW,SHRNK,PSHRNK,ERRCON,GAM,A21,A31,A32,A2X,A3X,
   * C21,C31,C32,C41,C42,C43,B1,B2,B3,B4,E1,E2,E3,E4,C1X,C2X,C3X,
   * C4X
    EXTERNAL derivs
```

```
      PARAMETER (NMAX=2800,SAFETY=0.9,GROW=1.5,PGROW=-.25,
     * SHRNK=0.5,PSHRNK=-1./3.,ERRCON=.1296,MAXTRY=1000)
      PARAMETER (GAM=1./2.,A21=2.,A31=48./25.,A32=6./25.,C21=-8.,
     * C31=372./25.,C32=12./5.,C41=-112./125.,C42=-54./125.,
     * C43=-2./5.,B1=19./9.,B2=1./2.,B3=25./108.,B4=125./108.,
     * E1=17./54.,E2=7./36.,E3=0.,E4=125./108.,C1X=1./2.,
     * C2X=-3./2.,C3X=121./50.,C4X=29./250.,A2X=1.,A3X=3./5.)

C     USES derivs,jacobn,lubksb,ludcmp

      INTEGER i,j,jtry,indx(NMAX)
      DOUBLE PRECISION d,errmax,h,xsav,a(NMAX,NMAX),dfdx(NMAX),
     * dfdy(NMAX,NMAX),dysav(NMAX),err(NMAX),g1(NMAX),g2(NMAX),g3(NMAX),
     * g4(NMAX),ysav(NMAX)
      xsav=x !Save initial values.
      call derivs(x,y,dydx)
      do i=1,n
        ysav(i)=y(i)
        dysav(i)=dydx(i)
      enddo !11
      call jacobn(xsav,ysav,dfdx,dfdy,n,NMAX)
      h=htry !Set stepsize to the initial trial value.
      do jtry=1,1  !23
        do i=1,n !Set up the matrix 1 -    !13
          do j=1,n !12
            a(i,j)=-dfdy(i,j)
          enddo !12
          a(i,i)=1./(GAM*h)+a(i,i)
        enddo !13
        call ludcmp(a,n,NMAX,indx,d) !LU decomposition of the matrix.
        do i=1,n !Set up right-hand side for g1.  !14
          g1(i)=dysav(i)+h*C1X*dfdx(i)
        enddo !14
        call lubksb(a,n,NMAX,indx,g1) !Solve for g1.
        do i=1,n !Compute intermediate values of y and x. !15
          y(i)=ysav(i)+A21*g1(i)
        enddo !15
        x=xsav+A2X*h
        call derivs(x,y,dydx) !Compute dydx at the intermediate values.
        do i=1,n !Set up right-hand side for g2.    !16
          g2(i)=dydx(i)+h*C2X*dfdx(i)+C21*g1(i)/h
        enddo !16
        call lubksb(a,n,NMAX,indx,g2) !Solve for g2.
        do i=1,n !Compute intermediate values of y and x.  !17
          y(i)=ysav(i)+A31*g1(i)+A32*g2(i)
        enddo !17
        x=xsav+A3X*h
        call derivs(x,y,dydx) !Compute dydx at the intermediate values.
        do i=1,n !Set up right-hand side for g3. !18
        g3(i)=dydx(i)+h*C3X*dfdx(i)+(C31*g1(i)+
     *     C32*g2(i))/h
```

```
      enddo !18
      call lubksb(a,n,NMAX,indx,g3) !Solve for g3.
      do i=1,n !Set up right-hand side for g4.  !19
       g4(i)=dydx(i)+h*C4X*dfdx(i)+(C41*g1(i)+
     *      C42*g2(i)+C43*g3(i))/h
      enddo !19
      call lubksb(a,n,NMAX,indx,g4) !Solve for g4.
      do i=1,n !Get fourth-order estimate of y and error estimate. !21
        y(i)=ysav(i)+B1*g1(i)+B2*g2(i)+B3*g3(i)+B4*g4(i)
        err(i)=E1*g1(i)+E2*g2(i)+E3*g3(i)+E4*g4(i)
      enddo !21
      x=xsav+h

    enddo !23 !Go back and re-try step.
    return
    END
```